WHOI-2012-09

Woods Hole Oceanographic Institution

Analysis of Deep Seafloor Arrivals Observed on NPAL04

by

Ralph A. Stephen, S. Thompson Bolmer, Ilya A Udovydchenkov, Matthew A. Dzieciuch, Peter F. Worcester, Rex K. Andrew, James A. Mercer, John A. Colosi and Bruce M. Howe

December 2012

Technical Report

Funding was provided by the Office of Naval Research under Contract No. N00014-10-1-0510

WHOI-2012-09

Analysis of Deep Seafloor Arrivals Observed on NPAL04

by

Ralph A. Stephen, S. Thompson Bolmer, Ilya A Udovydchenkov, Matthew A. Dzieciuch, Peter F. Worcester, Rex K. Andrew, James A. Mercer, John A. Colosi and Bruce M. Howe

Woods Hole Oceanographic Institution
Woods Hole, Massachusetts 02543

December 2012

Technical Report

Funding was provided by the Office of Naval Research under Contract No. N00014-10-1-0510

Approved for Distribution:

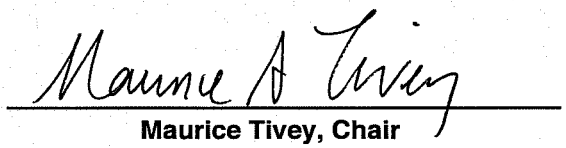

Maurice Tivey, Chair

Department of Geology and Geophysics

WHOI-2012-09

Analysis of Deep Seafloor Arrivals Observed on NPAL04

Ralph A. Stephen[1], S. Thompson Bolmer[1], Ilya A. Udovydchenkov[1], Matthew A, Dzieciuch[2], Peter F. Worcester[2], Rex K. Andrew[3], James A Mercer[3], John A. Colosi[4], and Bruce M. Howe[5]

December 3, 2012

Technical Report

1 Woods Hole Oceanographic Institution,
Woods Hole, MA, USA.

2 Scripps Institution of Oceanography,
La Jolla, CA, USA.

3. University of Washington,
Seattle, WA, USA.

4. Naval Postgraduate School,
Monterey, CA, USA.

5. University of Hawaii at Manoa,
Honolulu, HI, USA.

Abstract

This report gives an overview of the analysis that was done on Deep Seafloor Arrivals since they were initially presented in Stephen et al (2009). All of the NPAL04/LOAPEX (North Pacific Acoustic Laboratory, 2004/ Long Range Ocean Acoustic Propagation Experiment) data on three ocean bottom seismometers (OBSs) at ~5,000m depth and the deepest element of the deep vertical line array (DVLA) at 4250m depth has been analyzed. A distinctive pattern of late arrivals was observed on the three OBSs for transmissions from T500 to T2300. The delays of these arrivals with respect to the parabolic equation predicted (PEP) path were the same for all ranges from 500 to 2300km, indicating that the delay was introduced near the receivers. At 500km range the same arrival was observed throughout the water column on the DVLA. We show that arrivals in this pattern converted from a PEP path to a bottom-diffracted surface reflected (BDSR) path at an off-geodesic seamount.

Table of Contents

Table of Tables

Table of Figures

On NPAL04 Deep Seafloor Arrivals (DSFAs) were the largest amplitude arrivals observed on the OBSs from T500 to T3200. Prior to September 2012, the physical mechanism responsible for DSFAs was unexplained. There were five candidate explanations: a) Deep shadow zone arrivals (DSZA) which occur when acoustic energy is scattered vertically many wavelengths below a PE-predicted turning point (Dushaw *et al.*, 1999; Van Uffelen *et al.*, 2008a; Van Uffelen *et al.*, 2009; Van Uffelen *et al.*, 2006), b) Bottom-reflected surface-reflected paths along the source-receiver geodesic (In-plane BRSR), c) Bottom-diffracted surface-reflected paths along the source-receiver geodesic (In-plane BDSR), d) PE-predicted propagation to a near-by out-of-plane seamount with conversion to a seafloor interface wave (Out-of-plane IW), e) PE-predicted propagation to a near-by out-of-plane seamount with conversion to a BDSR path (Out-of-plane BDSR). Before addressing each of these in turn let's review the fundamental observations and present the procedure for identifying the out-of-plane conversion point on Seamount B (triangulation).

A) Fundamental Observations up to the 2009 JASA Paper

1) Detailed Analysis of Late Arrivals at T1600 (DVLA-L20-Hyd and OBS-S-Geo for M68.2)

The 2009 DSFA paper (Stephen *et al.*, 2009) addressed only arrivals on the South OBS from M68.2 transmissions at 350m depth. The key figure (Figure 1) compares the arrival pattern on the deepest element of the DVLA (DVLA-L20-Hyd) and the South OBS (OBS-S-Geo) with PE predictions **including bottom interaction.** Three arrival types were identified: a) PE-predicted (PEP), b) deep shadow zone (DSZA), and c) deep seafloor (DSFA). BRSR paths were included in the PE simulations but their SNR was insufficient at the receiver depths to be observed in the model traces.

2) Summary of Late Arrivals for T250 to T3200 (DVLA-L20-Hyd and OBS-S-Geo for M68.2)

The arrival patterns for all stations from T250 to T3200 are summarized in Figure 2. The PE time series in this figure **do not include bottom interaction** because the model traces in this case were too noisy. In the geophone and hydrophone data traces red indicates arrivals whose travel-time corresponds to PE predicted paths. The blue arrivals on DVLA-L20-Hyd are DSZA arrivals. There are 16 blue arrivals on the OBS (Figure 2a) that could be either DSZA arrivals, BRSR arrivals or DSFA arrivals.

Section 5e) of the technical report, Stephen et al (2008), discusses these 16 arrivals in detail. It includes figures similar to Figure 1 for the T500, T1000 and T2300 transmissions (with bottom interaction in the PE models) as well as individual time-front figures of PE-model-with-bottom-interaction results (T50 to T2300). The conclusions were: " Of the 16 arrivals discussed above three have been labeled "deep shadow zone" initially (vi, vii and viii) although they are too large in magnitude to be consistent with deep shadow zone events. If we consider these three as deep seafloor arrivals, of the sixteen total, four cannot be SRBR (iv, vi, xiii, and xiv) and twelve could conceivably be SRBR. Of the 12 that could be SRBR, eight correspond to a cloud in the PE model (i, ii, iii, v, vii, viii, xi, and xii), three could be extrapolated from time fronts at shallower

depths (ix, xv and xvi) and one is extrapolated from events at other ranges (x). Although arguments can be made to explain the arrival times of the twelve "SRBR" events in SRBR terms, more modeling would need to be done to explain the relative amplitudes and other characteristics of these events."

Figure 1: Comparison of model to data for T1600 to DVLA-L20-Hyd and OBS-S-Geo.

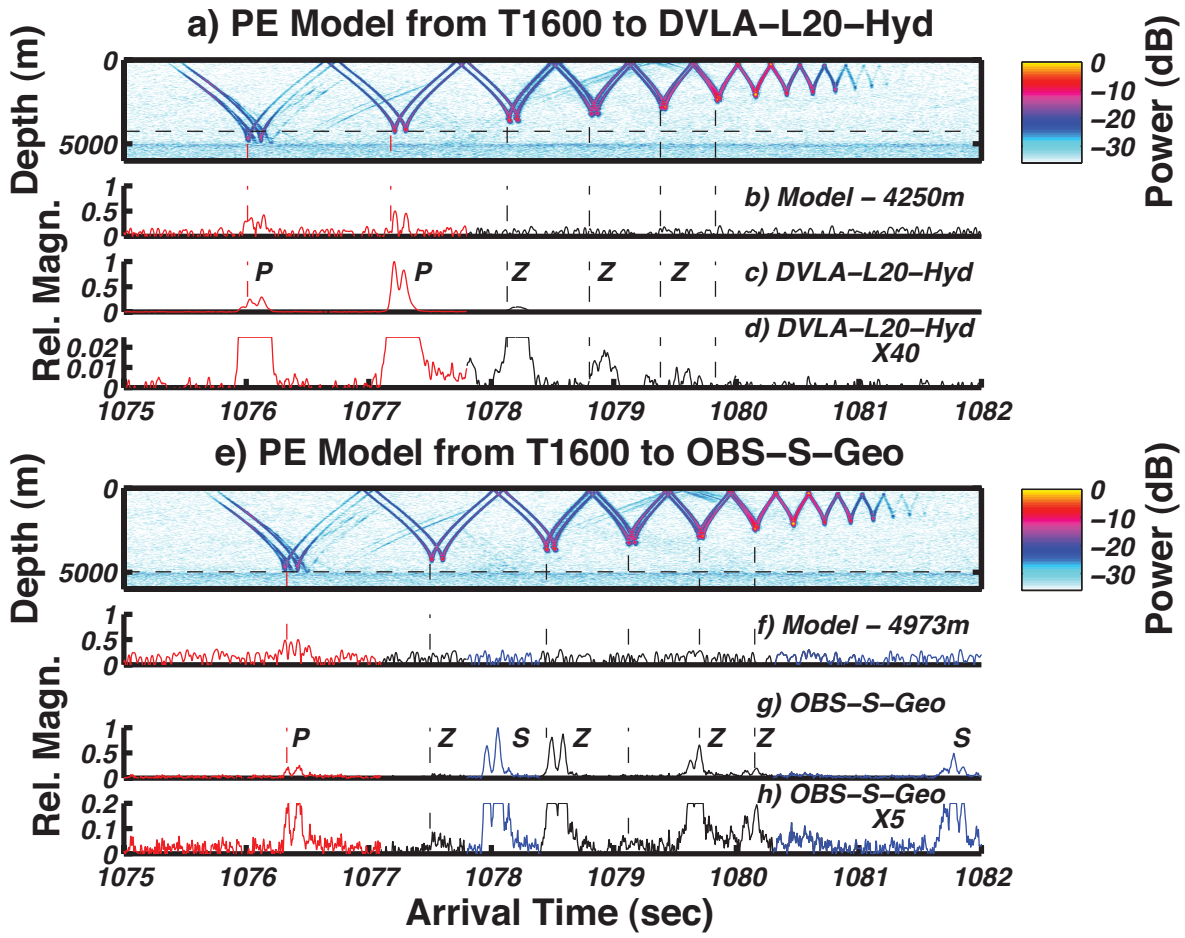

Figure 1 (Figure 4 of the 2009 paper): This figure compares the arrival structure on DVLA-L20-Hyd and OBS-S-Geo with PE (parabolic equation) model predictions for a range of 1600km. The PE models include bottom interaction. The top group of four panels (a-d) is the model-data comparison for DVLA-L20-Hyd and the bottom group (e-h) is for OBS-S-Geo. Within each group of four, the top panel is the time front diagram, the second panel is the model trace at the receiver depth (indicated by a horizontal dashed line in the time front diagram), the third panel is the data trace normalized to its maximum amplitude and the bottom trace is an expanded view of the data trace. Vertical dashed lines show the times of the turning points across all of the plots. Examples of the three arrival classes, "PE predicted" arrivals (P), "deep shadow zone" arrivals (Z) and "deep seafloor" arrivals (S) are indicated. The deep seafloor arrivals are an unexplained set of arrivals.

Figure 2: Model and data traces for DVLA-L20-Hyd and OBS-S-Geo (M68.2, 350m).

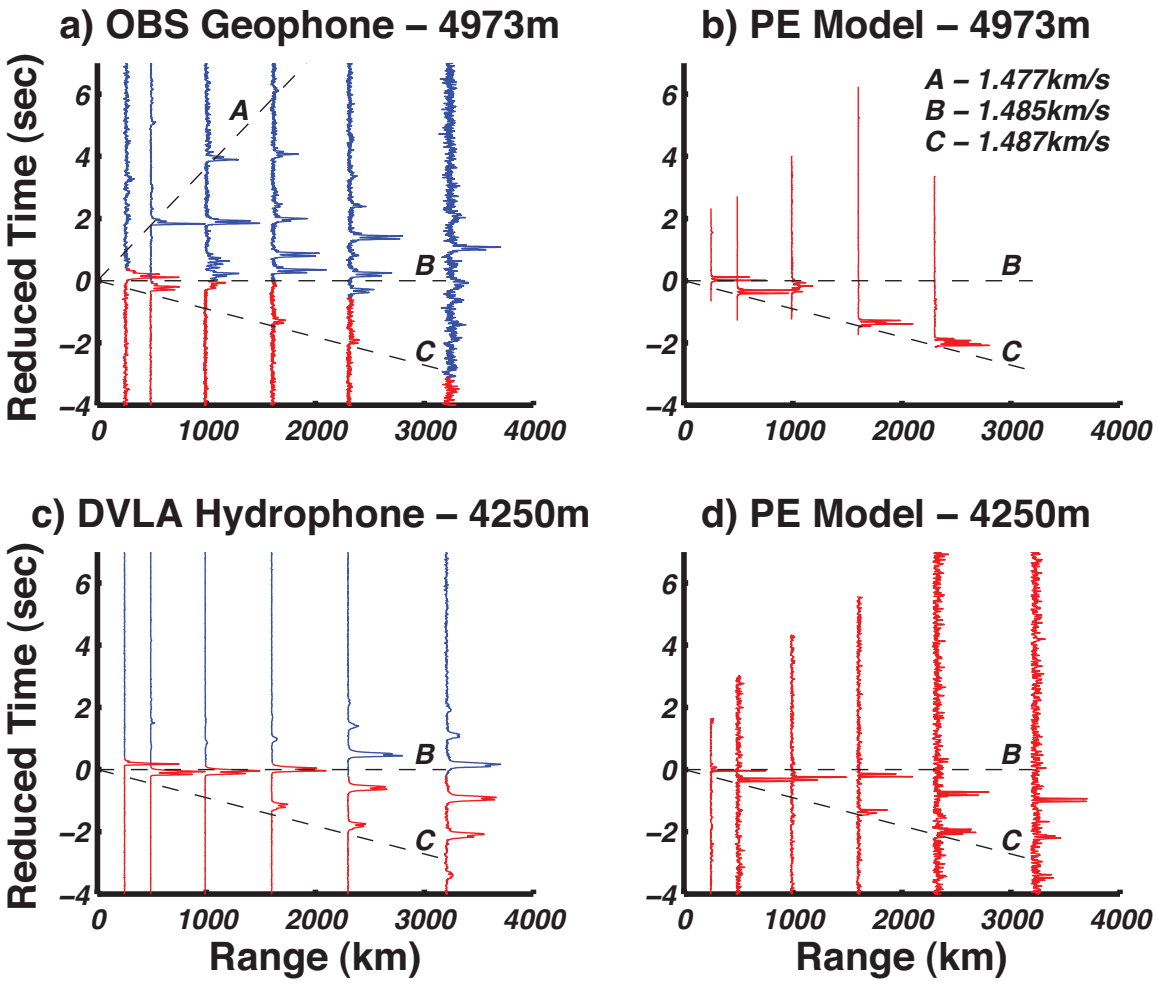

Figure 2 (Figure 5 of the 2009 paper): The stacked traces from the OBS vertical geophone on the seafloor (a) show many more arrivals than the deepest DVLA hydrophone (c) or the parabolic equation (PE) models (b and d). For the OBS geophone traces (a), events occurring with a sound speed faster than about 1.485km/s (roughly earlier than line B) are predicted by the PE but there are many "late arrivals". Dashed lines correspond to three relevant speeds: A- the apparent sound speed of the latest arrival at T500, T1000 and T1600, B - the apparent sound speed of the largest PE arrivals at the deepest hydrophone of the DVLA which seems to separate the known early arrivals from the late unknown arrivals and C - the apparent sound speed of the earliest arriving energy at the OBS and DVLA, which corresponds to the deepest turning energy. The time axis has been reduced by subtracting the range divided by 1.485km/s. The PE model for the South OBS (b) does not include bottom interaction but the PE model for the DVLA hydrophone (d) does include bottom interaction. [Compare with Figures 2-1 and 2-2 in Stephen et al (2008).] There is no indication of BRSR paths in the PE model at the DVLA-L20-Hyd depth (4250m). The model arrivals are all surface-reflected (SR) paths, which have turned in the deep ocean without hitting the bottom.

The analysis in the 2008 report was based on just DVLA-L20_Hyd and OBS-S-Geo, before the distinctive arrival pattern (highlighted in yellow) was identified on the three OBSs. A reinterpretation of these 16 arrivals is discussed in Section E below.

B) Fundamental Observations after the 2009 JASA Paper

1) Similarity of Arrival Patterns on DVLA-L20-Hyd and all three OBSs

After the 2009 JASA paper there were two significant developments. First, when we processed the East and West OBS data we saw the same distinctive arrival pattern on all three OBSs and it corresponded to the PE-predicted arrival pattern on DVLA-L20-Hyd (highlighted in yellow in Figure 3). The pattern occurred at different times with respect to the PE predicted arrivals for each OBS. The triangulation that was done to identify the source location of these arrivals will be discussed below in Section C.3.

2) Some features of deep seafloor arrivals

Figure 3 shows record sections (the incoherent stacks of all transmissions plotted as a function of range) for the M68.2 transmissions at the 350m source depth for all three OBSs and DVLA-4250. The record sections for the south OBS and DVLA-4250 were shown in Figure 5 of the 2009 paper (Stephen *et al.*, 2009) where they were compared with parabolic equation model results. Red indicates sections of the traces that are predicted by the parabolic equation method (PEP arrivals).

Inspection reveals the following features:
a) In general, the OBS vertical geophone traces have more arrivals than the DVLA-4250 hydrophone.
b) Most of the major events on DVLA-4250 are predicted by the PE. The later arrivals (in blue) at T2300 and T3200, and weakly at T1600, correspond primarily to deep shadow zone (DZA) arrivals, the evanescent tails beneath ray turning points (Van Uffelen *et al.*, 2009), as demonstrated in Figures 4 and 5 of Stephen et al. (2009).
c) On the south OBS there is an early, small amplitude, arrival at T1600 and T2300 that is predicted by the PE solution (line C, see Figure 5 of Stephen et al. (2009)). This is also on the west OBS out to T2300, so it appears to be a robust event. There is no indication of these PEP arrivals on the east OBS at T500 and greater.
d) On the south OBS there are larger amplitude arrivals at T1000 (smeared out), T1600 and T2300 that are not predicted by the PE solution. These are the blue arrivals that occur around line B that are not highlighted in yellow. On the west OBS there are corresponding arrivals at T1000 (strong) and at T1600 and T2300 (weak). On the east OBS this arrival appears clearly at T1000, but not at the other ranges. Because of this lack of consistency these arrivals will not be discussed further in this paper.

Figure 3: Data traces for DVLA-L20-Hyd and three OBSs (M68.2, 350m).

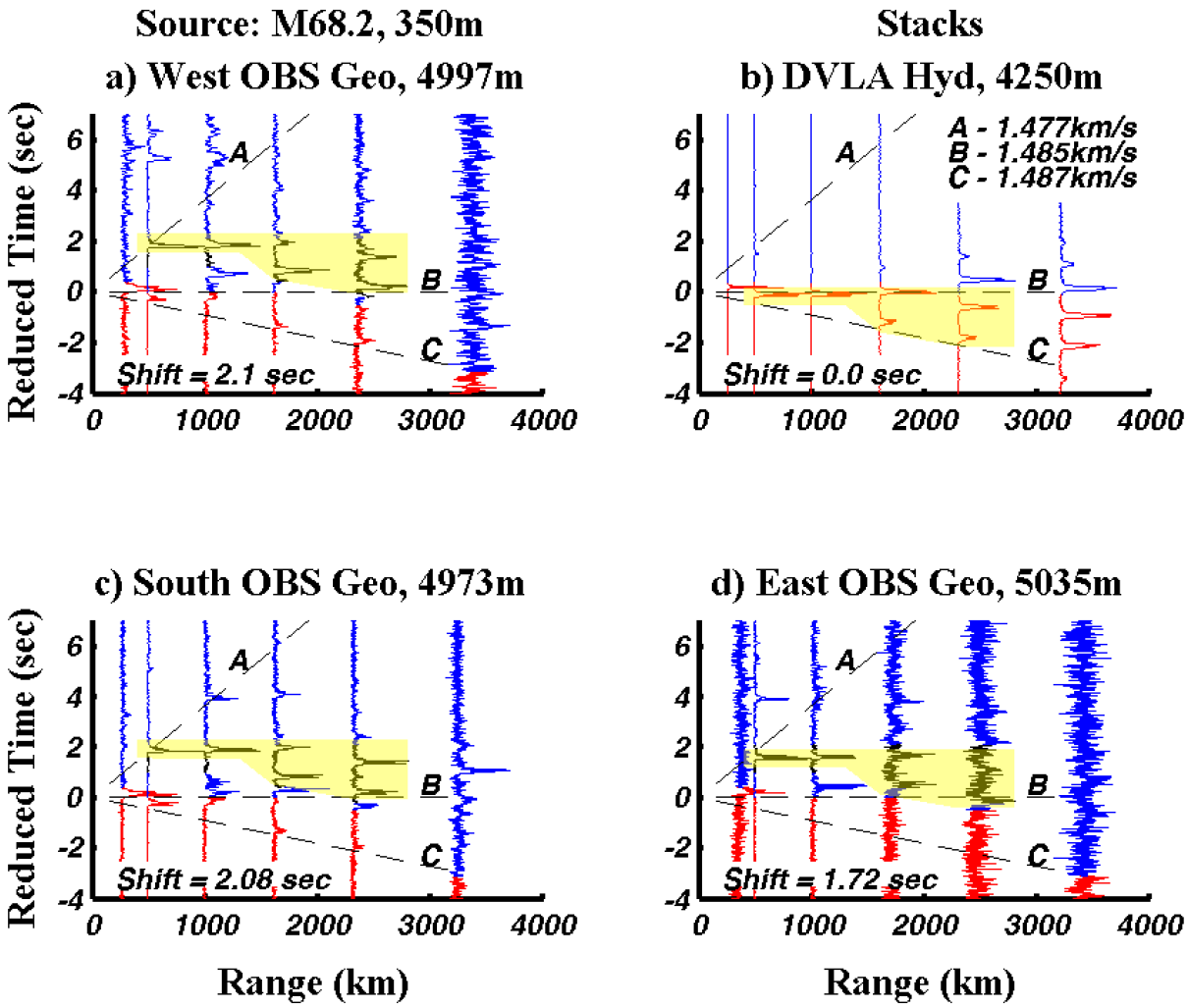

Figure 3 (Figure 2 in Stephen et al, submitted): Stacks of the replicated-correlated traces are displayed as a function of source range for the DVLA and the three OBSs. Reduced time is the actual travel time from the source minus the range divided by 1.485km/sec. The red section of each trace indicates the PE predicted arrivals and the blue trace indicates deep shadow-zone and deep seafloor arrivals as discussed in Stephen et al (2009). General features are discussed in the text. The seafloor arrivals shown in the highlighted yellow regions have a distinctive pattern for all three OBSs. The arrival pattern appears to be a delayed version (by about 2sec) of the pattern on the deepest element of the DVLA. The shifts of these arrivals with respect to the PE predicted arrivals on the DVLA are a constant regardless of range. The robustness of these arrivals over all three ocean bottom receivers is remarkable. Dashed lines correspond to three relevant speeds: A- 1.477km/s - the apparent sound speed of the latest arrival at T500, T1000 and T1600, B - 1.485km/s - the apparent sound speed of the largest PE predicted arrival at the deepest hydrophone of the DVLA which seems to separate the known early arrivals from the late unknown arrivals, and C - 1.487km/s - the apparent sound speed of the earliest arriving energy at the OBSs and DVLA. [Fig_OBS_Stacks_5_a4_new.jpg]

e) The DSF arrivals, highlighted in yellow, form a consistent pattern. This is most clearly seen on the south and west OBSs and the T500 to T1600 traces on the east OBS. Interestingly the arrival pattern is very similar to the PE arrival pattern on DVLA-4250. The yellow region is the same shape on all four figures but has been shifted in time as indicated. These arrivals will be discussed further below.
f) At 4sec reduced time and later there are arrivals on some traces on some OBSs. Although these are clear and have significant relative amplitudes, they do not seem to fit a pattern and will not be discussed further in this paper.
g) It is interesting that the single, large amplitude arrival in the stacks at T3200 to the south OBS is a DSF arrival. It does not appear on the east and west OBSs. It is even more interesting, however, that this arrival on the south OBS appears even on some single, 30sec transmissions after pulse compression (Figure 4).
h) Even though the OBSs are less than 4km apart, the number of detections and the SNRs vary dramatically for the three geophones (not shown). For example, for the west, south and east OBSs the SNRs (peak of signal to RMS of noise just prior to the arrival) of about 600 stacked vertical velocity traces at T3200 (source M68.2 at 500m depth) were 16, 25 and 15dB, respectively. The number of detections on single traces (for example Figure 4) were 13, 33 and 0, respectively. The south OBS, which is also the shallowest, has better SNRs than the other OBSs and this is consistent regardless of range to the source.
i) The DSF arrival structure is not particularly sensitive to the source carrier frequency or source depth as shown in Figure 5, for M75 at 800m depth and M68.2 at 500m depth. The arrivals between 0 and 2sec reduced time persist for T500 to T3200.

3) Energy Summary of PEP and DSFA Arrivals

The second development was a quantitative comparison of the RMS energy levels of the PE predicted and DSFA arrivals on DVLA-L20-Hyd and the three OBSs (Figure 10). The DSFA arrivals on the OBSs are 30-35dB quieter than the PE predicted arrival on the DVLA and, in fact, are even quieter, by 8 to 13dB, than the ambient noise on the DVLA. If the DSFA arrivals were propagating through the water column, perhaps on an out-of-plane bottom-diffracted-surface-reflected (BDSR) path they would not appear on single, unprocessed DVLA channels.

Figure 4: DSF arrivals on unstacked traces at 3200km range.

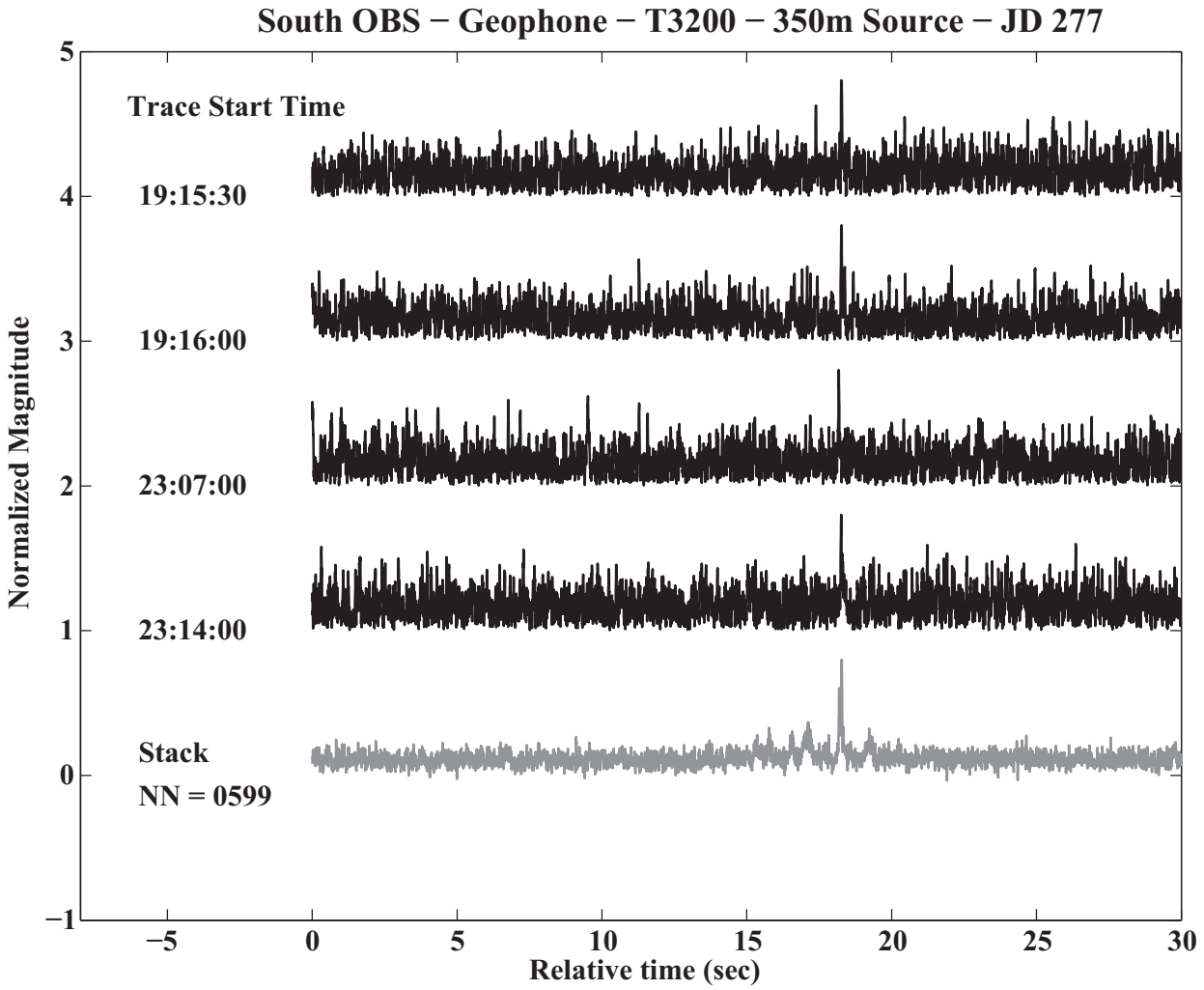

Figure 4: Four samples of unstacked traces (top) and the stack of 599 traces (bottom) are shown for propagation over 3200km range from the LOAPEX source at 350m depth as received on the vertical geophone channel of the south OBS at 4,973m depth. It is remarkable that transmissions are observed (at about 18sec) on single, unstacked traces in the deep shadow zone at this range. [Figure_03_TC_Geo_T3200.tif]

Figure 5: Data traces for DVLA-L20-Hyd and three OBSs (M75, 800m and M68.2, 500m).

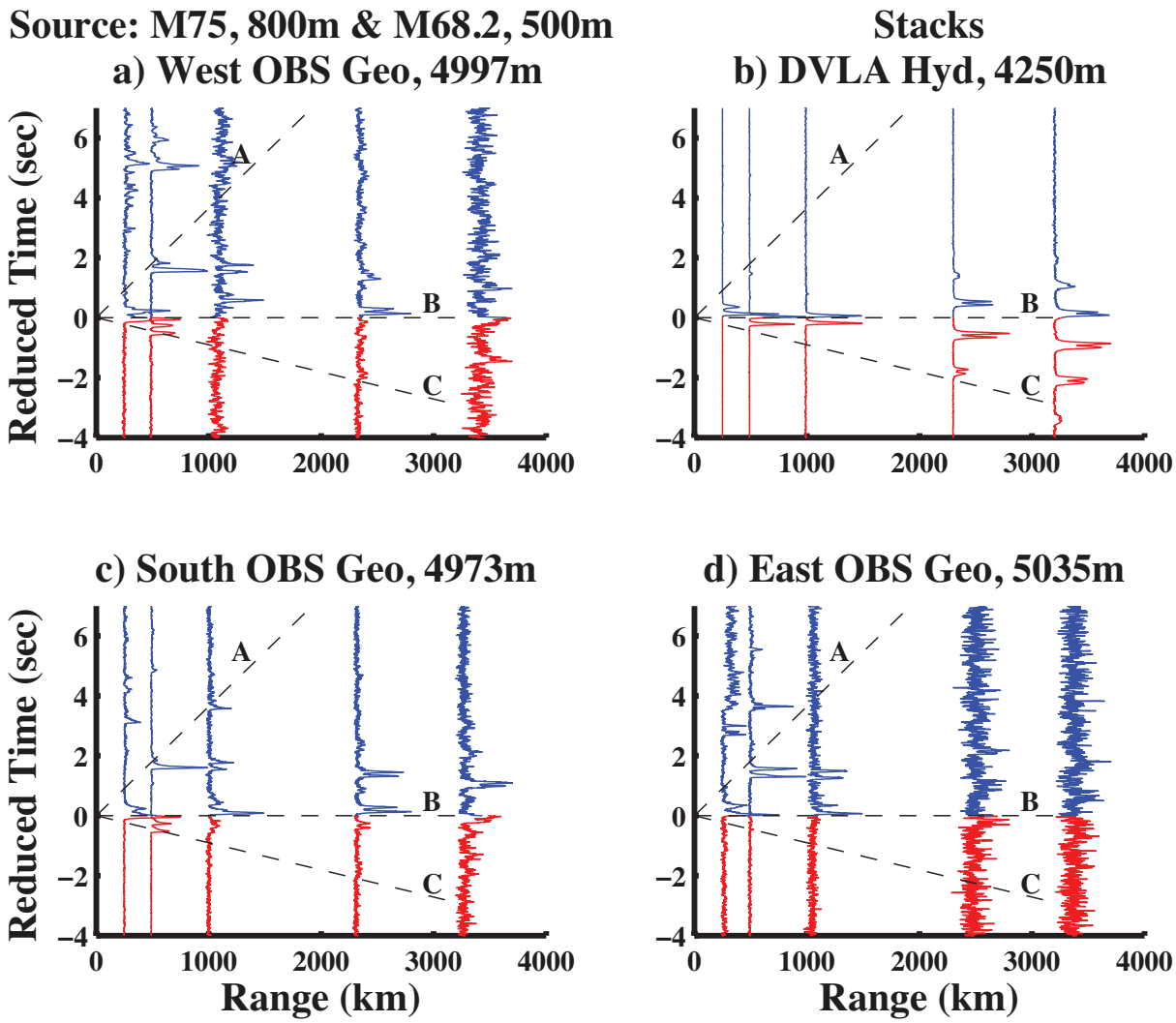

Figure 5: This record section combines traces for the M75 transmission format at 800m depth (at T250, T500 and T1000) with traces for the M68.2 transmission format at 500m depth (T2300 and T3200). They show a very similar arrival pattern to the record sections in Figure 2. [Fig_OBS_Stacks_5_a2_merged.tif]

C) Triangulation of the Distinctive Arrival Pattern (OBS Arrivals Only)

1) The Distinctive Arrival Pattern

From T500 to T2300 there is a section of DSFA arrivals on the OBSs that is identical to PEP arrivals on the DVLA-L20-Hyd traces but is delayed by about 2.0sec (yellow highlighted region in Figure 3). This section contains the largest amplitude arrivals on the OBSs. Since these arrivals are delayed a fixed amount regardless of range, the delay is introduced near the receivers. The similarity of the pattern on the OBSs with the pattern on the DVLA indicates that the "accordian pattern" of the acoustic arrivals at 4250m depth somehow appears, delayed by about 2.0sec, at 5000m depth. (The PE computed arrival patterns at 4250 and 4973m, which are quite different, are compared in Figure 2b and 2d.) Although the pattern for traces T500 to T2300 is robust, SNRs at T3200 are too poor to confirm that the pattern appears out to this range. At T250 where SNRs are good there is only a weak indication of later arrivals. PEP arrivals are not observed on the east OBS for these ranges possibly due i) to poorer SNR in general or ii) to the greater depth, and hence further from the PE turning points. (Depths of the south, west and east OBSs were 4973, 4997 and 5035m, respectively.) PEP arrivals were observed on the east OBS at T250 and these were used for the small clock correction.

Figures 6 and 8 show the same traces as Figure 3 (below) but grouped with respect to T-station and plotted as a function of range, as if the four receivers comprised a linear array. Figure 6 shows how well the PEP arrivals align on the DVLA and West and South OBSs after small clock corrections (about 0.2sec) that will be discussed further below. The time axis, from -2 to 2sec reduced time for T500 to T2300, spans the arrival times of the PE predicted and the first deep seafloor arrivals (shaded yellow in Figures 2 and 6). The first arrivals, occurring before 0sec reduced time and indicated in cyan on the DVLA-4250 trace and red on the OBS geophone traces, are PEP arrivals.

What is the small amplitude arrival, in magenta, at about 1.2sec reduced time on the DVLA-4250 trace at T500 (indicated by the arrow)? Figure 7 shows the time fronts, the stack of five minutes of transmissions corrected for array motion, for all of the available hydrophone elements on the DVLA for T500 at a source depth of 350m (sequence M68.2). The third arrival is the second largest event on the data trace but is still weak, about 35dB down from the peak amplitude on the DVLA. It occurs 1.678sec after the PEP arrival, is barely detectable in Figure 2b, and is the same event as indicated by the arrow in Figure 6a. It clearly corresponds to waterborne energy and has the characteristics of bottom-reflected surface-reflected (BRSR) energy. It will be shown below to have consistent travel time behavior with the DSF arrivals and both this event and the DSF arrivals are BDSR energy diffracted from Seamount B. This event is only observed on the DVLA at T500 and shorter ranges where it may be confused with BRSR. Similar arrivals were not observed at longer ranges (see Appendix B).

Figure 8 shows an expanded view, from -0.5 to 2.5sec reduced time, of Figure 6 that shows i) how well the six PE arrivals, in the yellow shaded region, on the DVLA align with the DSFA

arrivals on the South OBS after a 2.08sec delay and ii) how well these arrivals on the West and East OBSs align with the South OBS with delays of 0.015 and -0.365sec respectively. The OBS arrival times used to compute the DSF arrival conversion points are based on this figure. The DVLA-4250 traces (cyan) have been delayed 2.08sec to show the remarkable agreement in arrival time between the PEP arrivals on DVLA-4250 and the DSFA arrivals on the OBSs (except for the east OBS at T2300 which has poor SNR). Arrival times are picked for six events on the south OBS as indicated by the solid black lines. The dashed black lines on the west and east traces, which align well with the arrivals, are offset by 0.015 and -0.365sec respectively from the south picks, at all ranges. All six arrivals, across four ranges from T500 to T2300, occur on the three OBSs and the deepest hydrophone on the DVLA with just the three delays given in this paragraph. The "accordian" arrival pattern across the four ranges at 4250m depth on the DVLA appears identically on the three OBSs at about 5000m depth.

Of course there is nothing special about DVLA-4250. It is just a receiver near the bottom of the sound channel. But the separation of the two arrivals on T1600 and T2300 imply that whatever is scattering the energy must be at about 4250m depth (or deeper to allow for evanescent tails, Airy phases, below the turning points) and at a similar range from the DVLA. So a tentative hypothesis is that a seamount is protruding to about 4250m depth, the usual time front pattern from whatever range (at least between 500 and 2300km) hits this seamount, is coherently scattered, and reflects off the sea surface before arriving at the receivers.

We know that all of the arrivals vary slightly in arrival time and amplitude from transmission to transmission. To get a feeling for this variability we show segments of twenty individual pulse-compressed traces over 15minutes from T500 (Figure 9). The segments correspond to the PEP arrivals (on DVLA-4250, the south OBS and the east OBS), the DSF arrivals (on the south, west and east OBSs) and the BDSR arrival (on DVLA-4250). Of the four ranges in the arrival pattern T500 is the only range where we observe BDSR on DVLA-4250. The PEP arrival on DVLA-4250 has the most repeatable waveform. The BDSR arrival on DVLA-4250 has the least repeatable waveform and is essentially undetectable on unstacked traces.

Figure 6: DSF arrivals arranged as shot gathers.

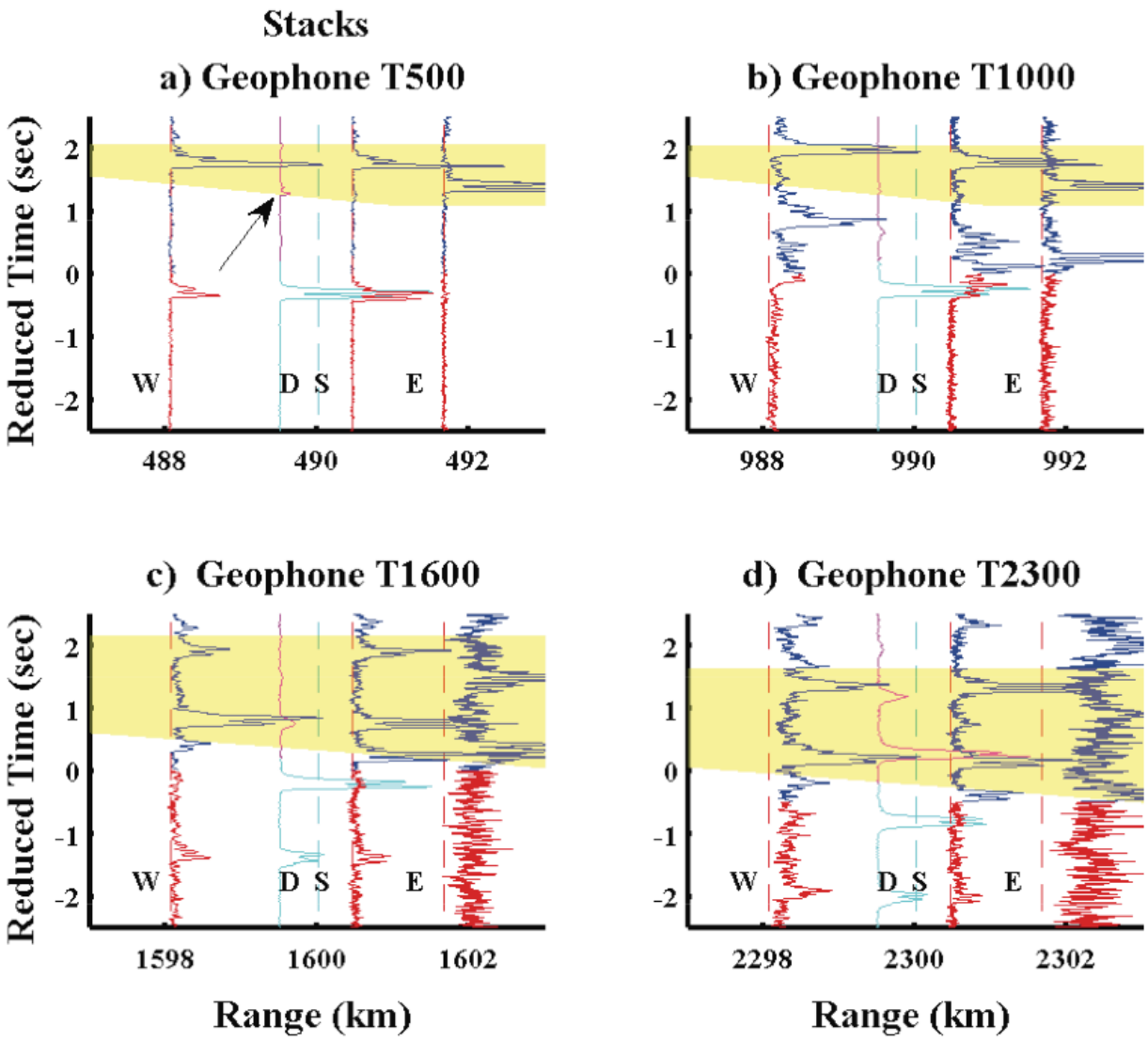

Figure 6: An expanded view of the traces in Figure 2 grouped with respect to T-station from T500 to T2300. The cyan/magenta line is the DVLA-4250 trace (D) and the red/blue lines are the OBS traces (west -W, south-S, and east-E). Red and cyan portions correspond to PEP arrival times. Blue and magenta portions correspond to later arriving energy that is not predicted by the PE solution. The yellow shading covers the corresponding region in Figure 2. The small amplitude arrival, in magenta, at about 1.2sec reduced time on the DVLA-4250 trace at T500 (arrow) will be shown below to be a BDSR arrival, the same physical event as the DSF arrivals on the blue traces highlighted in yellow. The late arrivals on the DVLA-4250 traces (magenta) at the other ranges are deep shadow zone (DSZ) arrivals. [Geo_Stacks_Fig_1_new_arrow_b.tif]

Figure 7: Data time fronts on the DVLA for T500.

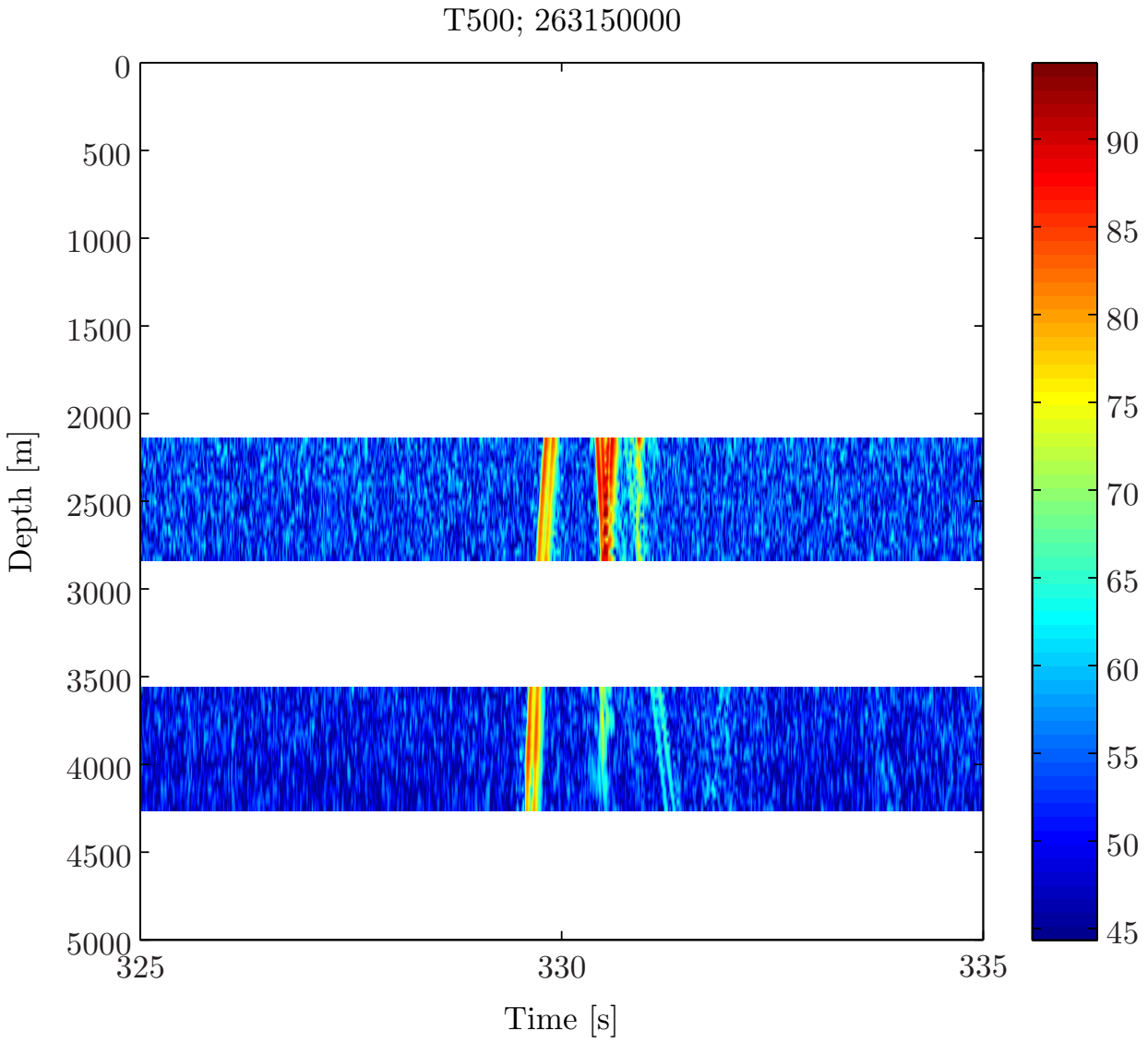

Figure 7: Time front display of the stack of five minutes of transmissions corrected for array motion, for the forty available hydrophone elements on the DVLA for T500 at a depth of 350m (sequence M68.2). The color bar is normalized to the peak amplitude on the plot and has a dynamic range of 50dB. The units are dB re: 1 microPascal. With the help of PE model results from Figure 15c, five arrivals can be observed on the bottom trace, from left to right: i) ~329.6sec - The prominent PE predicted (PEP) arrival; ii) ~330.5sec - A weak arrival corresponding to a DSZ arrival below the first turning point; iii) ~331.3sec - BDSR energy diffracted from Seamount B (see text); iv) ~331.7sec - very weak arrival, but detectable in Figure 5-19 of Stephen et al. (2008), corresponding to seafloor reflection of the BDSR arrival; and v) ~333.9sec - An extremely weak indication of energy on the lower half of the deep section of the DVLA, that appears to be a water multiple of BDSR. It corresponds to a similar, but clearer, event for the axial source at 800m depth (sequence M75)(see Figure B-5). [Figure_06_T500_68_2_Hz_350_m_addSVLA_off_LOAPEX_DVLA_processed_it_1.tif]

Figure 8: DSF arrival timing offsets.

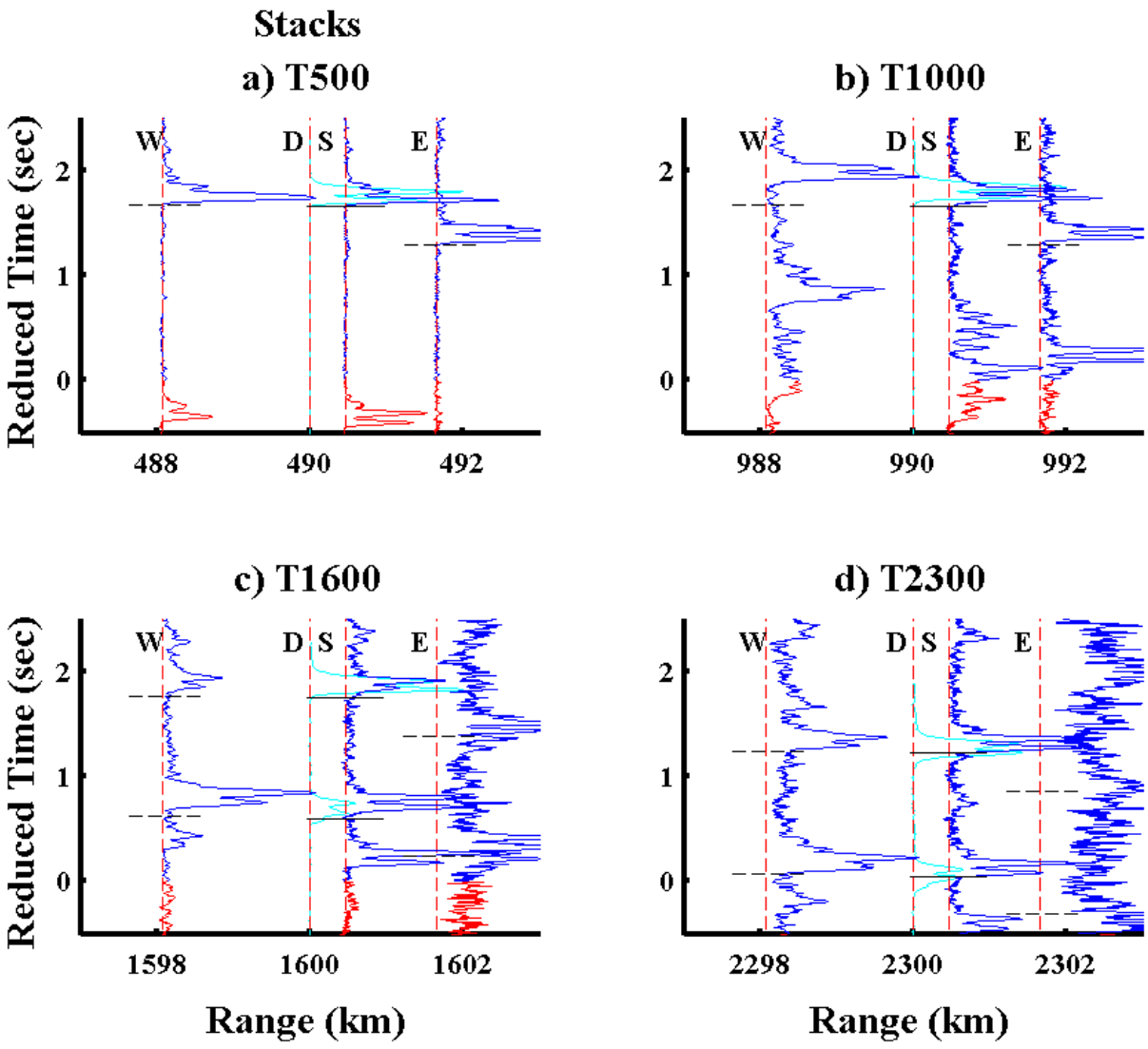

Figure 8: An expanded view of the late arrivals on the OBSs and DVLA-4250 from Figure 6 with the DVLA trace (cyan) delayed by 2.08sec at all ranges. The delayed DVLA-4250 arrivals correspond well with the arrivals on the south OBS (solid black lines). The dashed black lines on the west and east traces, which align well with the arrivals on the south OBS, are simply offset by 0.015 and -0.365sec, respectively, from the south picks at all ranges. [Geo_Stacks_Fig_2_new.tif]

Figure 9: Samples of the seven principal arrivals on unstacked traces.

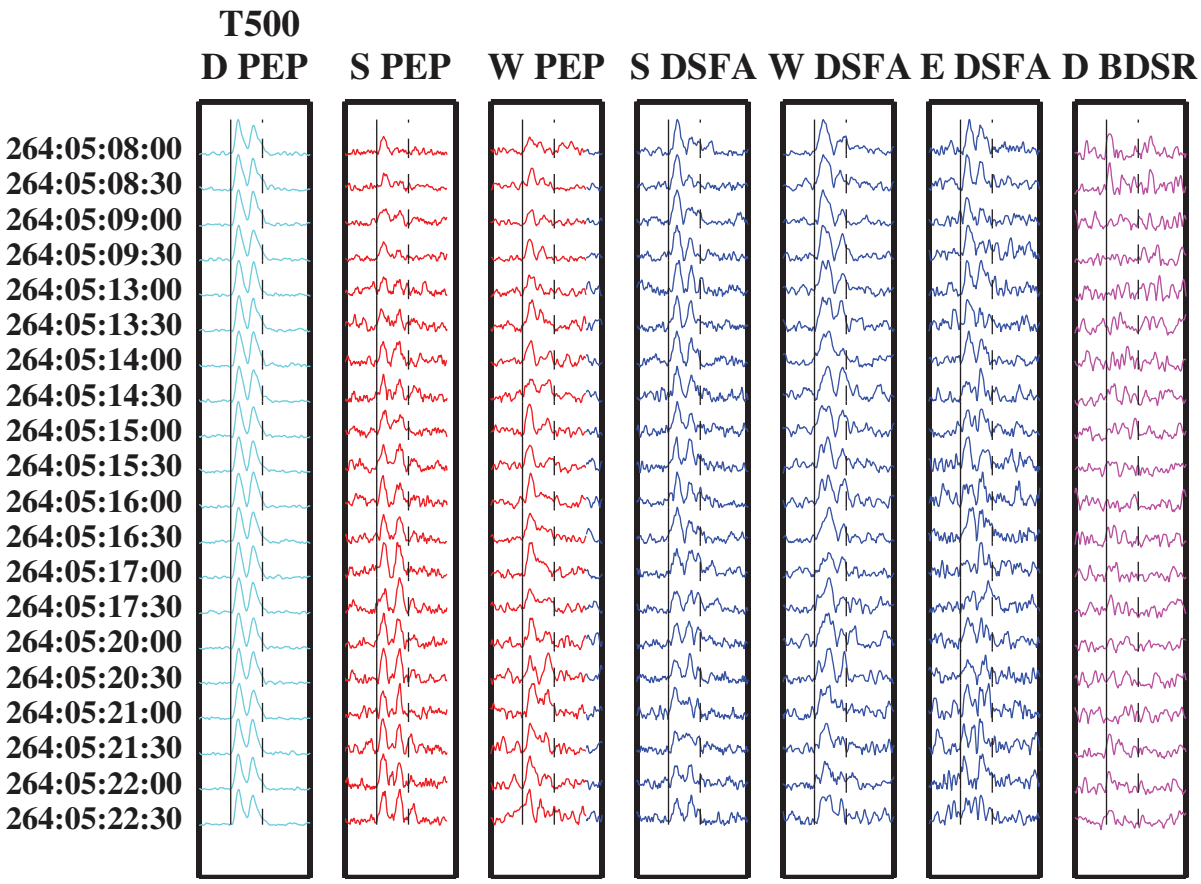

Figure 9: A sample of twenty individual pulse-compressed traces over 15minutes from T500 showing the variability of the "signals" through time. PE predicted (PEP) arrivals are shown for DVLA-4250 (D) and the south and west OBSs (S and W). Deep Seafloor (DSF) arrivals are shown for the south, west and east (S, W, and E) OBSs. The late arrival on DVLA-4250 is designated bottom-diffracted surface-reflected (BDSR) and is discussed in the text. "Signal" strength was computed as RMS levels between the vertical black lines, a width of 0.2sec. "Noise" strength was computed as RMS levels in the 0.2sec window prior to the signal. Over 400 traces like these were stacked to yield the T500 traces in Figures 2, 5, 6a and 8a and 473 transmissions were used to compute the signal and noise levels in Figure 10. [Figure_08_Geo_Traces_T500_Fig_6_020.tif]

Figure 10: Signal and noise levels of the seven principal arrivals.

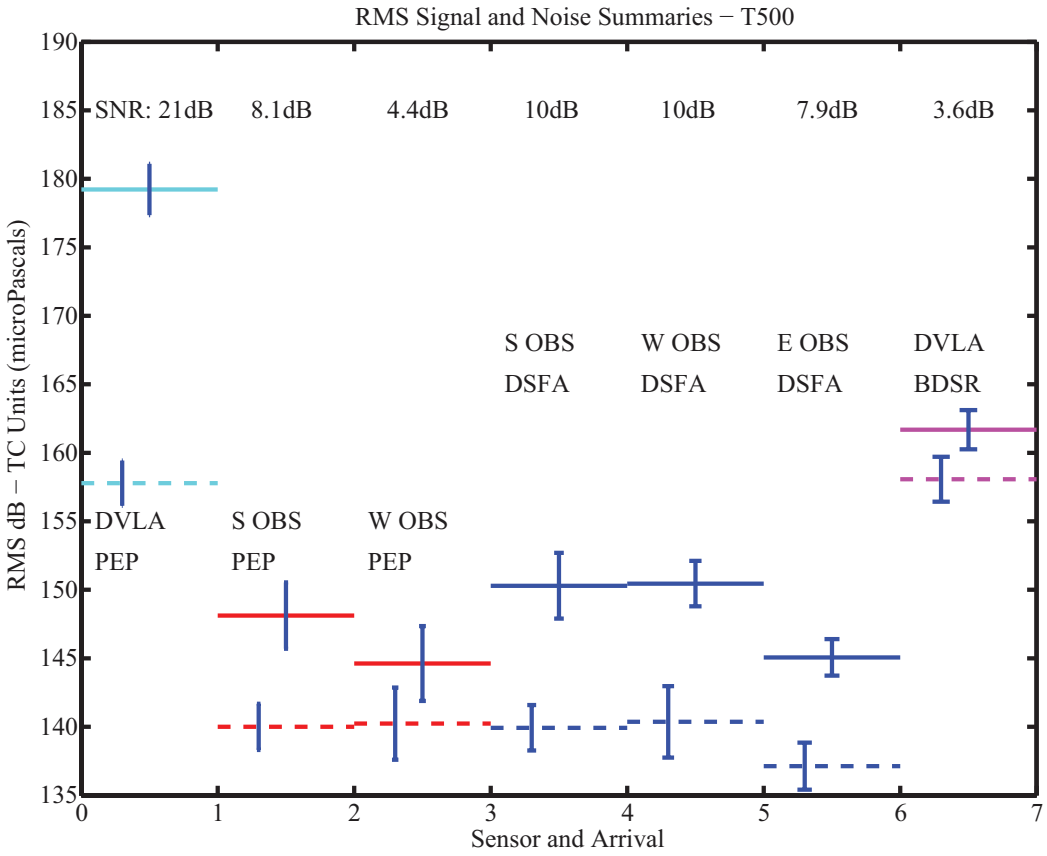

Figure 10 (Figure 6 in Stephen et al, submitted): Quantifying signal (solid lines) and noise (before the signal, dashed lines) for the seven arrivals in Figure 9. Some interesting points: a) The PE predicted (PEP) arrivals on the OBSs at 5,000m depth are over 30dB quieter than on the DVLA deepest element at 4,250m because of the evanescent decay below turning points (shadow zone arrivals (Van Uffelen *et al.*, 2009)) , b) Even though the noise on the OBSs is system noise, the ambient seafloor noise is more than 17dB quieter than at 4,250m. Ambient noise from distant sources is trapped in the sound channel above the conjugate depth (about 3,000m (Van Uffelen *et al.*, 2009)). If the sources of ambient noise were local and coming directly down from the surface one would expect noise levels at 4,250m and 5,000m to be similar. c) In an RMS sense the DSFA arrivals are the largest arrivals on the OBSs. On the east OBS the PE predicted arrival was undetectable from the ambient noise. d) From arrival time analysis the DSFAs are a delayed replica (by about 2sec) of the PE predicted arrival at 4,250m on the DVLA. The DSFA arrivals on the OBSs are 30-35dB quieter than the PE predicted arrival on the DVLA and, in fact, are even quieter, by 8 to 13dB, than the ambient noise on the DVLA. If the DSFA arrivals were propagating through the water column, perhaps on an out-of-plane bottom-diffracted-surface-reflected (BDSR) path they would not appear on single, unprocessed DVLA channels. (All signal and noise levels are RMS values in the units of the time compressed (TC) pressure time series in microPascals. For the OBSs, vertical particle motion has been converted to "pseudo-pressure" as explained in the text.) [Geo_RMS_T500_S&N_Summary_2012_Noise1_6.jpg]

As a preliminary hypothesis it appears that sound in the PE predicted 4250m time front pattern (Figure 2d) for ranges from 500 to 2300km hits a seamount that protrudes to this depth, is coherently scattered, and travels a separate path to the receivers, arriving with about a 2sec delay in reduced time. These delayed arrivals are strong on the OBSs but relatively weak on DVLA-L20-Hyd because either a) the ambient noise at the OBSs is very much quieter than at the DVLA or b) this converted energy is stronger near the seafloor.

In summary, the DSFA arrival pattern, highlighted in yellow in Figure 3, is fixed with respect to the PE predicted arrival time for all four ranges and all three OBSs. Once the clock offsets and drifts have been applied (based on aligning the PEP arrivals with the PE model waveforms, see below), the delay between the PE predicted arrivals on the DVLA and the DSFA arrivals on the south OBS is fixed at 2.08sec for all ranges from T500 to T2300. Similarly the offset of the DSFA arrivals on the east and west OBSs is fixed with respect to the DSFA arrivals on the south OBS by -0.365sec and 0.015sec, respectively. The BDSR arrival on DVLA-4250, for T500, occurs 1.678sec after the PEP arrival.

2) Ranges, Timing and Clock Drifts

The ranges, timing and clock drifts for the OBSs and DVLA-L20_Hyd on NPAL04 are summarized in Section 5g and Tables 5-1 and 5-2 of Stephen et al (2008). These values were used for the 2009 paper and Figure 3 below (Figure 2 in Stephen et al, submitted). The ranges from the T-stations to the receivers used in our analysis have not changed from the 2008 report. We do not correct for mooring motion. We use a single range value for each T-station receiver pair (Table 5-2 of the 2008 report). These ranges were used by Matt Dzieciuch for the PE models in Fall 2007, without bottom interaction, and in Spring 2008, with bottom interaction.

For time, we assumed that whoever provided the data did the best job they could to provide correct, absolute, GPS time. We made no attempt to fix absolute times but focused on getting the arrival times between the T-stations and receivers "correct". We assumed that the PE model gave the "correct" arrival time (or at least a standard reference arrival time). Then we logged the time shift necessary for each receiver to get the "first PE" arrival in the stacked data traces (same as in Figure 3) to align with the model traces. This appeared to be pretty much constant with respect to range so we expressed the "time shift" as a range independent "offset" plus a smaller "drift" that varied with T-station. These values for the four receivers (DVLA-L20_Hyd and the three OBSs) and for stations T500 to T2300 are given in Table 1 (Table 5-1 of the 2008 report).

The preliminary clock offsets and drifts that were published in the 2008 Technical Report (Table 1) were based on lining-up arrivals in the time front diagram figures (eg. Figure 5.22 in the report) which had a course time scale (10sec over 4inches). In the 2008 Technical Report and 2009 paper we obtained consistent results to a resolution of 0.20sec which was fine since we were distinguishing arrivals that were seconds apart. For the triangulation work we wanted more accurate arrival times.

In September 2009 we overlaid data with model time series and applied shifts to get the "PE arrivals" to align, but we used a finer time scale (0.5secs over 2inches) than in the earlier work. We assumed that the PE model was the "correct" time. SNR varied with range and receiver, so

the ease of lining-up arrivals varied. T250 and T500 worked pretty well, T2300 was dicey. We did this for DVLA-L20-Hyd and the geophone channels on the three working OBSs. An "offset" was chosen for each data channel, based on the high SNR T250, and then individual "drifts" were assigned for each channel at each T-station. (The drift at T250 is zero by definition.) When waveforms were dramatically different, the usual issues arose whether to pick first breaks, first peaks or best overall fit to the whole waveform. Some subjective judgment was applied but all results are plotted in Appendix A so folks can see for themselves what the fits are. When SNR is good (eg the DVLA at T500) timing is good to about 0.02sec. When arrivals can be picked poorly the timing error is about 0.05sec (eg the West OBS at T1000 to T2300). These compare with estimated errors of 0.2sec in the 2008 report and 2009 paper. Sometimes SNR was so poor on either the model or the data that no arrival could be picked (eg the DVLA at T2300, Figure A-5).

The agreement in waveform between data and the PE model can be remarkable (eg for the DVLA at T500 and T1000, Figure A-5, and the South OBS at T500. Figure A-2). On the other hand there are no observable PE arrivals at T500 or above on the East OBS (stacks or individual traces at any source depth, Figure A-3). The East OBS is the deepest at 5035m and possibly all of the PE paths are turning above it or these deep paths have either been blocked or distorted by shallower bathymetry along the geodetic. So there is no way to check the timing of the East OBS at ranges of T500 and beyond. We were able to get a good offset for the East clock from T250 and we used this value without drift for T500 through T2300.

The offsets and drifts in Table 2 were used for Figures 6 and 8. There are three take home messages from these figures: i) The distinct DSFA arrival pattern on the three OBSs is a precise delayed replica of the PEP arrival pattern on DVLA-L20-Hyd (highlighted in yellow in Figure 3). ii) The delays required to get the DSFA arrivals on the OBSs to align with the PEP arrivals on DVLA-L20-Hyd are 2.080sec, 2.095sec and 1.715sec for the South, West and East OBSs respectively. The delays are the same for all ranges from T500 to T2300. These delays are based on the T500 traces where SNR and timing are good and the resolution is typically 0.020sec. iii) Only eight numbers are necessary to give the arrival time of the six DSFAs on all three OBSs from T500 to T2300. Once the DSFA arrival times are known for the South OBS (for the six major arrivals in the yellow highlighted region, indicated by solid lines in Figure 8 and given in Table 3), the DSFA arrival times on the other two OBSs can be predicted by applying one delay each (dashed lines in Figure 8).

It appears here that the DSFA arrival is occurring first on the East OBS but this is just an artifact of displaying the data in reduced time (see Table 4). The actual unreduced DSFA times at T500, for example, for the three OBSs are 331.934, 330.338 and 332.376sec for the South, West and East OBSs, respectively.

Table 1: Summary of timing offsets and drifts - 0.20sec resolution
(from Stephen et al 2008)

	DVLA	South OBS	West OBS	East OBS
T500 - offset - drift	-0.20 -0.02	-0.05 -0.05	-0.05 0.0	0.20 -2.15
T1000 - offset - drift	-0.20 0.0	-0.05 0.0	-0.05 0.0	0.20 0.0
T1600 - offset - drift	-0.20 0.0	-0.05 0.0	-0.05 0.0	(1) (1)
T2300 - offset - drift	-0.20 0.0	-0.05 0.0	-0.05 0.0	(1) (1)

(1) The East OBS had the worst SNR on the geophone and the timing seemed flaky. Perhaps the poor SNR was a result of stacking traces with poor timing. The -2.15sec drift could have been a misidentified arrival. The West and East OBSs were not analyzed in the published work up to 2009.

Table 2: Summary of timing offsets and drifts - 0.02sec resolution
Offsets and drifts for the triangulation work (2012 submitted manuscript)

	DVLA	South OBS	West OBS	East OBS
T250 - offset	-0.220	-0.095	-0.035	-0.195
T500 - drift	0.000	-0.020	-0.015	(1)
T1000 - drift	-0.018	-0.020	0.165	(1)
T1600 - drift	0.000 (2)	0.010	0.005	(1)
T2300 - drift	0.000 (2)	0.02	0.015	(1)

(1) SNR for the PEP arrival on the East OBS was too poor to get a reliable clock offset at T500 to T2300.
(2) At T1600 and T2300 waveforms were not consistent enough on DVLA-L20-Hyd to get a good overall pick. At T1600 the first break looks good.

Table 3a: DSF arrival times and delays from Figure 8.
(all times in seconds)

Reduced arrival times on South OBS:	
T500 DSFA	1.655
T1000 DSFA	1.65
T1600 first DSFA	0.60
T1600 second DSFA	1.75
T2300 first DSFA	0.05
T2300 second DSFA	1.22
Delay times relative to South OBS:	
West OBS - DSFAs	0.015
East OBS - DSFAs	-0.365
DVLA-L20_Hyd - PEP arrivals	-2.080

Table 3b: PEP arrival times and delays from Appendix A.
(all times in seconds)

Reduced arrival times at T500	
South PEP	-0.445
West PEP	-0.400
DVLA PEP	-0.425
Delay times relative to T500:	
T1000	-0.005
T1600 (to first PEP arrival)	-1.055
T1600 (to second PEP arrival)	0.095
T2300 (to first PEP arrival)	-1.605
T2300 (to second PEP arrival)	-0.435

Table 4: Example of reduced and unreduced times for the DSFA at T500

	South OBS	West OBS	East OBS
T500 DSFA reduced arrival time (Figure 8 and Table 3)	1.655	1.670	1.290
Range from T500 to OBS	490.4640	488.0724	491.6623
Reduction time shift - range to T500 divided by 1.485km/s.	330.279	328.668	331.086
DSFA unreduced arrival time at OBS	331.934	330.338	332.376

Table 5: Summary of PEP group velocities
(All values in km/sec)

	DVLA_L20_Hyd	South OBS	West OBS	Average
T500	1.4869	1.4870	1.4868	1.4869
T1000***	1.4860	1.4860	1.4859	1.4860
T1600	1.4870	1.4871	1.4870	1.4870
T2300	1.4869	1.4870	1.4869	1.4869

*** - This slow group velocity for T1000 is based on the "observed" first PEP arrival (see Appendix A). From the PE model results for T1000 (Figure 4-2 of the 2008 Technical Report for example) the "observed" first PEP arrival clearly corresponds to the second branch of the accordion. The true first branch passes over the receivers at 4250 and ~5000m depth. A PEP group velocity of 1.4869km/sec was used for the triangulation work.

Table 6: Six seamount summary of linear regression parameters

Summary of the DSFA phase and group speeds with correlation coefficients and least square errors of the linear regression for phase speed.

All speeds in km/sec. Least square (LSQ) error in seconds.

	T500	T1000	T1600	T2300
PE Group Speed	1.4869	1.4860	1.4855	1.4858
Seamount A - LSQ error	1.2300	1.2300	1.2300	1.230
- Correlation Coeff.	0.582	0.581	0.581	0.581
- DSFA Phase Speed	1.9099	1.9124	1.9134	1.9139
- DSFA Group Speed	2.1710	2.1565	2.1510	2.1489
Seamount B - LSQ error	**0.0817**	**0.0828**	**0.0833**	**0.0835**
- Correlation Coeff.	**0.999**	**0.999**	**0.998**	**0.998**
- DSFA Phase Speed	1.6310	1.6314	1.6315	1.6316
- DSFA Group Speed	1.3186	1.3175	1.3170	1.3172
Seamount C - LSQ error	0.1930	0.1920	0.1920	0.1910
- Correlation Coeff.	0.992	0.992	0.992	0.992
- DSFA Phase Speed	1.7427	1.7429	1.7430	1.7431
- DSFA Group Speed	1.2914	1.2907	1.2904	1.2906
Seamount D - LSQ error	0.8480	0.8470	0.8460	0.8460
- Correlation Coeff.	0.829	0.829	0.829	0.830
- DSFA Phase Speed	2.0262	2.0255	2.0253	2.0252
- DSFA Group Speed	1.6812	1.6696	1.6653	1.6637
Seamount E - LSQ error	0.3150	0.3160	0.3160	0.3160
- Correlation Coeff.	0.978	0.978	0.978	0.978
- DSFA Phase Speed	1.5427	1.5433	1.5435	1.5436
- DSFA Group Speed	1.5317	1.5248	1.5222	1.5215
Seamount F - LSQ error	0.1580	0.1590	0.1590	0.1590
- Correlation Coeff.	0.995	0.995	0.994	0.994
- DSFA Phase Speed	1.5868	1.5873	1.5875	1.5876
- DSFA Group Speed	1.4946	1.4890	1.4868	1.4864

Table 7a: Example of the triangulation procedure to the three OBSs

Example of the triangulation procedure for transmission from T500 to DSFAs on the three OBSs and for a conversion point on Seamount B (Figure11, 33deg28.1'N, 137deg51.0'W) [33.468degN, 137.850degW, lat_ind = 12, lon_ind =12 in scat_range_3.mat]

	South OBS	West OBS	East OBS
DSFA unreduced arrival time to OBS (from Table 4, sec))	331.934	330.338	332.376
Range from T500 to Conversion Point (CP, km)	473.6202	473.6202	473.6202
PE group speed from T500 to DVLA used as a proxy to the CP (from Table 5, km/sec)	1.4869	1.4869	1.4869
PE arrival time to CP (sec)	318.527	318.527	318.527
Residual time (from CP to OBS)(sec)	13.407	11.811	13.849
Range from CP to OBS (km)	17.3678	14.7129	18.1149

Table 7b: Example of the triangulation procedure to DVLA-4250

Triangulation procedure for transmission from T500 to the BDSR arrival on the DVLA and for the same conversion point on Seamount B as above.

	DVLA
BDSR unreduced arrival time to DVLA (from caption to Figure 15, sec)	331.3
Range from T500 to Conversion Point (CP, km)	473.6202
PE group speed from T500 to DVLA used as a proxy to the CP (from Table 5, km/sec)	1.4869
PE arrival time to CP (sec)	318.527
Residual time (from CP to DVLA)(sec)	12.773
Range from CP to DVLA (km)	16.5146

Table 7c: Example calculation to predict the BDSR arrival times

*Example calculation to predict the BDSR arrival time at the DVLA and South OBS (Figure 15c), assuming the same conversion point on Seamount B as above.***

	T500 to DVLA Location	T500 to OBS South Locations
PEP direct to receiver (Table A-1)	329.542sec	329.834sec
PEP to Seamount Conversion Point (CP) (Table 7a and b)	318.527sec	318.527sec
Residual time of DSFA/BDSR from CP to receiver - observed	329.542+1.758*-318.527 =12.773sec	13.407sec (Table 7)
Residual range of DSFA from CP to receiver - observed	16.5146km (Table 7b)	17.3678km (Table 7a)
Ray tracing BDSR time from CP (at 4250m depth) to receiver (at actual receiver depth) - from tt_totals mat file	12.657sec	13.113sec
Predicted BDSR arrival time	331.18sec	331.64sec
DSFA arrival time	331.3sec	331.95sec

* Measured from PEP to BRSR time in Figure 15a. 329.542 + 1.758 = 331.3, the BDSR unreduced arrival time to the DVLA (from caption to Figure 15, sec)

** Better agreement can be obtained by including the BDSR arrival at the DVLA in the triangulation process as discussed in the text and Figures 18 and 19.

3) Triangulation

What process can 1) generate DSFA arrivals on the South, West and East OBSs with arrival times (in unreduced time) from T500 of 332.359, 330.763 and 332.801sec, about two seconds later than the PEP arrivals and 2) replicate the PEP arrival pattern for 4250m depth at 5000m depth? Some conversion of PEP arrivals to a slower or longer path at a point near the receivers is required and the depth of the conversion point must be near 4250m. To locate candidate conversion points we use the triangulation procedure summarized in Figure 11, Figure 12 and Table 7.

We seek a conversion point that has a depth around 4250m and yields linear travel-times across the array of three OBSs (Figure 11). We use the group speed of the PE predicted arrivals at the DVLA (Table 6) and the range from the transmission station to the scattering point (black line) to compute the time spent on the PE-predicted path to the scattering point. This time would be the same for all three OBSs. Then we plot the "residual time" for the DSFA arrival at each OBS versus the range from the scattering point to each OBS (yellow lines) to see if the travel-times to the OBSs are "consistent" for an arrival from that point (Figure 12). "Consistency" is measured by the linearity (correlation coefficient and least square error) of the travel-times across the array. The points with the largest correlation coefficient and the smallest least square error would be the most likely points for the path conversion.

Figure 11: DSFA path geometry (OBS arrivals only).

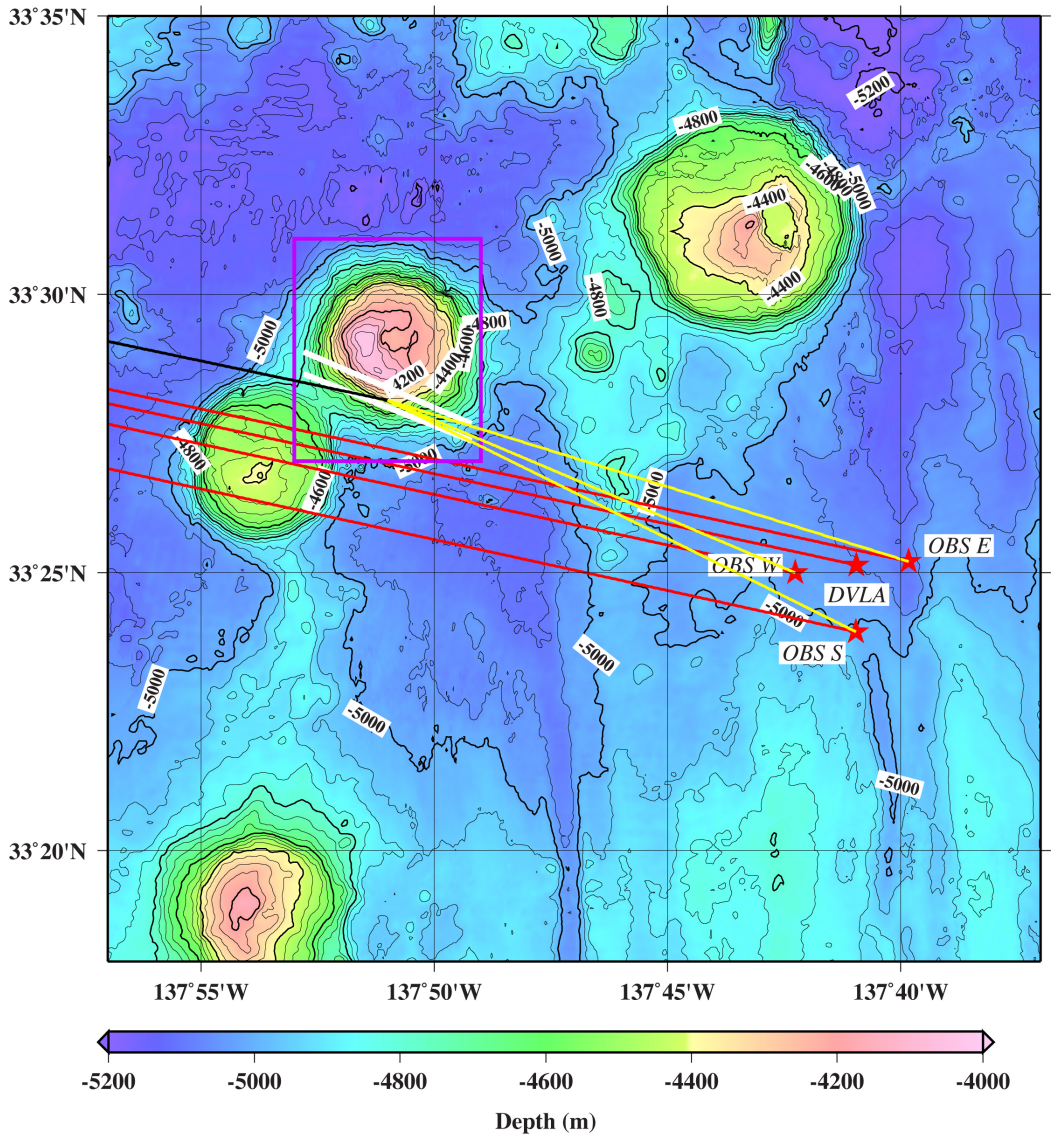

Figure 11: The locations of the three OBSs and the DVLA with their geodetic paths (red lines) to the source locations are overlain on swath map bathymetry. This bathymetry is higher resolution but is available over a much smaller area than the satellite derived bathymetry in Figure 1. The DSFA pattern on the OBSs (Figure 2) is consistent with conversion from a PE predicted path from the source to the seamount (black line) to some unknown path from the seamount to the OBSs (yellow lines) at a seamount (Seamount B in this example), probably out of the sagittal plane. Of all six seamounts in Figure 1, Seamount B gave the most linear fit of the DSFA arrival times (Table 6). A search was then carried out within the maroon box to find the points with the most linear DSFA arrival times at the OBSs. Points with a least-square fitting error of 0.02sec (the estimated travel time error) or less are bounded by the two white lines. Specific values for the conversion point shown are given in Table 7a. [VLA_region_4-2.jpg, error surfaces are generated in TT_analysis_T500_4_2012.m.]

Figure 12: Linear regression example of DSF arrivals (OBS arrivals only).

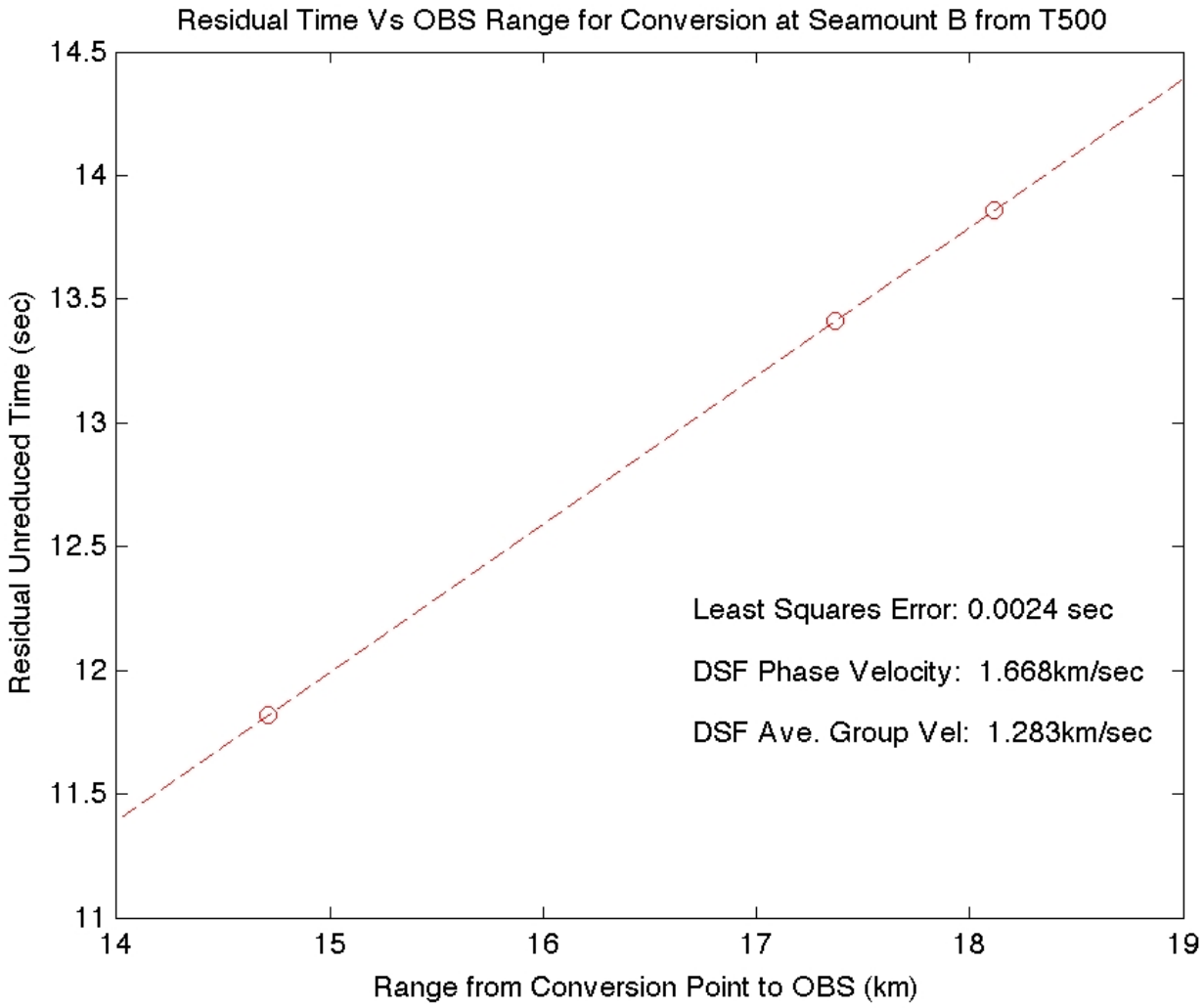

Figure 12: Example of linear regression of the points in Table 7a for a transmission from T500 to a conversion point on the side of Seamount B. "DSF Phase Speed" is the inverse slope of the line. "DSF Ave. Group Vel," is the average of the ranges to each OBS from the conversion point divided by the residual time. The conversion point used is the same as the one shown in Figure 11. Calculations like this were done over two test grids: one covering all six seamounts (Figure 13) and one covering just Seamount B (Figure 14). [TT_Analysis_2012.jpg]

This procedure was carried out for three test-point strategies. First we considered a single test point on each of the six seamounts near the NPAL04 receivers (Table 6). Seamount B had the smallest least-square error and the greatest correlation coefficient. Second we considered a grid of test points over the entire area encompassing the six seamounts (Figure 1 of Stephen et al (submitted)). This was a grid of points at 1minute intervals from 33deg15'N to 33deg45'N and 138deg 20'W to 137deg 40'W (scat_range_4 computed in obspe_RAS_Scat_4.m). Contours of the error surface are shown in Figure 13. The least square (LSQ) errors form a cone to the northwest and graze Seamount B. Third we considered a dense grid over just Seamount B (magenta box in Figure 11). This was a grid of points at 0.1minute intervals from 33deg27'N to 33deg31'N and 137deg 53'W to 137deg 49'W (scat_range_3 computed in obspe_RAS_Scat_3.m). Contours for this error surface are shown in Figure 14 and the 0.02sec error contour is overlain on the bathymetry in Figure 11. Figures 13 and 14 are the error surfaces for T500. Error surfaces for T1000, T1600 and T2300 were also generated by the same procedures and the results are similar. It is remarkable that the 0.02sec error contours graze Seamount B between the 4200 and 4400m contours, since the procedure for locating conversion points in the second and third strategies is independent of bathymetry.

Specific values for the conversion point in Figure 11 are given in Table 7a. The phase speed across the array of OBSs is 1.668km/sec and the average group speed to the three OBSs is 1.283+/- 0.033km/sec

D) Candidate Explanations for DSFAs

There are five candidate explanations for DSFAs: 1) Deep shadow zone arrivals (DSZA) which occur when acoustic energy is scattered vertically many wavelengths below a PE-predicted turning point (Dushaw *et al.*, 1999; Van Uffelen *et al.*, 2008a; Van Uffelen *et al.*, 2009; Van Uffelen *et al.*, 2006), 2) Bottom-reflected surface-reflected paths along the source-receiver geodesic (In-plane BRSR), 3) Bottom-diffracted surface-reflected paths along the source-receiver geodesic (In-plane BDSR), 4) PE-predicted propagation to a near-by out-of-plane seamount with conversion to a seafloor interface wave (Out-of-plane IW), 5) PE-predicted propagation to a near-by out-of-plane seamount with conversion to a BDSR path (Out-of-plane BDSR).

1) Deep shadow zone arrivals (DSZA)

Deep shadow zone arrivals (DSZA, (Dushaw *et al.*, 1999; Van Uffelen *et al.*, 2008a; Van Uffelen *et al.*, 2009; Van Uffelen *et al.*, 2006)) can be ruled-out as an explanation for deep seafloor arrivals by the analysis shown in Figure 1 for T1600 (Figure 4 of the 2009 paper). Although some energy arrives at the OBSs at times corresponding to caustics of the PE predicted time fronts, there are large amplitude, late arrivals that occur between caustics and even after the PE predicted coda. Similar analysis was done for T500 to T2300 with similar results and is discussed in Section 4 of Stephen et al (2008). Some arrivals tentatively identified as DSZA in the 2008 and 2009 work, could actually be DSFA. This is discussed in Section E below.

Figure 13: Least-square error surface covering all six seamounts (OBS arrivals only).

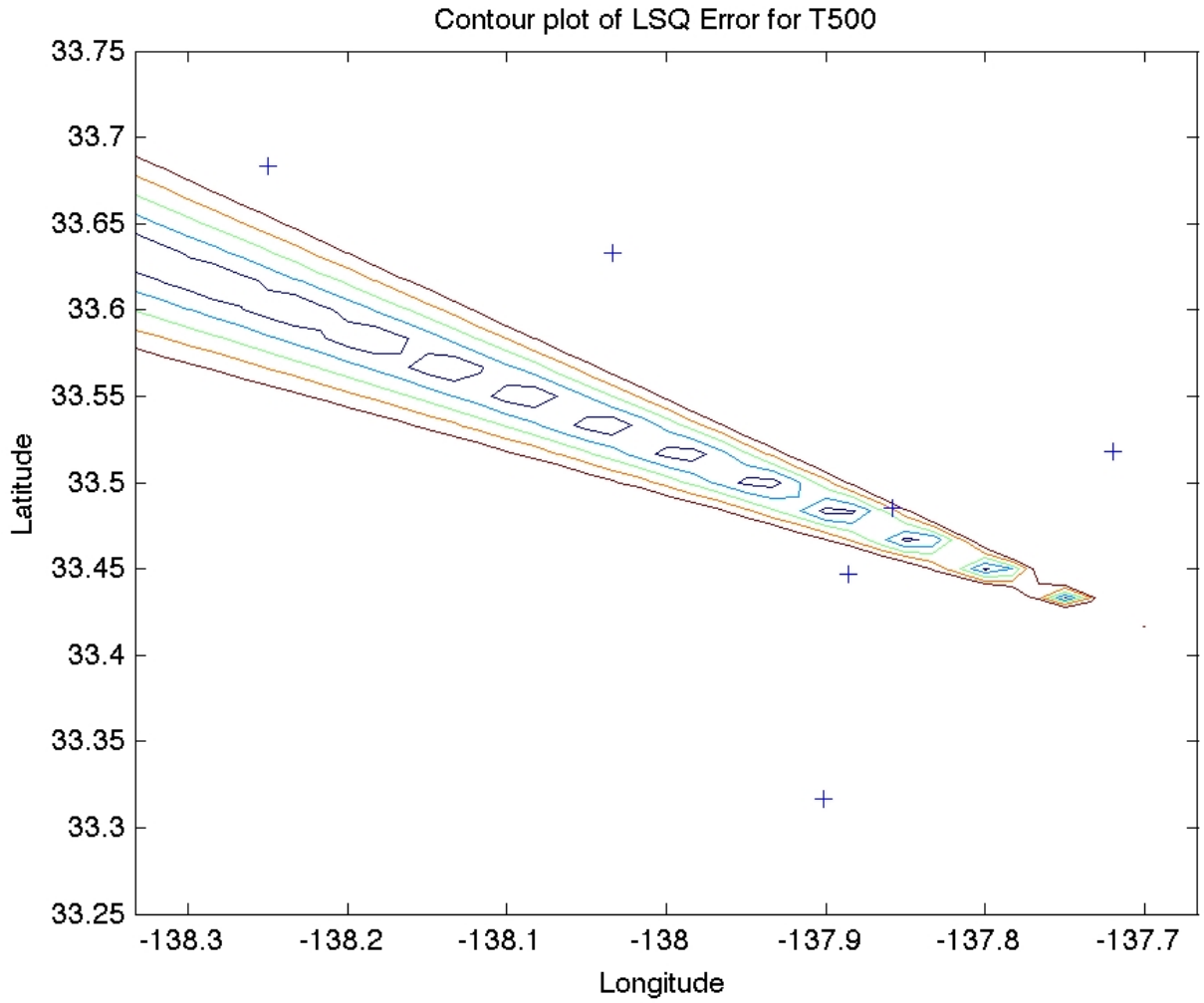

Figure 13: Contour plot of the least-square error surface over an area covering all six seamounts in the vicinity of the NPAL04 receivers. Crosses are the seamount locations (see Figure 1 of Stephen et al, submitted). Triangulation of arrivals for all four T stations indicates that the scattering is occurring at Seamount B. Triangulation only depends on T station locations (on which it is insensitive), OBS and DVLA locations, DSFA arrival times at the OBSs and PE arrival time at the DVLA. From the latter we get the PE propagation velocities for each T station which we assume is constant across the seamount area for each T-station. (PE propagation velocities to the OBSs and DVLA are consistent.) From a test location we know the range to the T-stations, the DVLA and the OBSs very accurately so with the PE propagation speed we get an arrival time from the T-station to the conversion point. This is subtracted from the DSFA arrival time. The remainder is plotted versus range from the conversion point to the receiver. The LSQ error is the error of the straight line fit to these three points (Figure 12). So the procedure does not assume a propagation mechanism from the seamount to the DVLA and OBSs. The slope of the line in Figure 12 gives the horizontal phase speed across the OBS array. The contour values are 0.02, 0.04, 0.06, 0.08 and 0.10 for blue, cyan, yellow, red and brown respectively. [SM_B_grid_2012_5.jpg]

Figure 14: Least-square error surface covering Seamount B (OBS arrivals only).

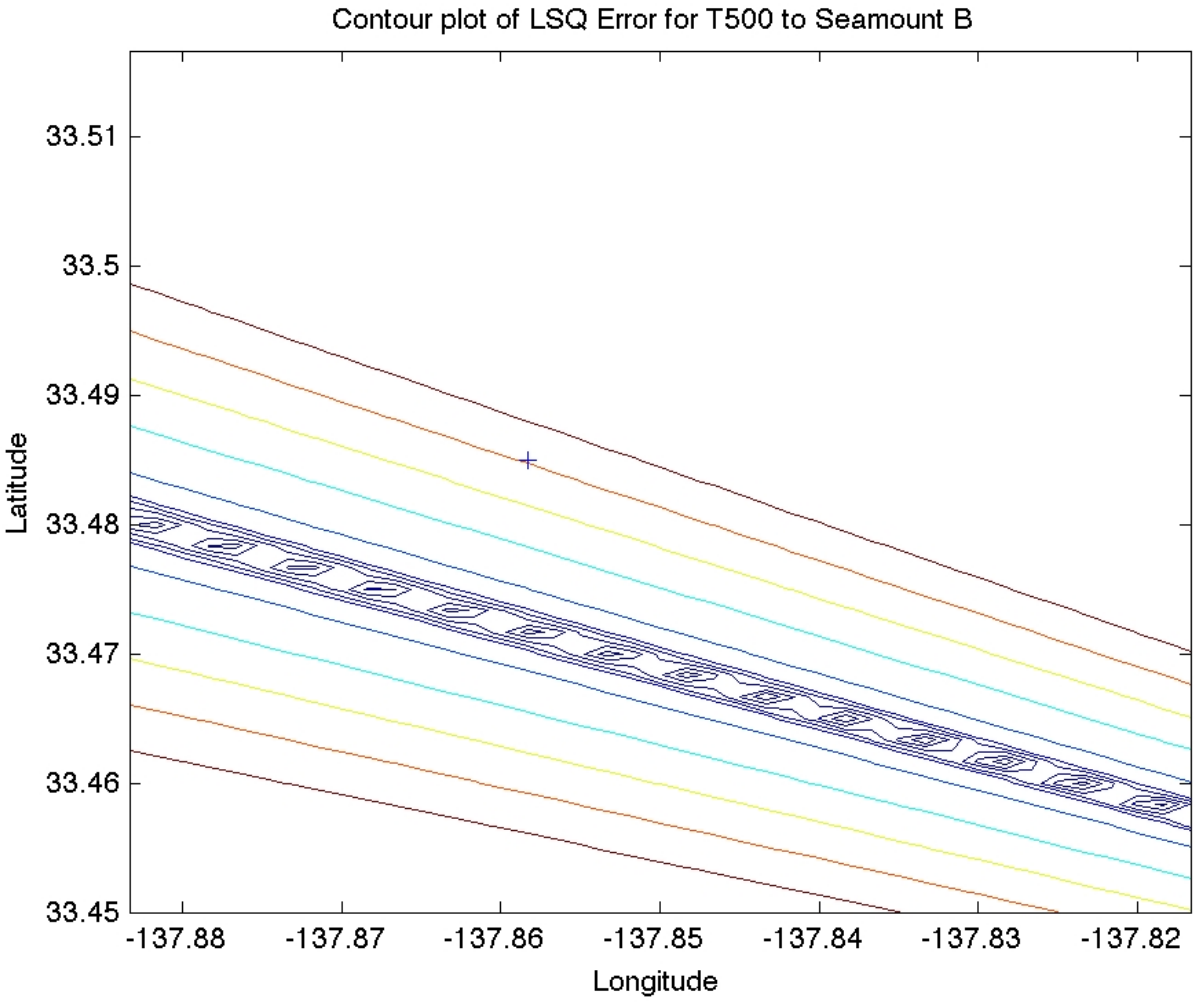

Figure 14: Same as Figure 13 for a detailed area over just Seamount B. The contour values are 0.02 and less, 0.04, 0.06, 0.08 and 0.10 for blue, cyan, yellow, red and brown respectively. The contours for 0.020sec LSQ error are overlain on the map in Figure 11. [SM_B_grid_5.jpg]

2) Bottom-reflected surface-reflected paths along the source-receiver geodesic (In-plane BRSR).

Section 5 of Stephen et al (2008) discusses the SRBR story, based on analysis of just the DVLA and South OBS data, in detail. It summarized the SRBR story as follows: " Are the 'deep seafloor arrivals' observed on the OBS SRBR? The arrival time of many [12 of 16] of the deep seafloor arrivals agrees at least approximately with SRBR. Other aspects of SRBR must be satisfied, however:
i) Deep seafloor arrivals in the OBS data are the largest events by far on the traces. They are much larger than PE predicted and deep shadow zone arrivals.
ii) So far none of the NPAL investigators has observed SRBR arrivals on the DVLA or SVLA for M68.2 LOAPEX transmissions at ranges of T500 and beyond. So for the model SRBR events to agree with the data we need to increase the magnitude of SRBR relative to PE and deep shadow zone arrivals at the seafloor while simultaneously decreasing the magnitude of SRBR relative to PE predicted at SVLA and DVLA depths (particularly above 3000m). This is a tall order.
iii) In contrast to deep shadow zone arrivals which decay in amplitude with increasing depth below turning points, the deep seafloor arrivals appear to decay with increasing height above the seafloor. It would be strange for SRBR to appear louder at the seafloor, except perhaps for up to a six dB gain that could be expected from constructive interference of incident and reflected waves.
iv) The SRBR "events" at the seafloor in the PE models are diffuse clouds of slightly stronger energy. [Time series of PE model data with bottom interaction, eg Figure 2d at 4250m depth, do not show any discrete arrivals that could correspond to SRBR paths.] The observed deep seafloor arrivals, on the other hand, are large amplitude, discrete events. In many cases the deep seafloor arrivals have the double-peak structure that is characteristic of the PE and deep shadow zone arrivals. The deep seafloor arrivals in the data are not smeared like the arrival clouds in the models."

For the long ranges considered here, the best predictor of BRSR arrival times would be the PE modeling done by Matt that included a simple bottom description and Smith and Sandwell bathymetry. Unfortunately the PE model with bottom interaction (Figure 2d and Figure 2-2 in Stephen et al (2008)) did not show any discrete arrivals that correspond to BRSR paths.

The strongest argument prior to 2009 for ruling out BRSR (and in-plane and out-of-plane BDSR) paths as an explanation for DSFAs was that no one studying the SVLA and DVLA data had identified BRSR arrivals in the VLA data. This was not entirely true. As discussed in the 2008 report Van Uffelen saw BRSR arrivals for 250Hz transmissions at T500 and (weakly) at T1000 and Udovydchenkov saw weak BRSR at T500 for 75Hz ("axial") transmissions. An open question at the time was: "Why is SRBR greater at 250Hz than at 75Hz?"

Since 2009 there have been three developments. First, Ilya published his paper on the importance of considering in-plane bottom reflections in the modal analysis of the SVLA data (Udovydchenkov *et al.*, in press).

Second, in the Spring of 2012 I did some analysis of RMS energy levels for DSFAs and PE predicted (PEP) arrivals on the three OBSs and the deepest element of the DVLA (Figure 10).

This analysis indicated i) that the DSFAs appeared loud on the OBSs because the ambient noise floor of the OBSs was almost 20dB quieter than at the deepest element on the DVLA, about 750m above the seafloor, and ii) the DSFA energy level was quieter than the ambient noise level on DVLA-L20-Hyd. On a single element basis one would not expect to see DSFAs on the DVLA elements even if they were in the water column.

Third, in August 2012 we noticed that there actually is a DSFA arrival on DVLA_L20_Hyd for T500 at ~331.3sec in Figure 15a. In a reprise of his 2008 work, Ilya has displayed the DVLA data with a high dynamic range (at least 50dB) and sees weak arrivals corresponding to BRSR or BDSR (Figure 15 and Appendix B). BRSR and BDSR arrivals are weakly indicated by linear streaks of color that are essentially in the noise (Figure 7). They would be difficult to identify solely in the time series of a single hydrophone (eg the bottom hydrophone, Figure 15a). If the arrival is seen in the PE model (Figure 15b) then it could be BRSR or possibly in-plane BDSR; if not, it could be out-of-plane BDSR. This will be discussed further under bullet 5) on out-of-plane BDSR.

3) Bottom-diffracted surface-reflected paths along the source-receiver geodesic (In-plane BDSR)

Diffractions from seafloor roughness are essentially ubiquitous in the deep ocean. Most 3.5KHz echo sounder records, for example, are just a continuous series of diffraction hyperbolae from in-plane and out-of-plane bathymetric features.

In-plane BDSR differs from BRSR in at least two ways. First, for a laterally homogeneous bathymetry or a smoothly varying bathymetry, the reflection points at the seafloor for BRSR are constrained by the source-receiver geometry. For in-plane BDSR the diffraction points can be pretty much anywhere in the sagittal plane containing the source and receiver provided that the diffracting bathymetry (eg at a seamount) is insonified by the source. Second, diffracted arrivals are typically much weaker than reflected arrivals. Stephen and Swift (1994) estimate that they are about 20 to 30dB weaker based on numerical simulations. If one thinks about diffraction as a secondary scattering from a point heterogeneity the transmission loss from the secondary point starts out as spherical (proportional to 1/r^2) compared to cylindrical for long range propagation (proportional to 1/r).

To check for in-line diffraction points, we looked at the locus of scattering locations that would result in a two second delay at the DVLA (Figure 16). This would be credible if you had no confidence at all in the different DSFA arrival times at the OBSs. You only believe that something is coming in 2.08 seconds late and you assume that the path to the diffraction point is traversed at the PEP group speed (1.4869km/sec). Assume that the conversion process is occurring in-line with the geodetic to the DVLA and that the 2.08sec delay (which is near the DVLA location) is due solely to a reduced propagation speed from the diffractor to the DVLA location, the "last leg" speed (Figure 16b). Conversion to really slow shear velocities typical of soft sediments (0.6km/sec or less) would require conversion within the OBS array and can be disregarded immediately. Conversion at Seamount C, which might be reasonable since its peak is above 4400m, would require a "last leg" speed of about 1.3km/sec. This is consistent with the

group speed for the point on Seamount B, determined by triangulation (Section C.3. above), of 1.283+/- 0.033km/sec. At the moment, we rule out In-plane BDSR as a DSFA mechanism because we believe the DSFA arrival times are accurate and that the triangulation procedure is valid.

Figure 15: Detailed analysis of the arrivals from T500 to the DVLA.

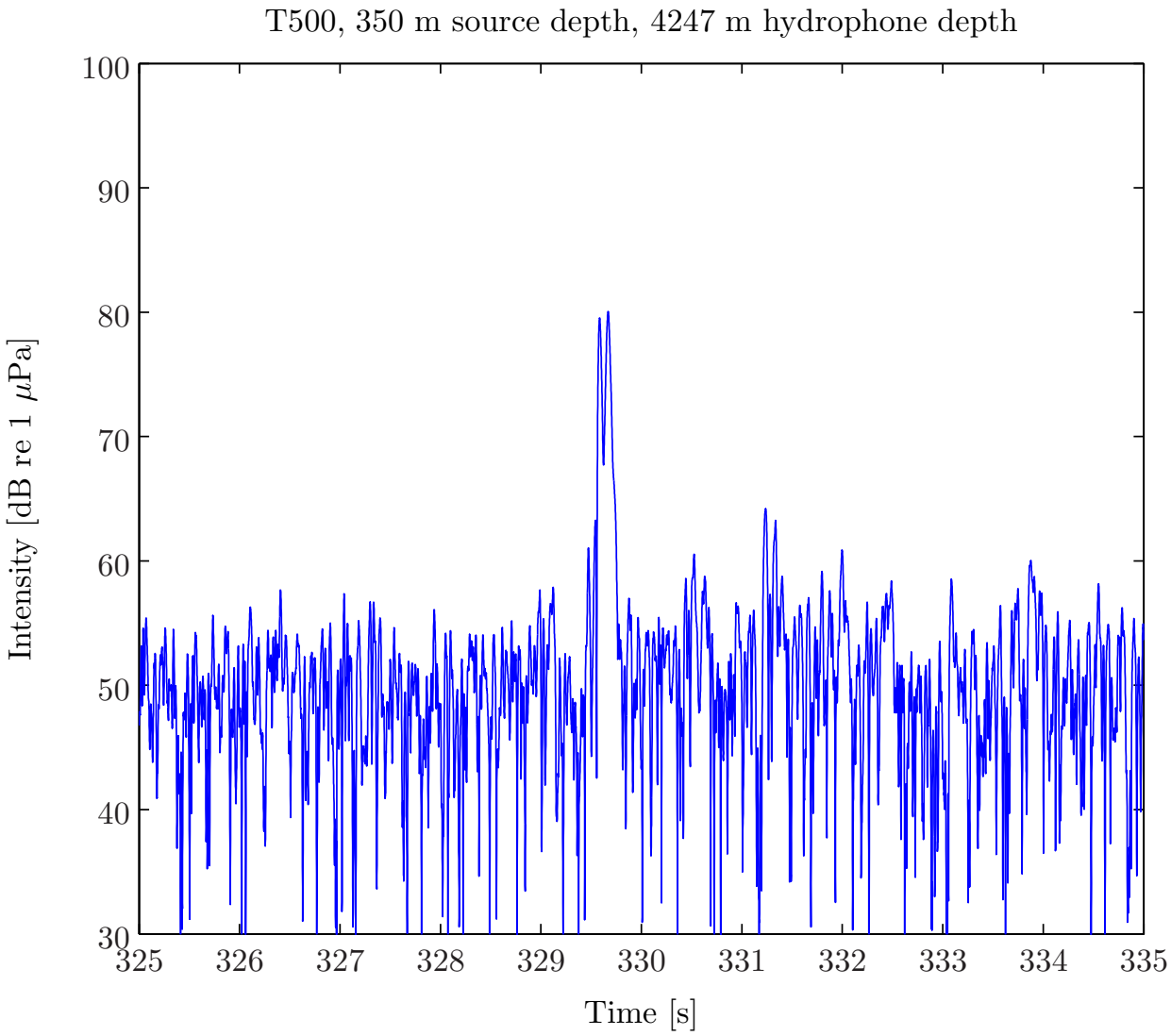

15a) [fig3a_T500_DVLA_H40.pdf]

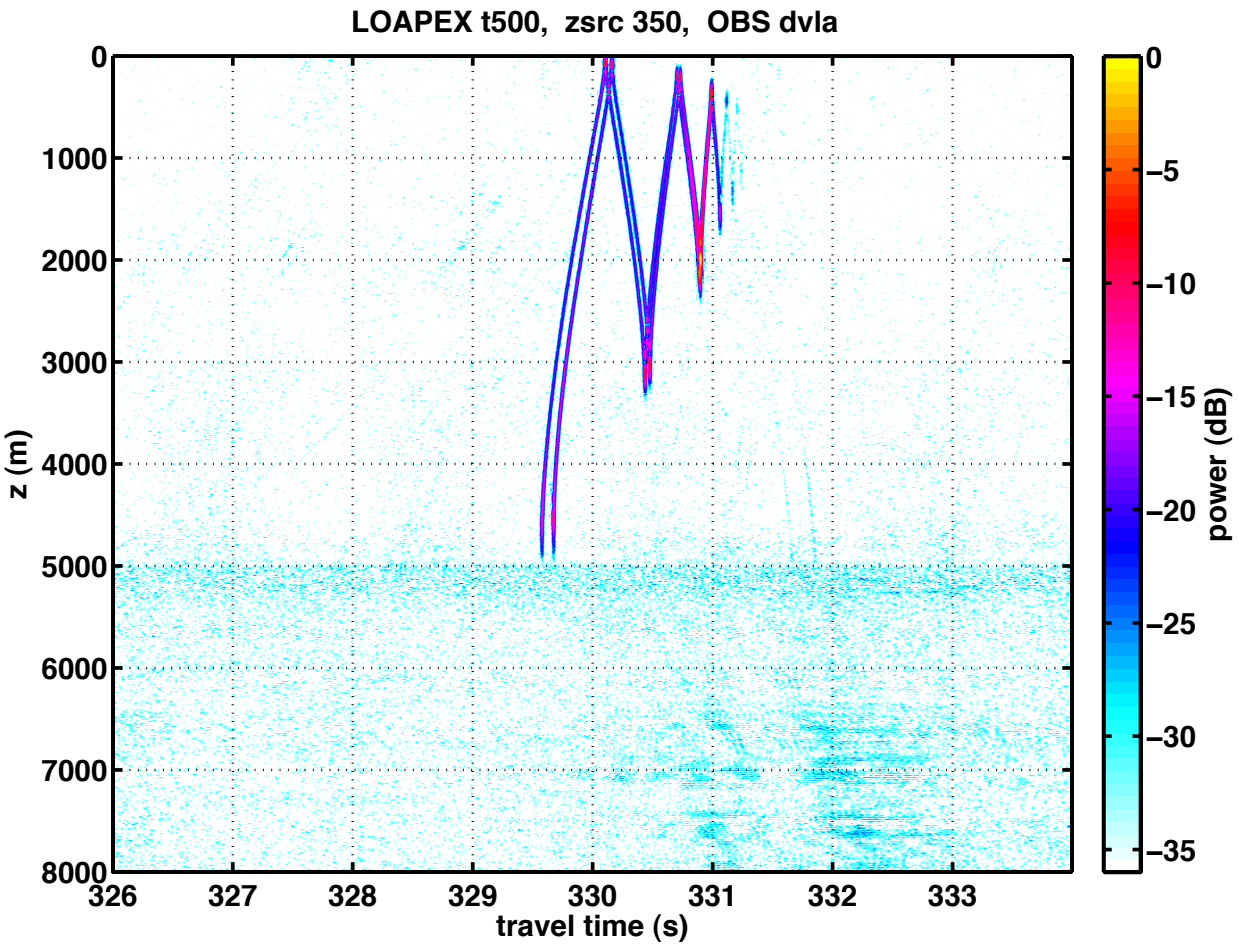

15b) [obstf.t500.z350.dvla.pdf]

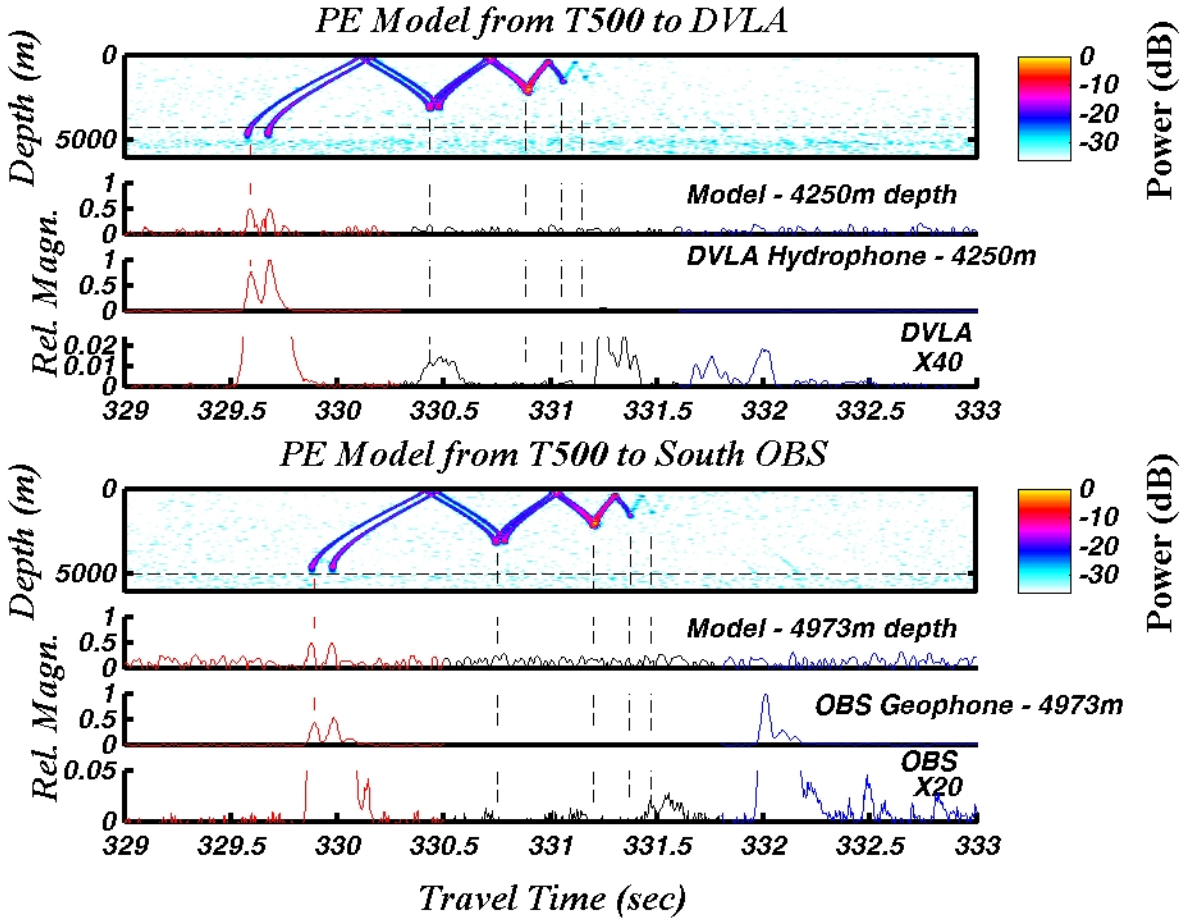

15c) Figure 5-19 from Stephen et al (2008).

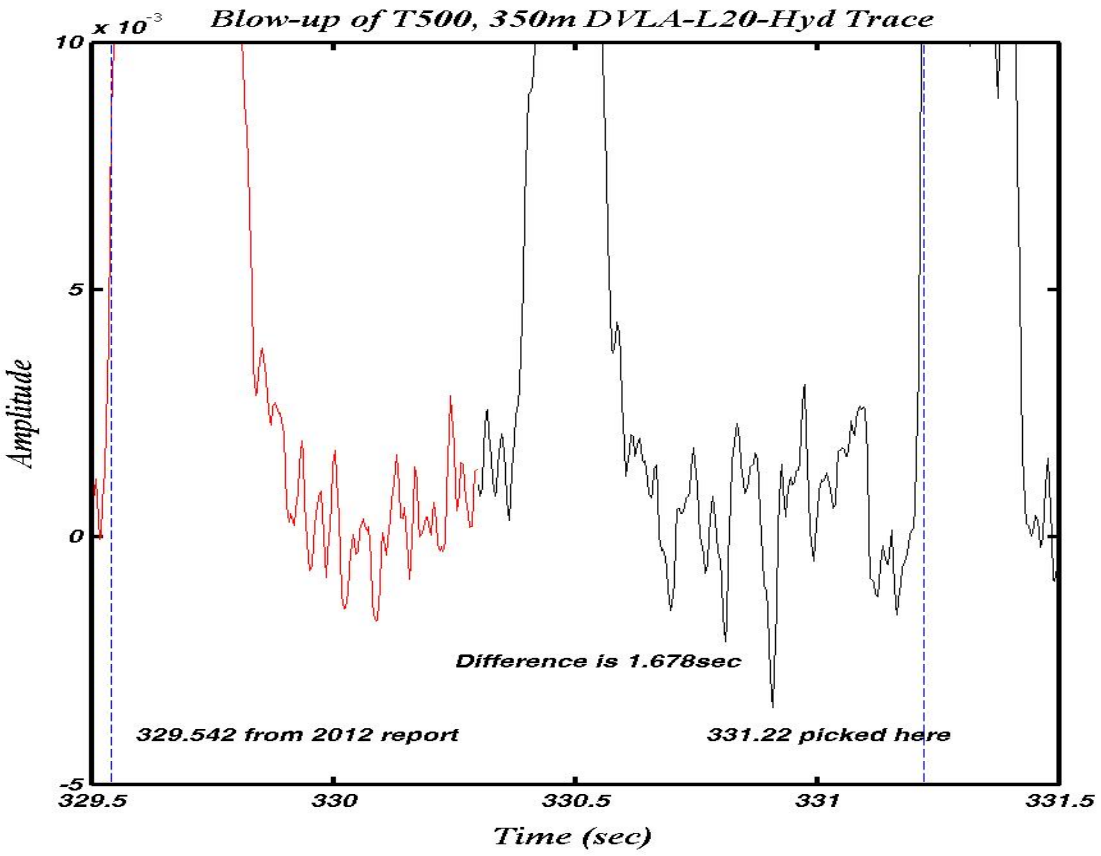

15d) [Fig_4c-500_Detail.j

Figure 15: a) Time series for the bottom element in Figure 7. b) The PE model results from Matt for the DVLA. c) Model-data comparisons from T500 to the DVLA and South OBS from Stephen et al (2008). The time series (a) is similar to the T500 DVLA trace in Figure 2c. [The trace here is the stack of 5minutes of data correcting for array motion; the trace in Fig 2c is the stack of all available data without correcting for array motion.] d) Blow-up of the trace in a), showing the time separation between the PEP arrival and the BDSR arrival. This time is used in the triangulation procedure.

Four arrivals in the DVLA time series can be identified, with the help of the full array display and the model: i) ~329.6sec - The prominent PE predicted (PEP) arrival; ii) ~330.5sec - A weak arrival corresponding to a DSZA below the first turning point; iii) ~331.3sec - The second largest event on the data trace but still weak, about 30dB down from the peak amplitude on the DVLA. It occurs ~1.7sec after the PEP arrival, is barely detectable in Fig 2c, and is the same event as indicated by the arrow in Figure 6a. It clearly corresponds to waterborne energy and has the characteristics of bottom-reflected surface-reflected (BRSR) energy. It will be shown below to have consistent travel time behavior with DSFAs and is BDSR energy diffracted from Seamount B. iv) ~331.7sec - very weak arrival, but detectable in Figure 5-19 of Stephen et al (2008), corresponding to seafloor reflection of the BDSR arrival. There is a fifth arrival at ~333.9sec which is an extremely weak indication of energy on the lower half of the deep section of the DVLA. It appears to be a water multiple of BDSR. It corresponds to a similar, but clearer, event for the axial source at 800m depth (sequence M75, Figure B-5).

Figure 16: Hypothetical in-plane and out-of-plane diffraction points.

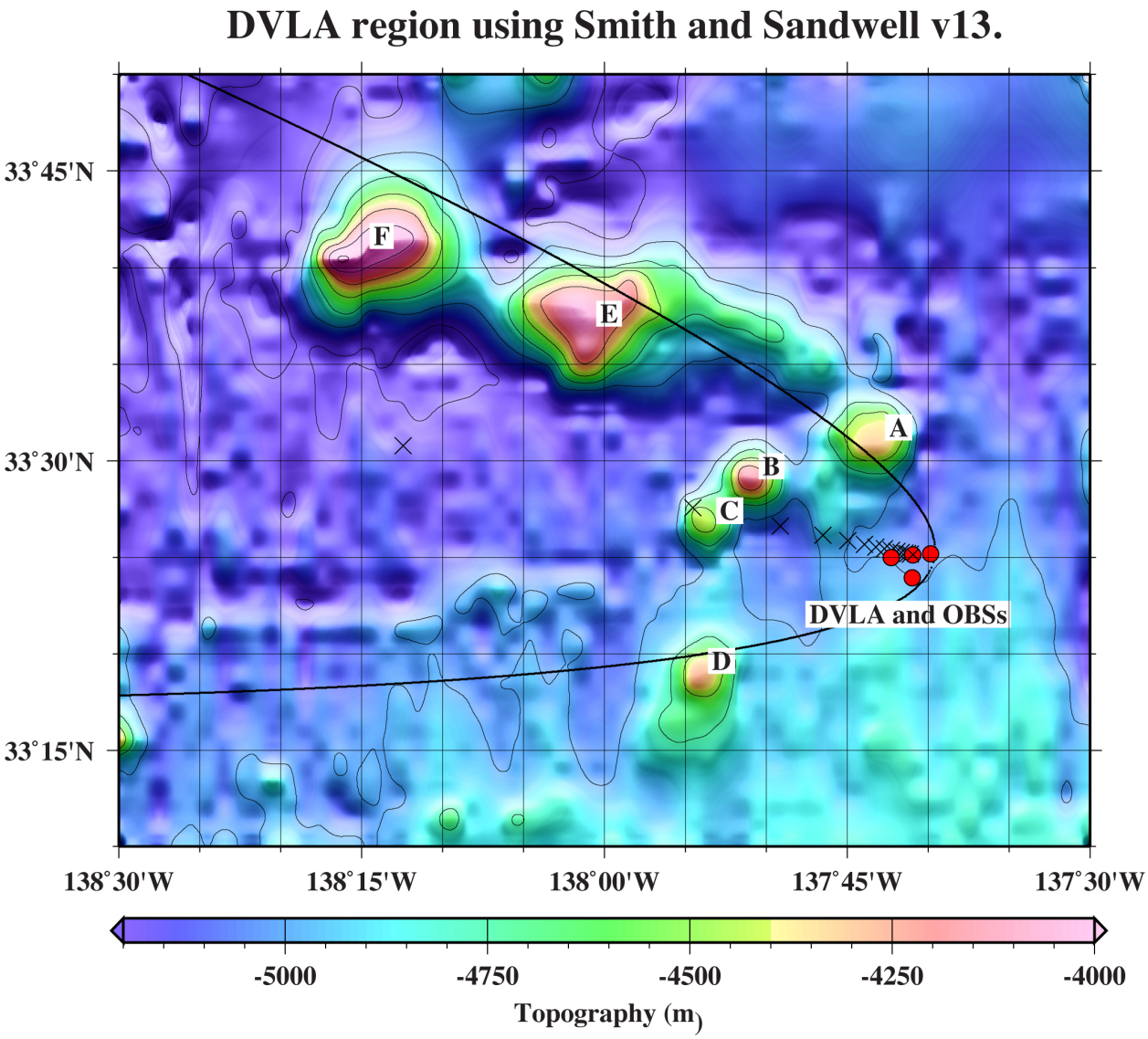

16a) [DVLA_seamounts_region_Bounces]

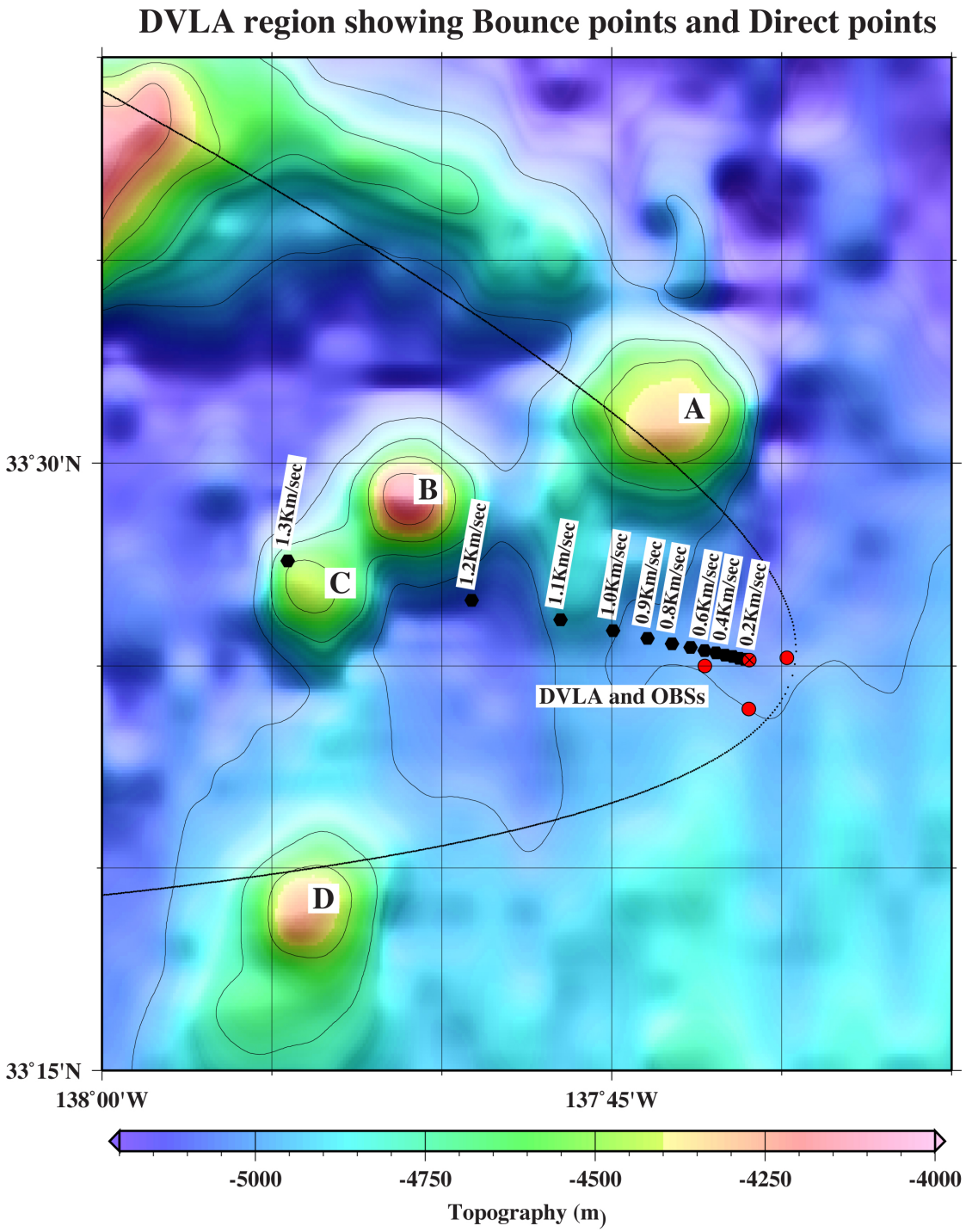

16b) [DVLA_seamounts_region_Refracts]

Figure 16: Locations of in-plane diffraction points (crosses and filled circles) at various "last-leg" group velocities and the locus of out-of-plane diffraction points (ellipse) for a "last-leg" group speed of 1.540km/sec. The ellipse and diffraction points are the same in the two figures. They are just plotted at different scales.

In section 5) below we discuss in detail the BDSR mechanism for out-of-plane diffractors. "RMS Offset" is a measure of how closely the BDSR ray tracing predictions come to matching the observed arrival time residuals. Figure 20 shows the RMS offset map for a large area covering all six seamounts in the vicinity of the DVLA for diffractor depths of 4250 and 4400m. Plus marks indicate the locations of the six seamounts and the box is the detailed area over just Seamount B. Seamount C, just to the southeast of the box, has an RMS offset of 0.6sec. [These values are slightly dependent on scatterer depth.] Much lower values of RMS offset, around 0.1sec, are found along the geodesics further to the east of Seamount C where the water depth is 5,000m or so, too deep to be a valid conversion point. Similar RMS offset values are also observed in the southeast corner of the box, on the flanks of Seamount B where water depth is about 4400m. [The estimated error of the arrival time picks was 0.02sec.] We rule out In-plane BDSR as a DSFA mechanism and discuss Out-of-plane BDSR in Section 5.

4) PE-predicted propagation to a near-by out-of-plane seamount with conversion to a direct bottom diffracted path (Out-of-plane BD).

To check for direct diffractions from out-of-plane points, we did a similar analysis to 3) above, assuming that the path to the Seamount is traversed at the PEP group speed (1.4869km/sec) and that the DSFA path is traversed at a typical sediment or lower ocean compressional speed (1.540km/sec) (ie. a direct diffraction from the top of the seamount) and requiring the event to come late by 2.08 seconds. This mechanism also requires that you ignore the different DSFA arrival times at the OBSs. The resulting ellipse is shown in Figure 16. Interestingly the loci pass over seamounts A, D and E. So sound could hit any point under this ellipse and the diffractions could travel directly, more or less horizontally, at the deep water sound speed, to the receivers.

In Section 5 we show that late arrivals are observed on the DVLA and that these are consistent with Out-of-plane BDSRs. These arrivals have moveout along the DVLA, they are not hitting the DVLA broadside. We conclude that DSFAs are not direct diffractions from any of the six seamounts.

5) PE-predicted propagation to a near-by out-of-plane seamount with conversion to a BDSR path (Out-of-plane BDSR).

BDSR is a mechanism that requires serious consideration. This path consists of a segment from the T-station to a seamount, that protrudes to about 4250m depth, at the PEP group speed (1.4869km/sec). The diffracted energy from the seamount is reflected from the surface and back down to the OBSs. (The direct diffracted path was ruled out as a mechanism in bullet 4) above, because it was not consistent with the observed DSFA arrival times at the OBSs. Bathymetric profiles across the seamounts, which may pertain to this argument are given in Appendix C.) One caveat of this hypothesis is that the observed late arrivals on the DVLA arrays (Appendix B) may not be strictly in-plane BRSR, as commonly assumed, but are in fact out-of-plane BDSR. [A check with PE modeling, which addresses in-plane BRSR only, would be good here.]

In a first quick-look phase, we considered BDSR paths from all six seamounts assuming that the diffraction occurred from the shallowest point of the seamount (Appendix C) and that the OBSs were at a depth of 5,000m. Seamount B came the closest to matching arrival times with an offset

of 0.249sec (Figure C-5). Changing the scatterer depth (or the receiver depth by say 375m could delay the predicted offsets for Seamount B enough to get good agreement. The observed phase velocities across the OBS array (1.631km/sec (crude) or 1.6484 km/sec (accurate)) could not be matched for Seamount B ranges by varying the scatterer depth from 3,640m to 4,400m depth (Figure C-6). The residual times and ranges for the "crude" calculation (Figure C-4 for example) assume that the scattering point is at a point on each seamount that was picked by hand (../NPAL_09/Geometry/scat_range computed in obspe_RAS_Scat.m). The "accurate" phase velocity was based on a point in the finer grid (scat_range_3) but I am not sure which one (this should be checked). Note that for the conversion point on the side of Seamount B used in the sample calculation above the DSFA phase velocity was 1.668km/sec (Figure 12), which is still not well matched by the ray tracing results in Figures C-5 and C-6.

At the end of this first phase, it was concluded that a scatterer on Seamount B could achieve a reasonable fit (in time) to the residual times and ranges based on the BDSR hypothesis, but that the slope of the arrival time curve, the phase velocity across the array, could not be matched.

The second phase started in August 2012, when we noticed that at least one late arrival on DVLA-L20-Hyd could be related to the DSFAs on the OBSs. We started with Figure 15 which shows DVLA and OBS-South model and observed data for the 350m source at T500. Three arrivals are evident on the lower element of the DVLA (Figures 7 and 15a). In Ilya's time the arrivals at the bottom element (DVLA-L20_Hyd) are occurring near 329.6sec (PEP), 330.5sec (DSZA) and 331.3sec. [These arrivals are also seen in the DVLA x40 trace in Figure 15c. This trace is the stack of all available transmissions, but Ilya's trace is the stack of just 5minutes of transmissions.] The third arrival is the second largest event on the data trace and is clearly a full water column arrival (ie. BRSR or BDSR) since it corresponds to a line of arrivals in Figure 7. There is an extremely weak indication of the reflection of this energy from the seafloor (see Figure B-6). We will show that this arrival on DVLA-L20-Hyd is a DSFA just like the DSFA near 332sec at T500 on the South OBS (Figure 15c, and near 2sec reduced time on Figure 2a). We will also show that this DVLA-L20-Hyd arrival and all the arrivals highlighted in yellow in Figure 3 are BDSR arrivals from Seamount B. [This is event i) in Section 5e) of Stephen et al (2008). Note that the event at 332sec on the DVLAx40 trace in Figure 15c) is not observed on the time series in Figure 15a).]

Could the late (BDSR) arrival on the DVLA be the same as the DSFA arrivals, highlighted in yellow, on the OBSs? Table 7b summarizes the computation of the residual time and range for the BDSR arrival on the DVLA as if the BDSR was diffracted from the same conversion point (CP) as the DSFAs in Figure 11. This point is added to the DSFA arrival time plot in Figure 17. The BDSR arrival occurs slightly earlier than predicted for DSFAs, most likely because DVLA-L20-Hyd is shallower than the OBSs by about 750m.

Figure 17: Linear regression example of DSF arrivals (OBS and BDSR arrivals).

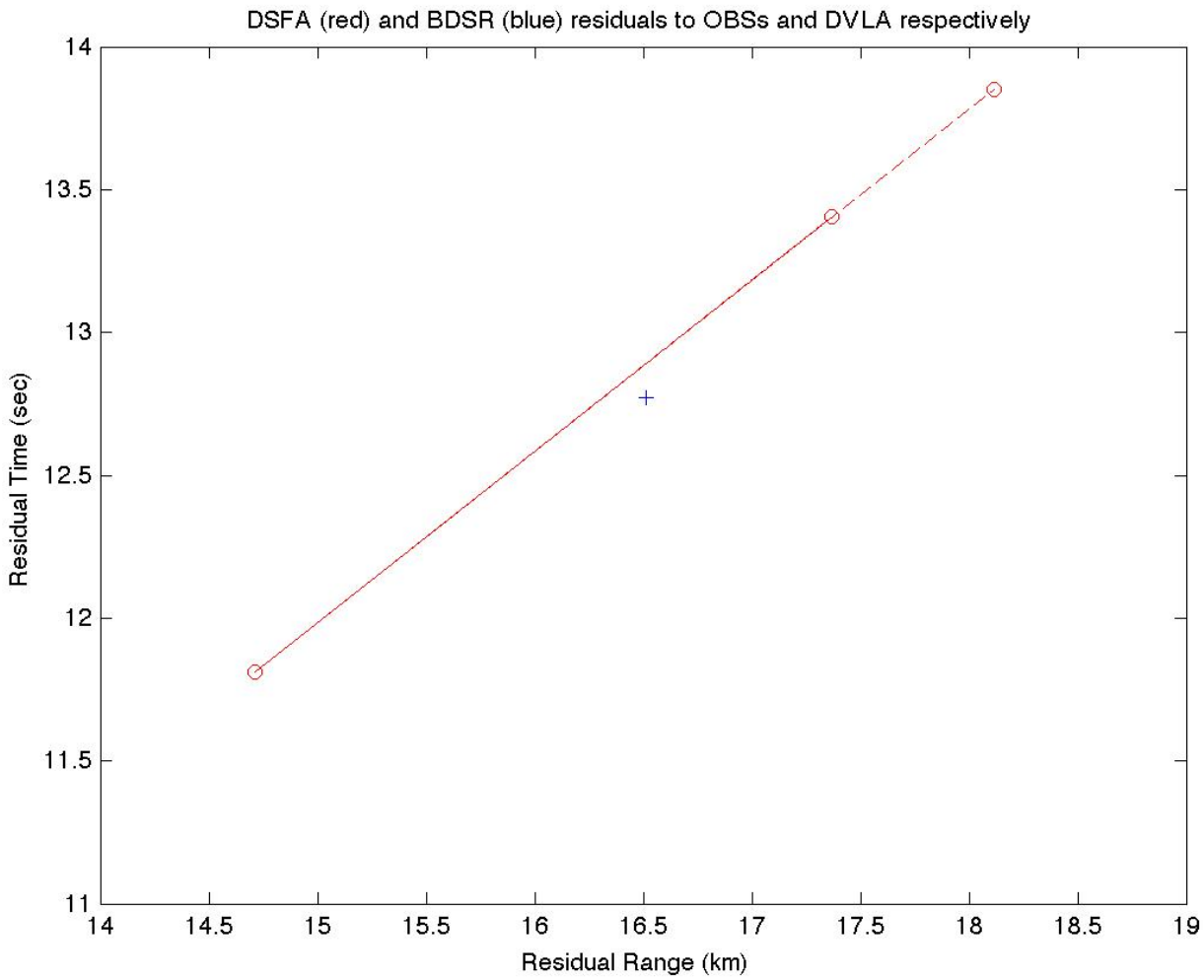

Figure 17: As Figure 12 but with the BDSR arrival at the DVLA added. It appears that DSFAs and BDSR arrivals are the same thing. The BDSR arrival occurs earlier than predicted because the DVLA element is shallower (~4250m versus ~5000m). Receiver depth was not considered in calculating this figure.

In a third phase, we included the DVLA arrival in the triangulation procedure (Section C-3) under the assumption that it was following a BDSR path and obtained acceptable results. As earlier we did not consider the depth of the CP in computing the T-station to CP time but, unlike earlier, we did consider the depths of the CP point and receivers in computing the travel-time curve for the CP to receiver path (Figure 18). We used these depth dependent travel-time curves for two things: a) first we used these curves to determine a "correction" to the observed arrival times (for the three OBSs and DVLA-L20_Hyd) to reduce them to a common datum, chosen as the depth of the West OBS (4,997m). b) In working with and displaying the ray-traced travel-times we chose a range of source (CP) depths from 4200- 4450m to the depth of the West receiver. The resulting travel-times are summarized in Figure 19. Goodness of fit was determined three ways: a) the RMS offset of the ray-traced arrival time from the observed arrival time at the four receiver ranges, b) the phase speed (inverse slope) difference between the observed and modeled linear fits, and c) the least-square error of the linear fit to the observed arrival times (as was done for the triangulation procedure in Section C-3).

The error surface for the RMS offset on the one-minute grid covering all six seamounts is shown in Figure 20. A box has been drawn around Seamount B indicating the location of the detailed 0.1minute grid. Plus signs indicate the location of the six seamounts. The values are computed for a CP depth of 4400m but much of the area of the least values has water depths much greater than this, and can be excluded from consideration. (Similar plots were made for CP depths from 4200 to 4450m and the contours did not change much.)

The RMS offset error surface for the 0.1minute grid surrounding Seamount B is given in Figure 21. Figure 22 shows the 0.1sec RMS offset contour overlain on the 4200 and 4300m isobaths for Seamount B. The points with the least RMS offset are located over water depths exceeding 4400 and are ruled out because the DSFA arrival pattern corresponds to conversion at a water depth around 4250m. Also shown on Figure 22 are the LSQ Error contours for 0.05sec and the phase speed difference contours for 2%. No single point meets all four criteria. We chose two points as compromises between RMS offset, phase speed difference, lsq fit and water depth. The locations and error values for these points, test points # 1 and #2, are given in Figure 19 assuming a 4250m source depth.

Figure 23 is a revised version of Figure 11, showing the PEP and BDSR trajectories for test point #1 based on including the DVLA arrival in the triangulation analysis. The error surfaces above were computed for a conversion depth of 4250m In future work it may be worthwhile to compute error surfaces using the actual depths at the test locations on Seamount B. Figure 24 shows a bathymetry map of Seamount B for the area of the 0.1minute grid. This map was generated from an interpolated bathymetry data base with values at every 0.1minute interval in latitude and longitude.

Figure 18: Example of a) ray tracing diagram and b) travel-time curve.

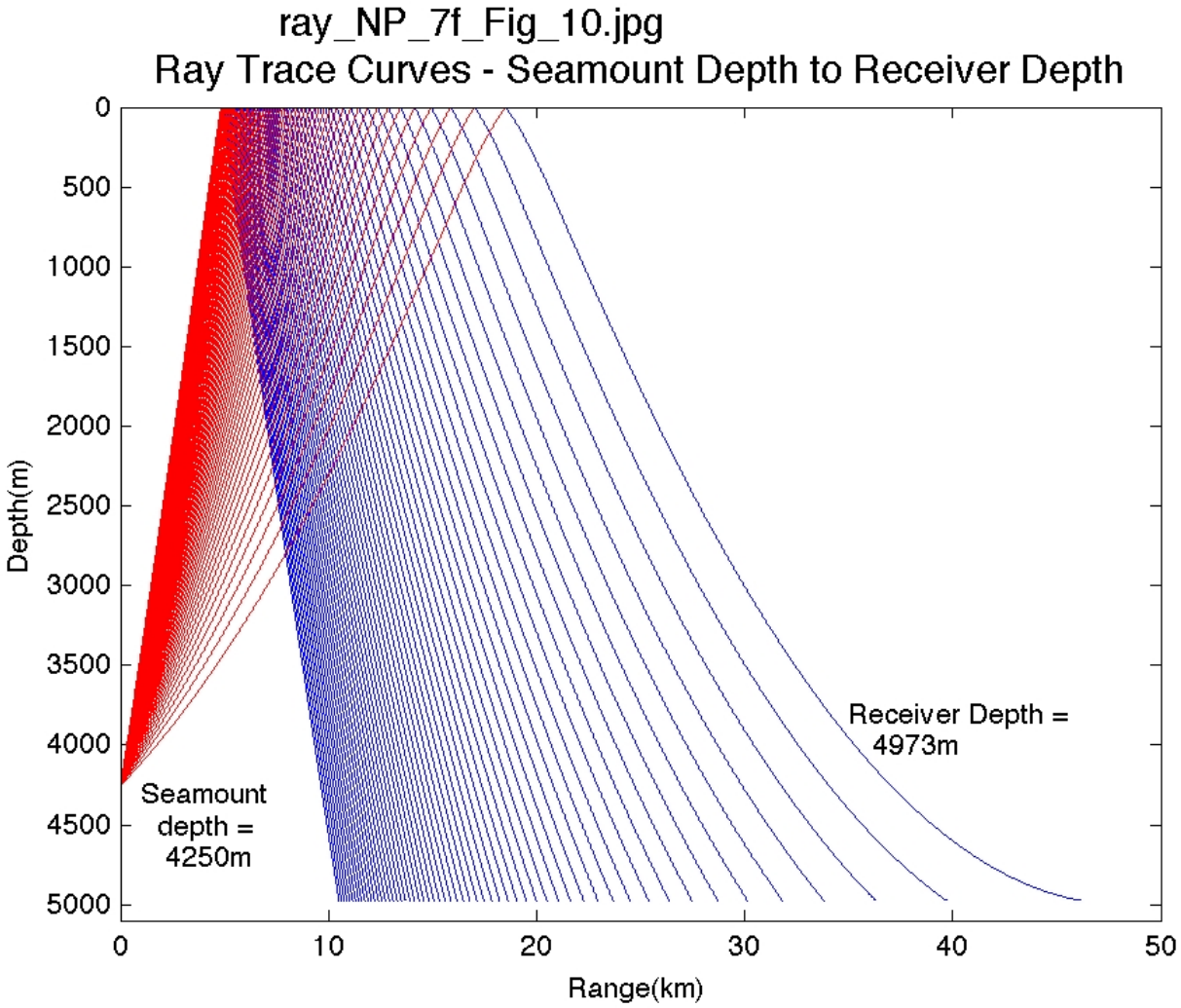

Figure 18a:

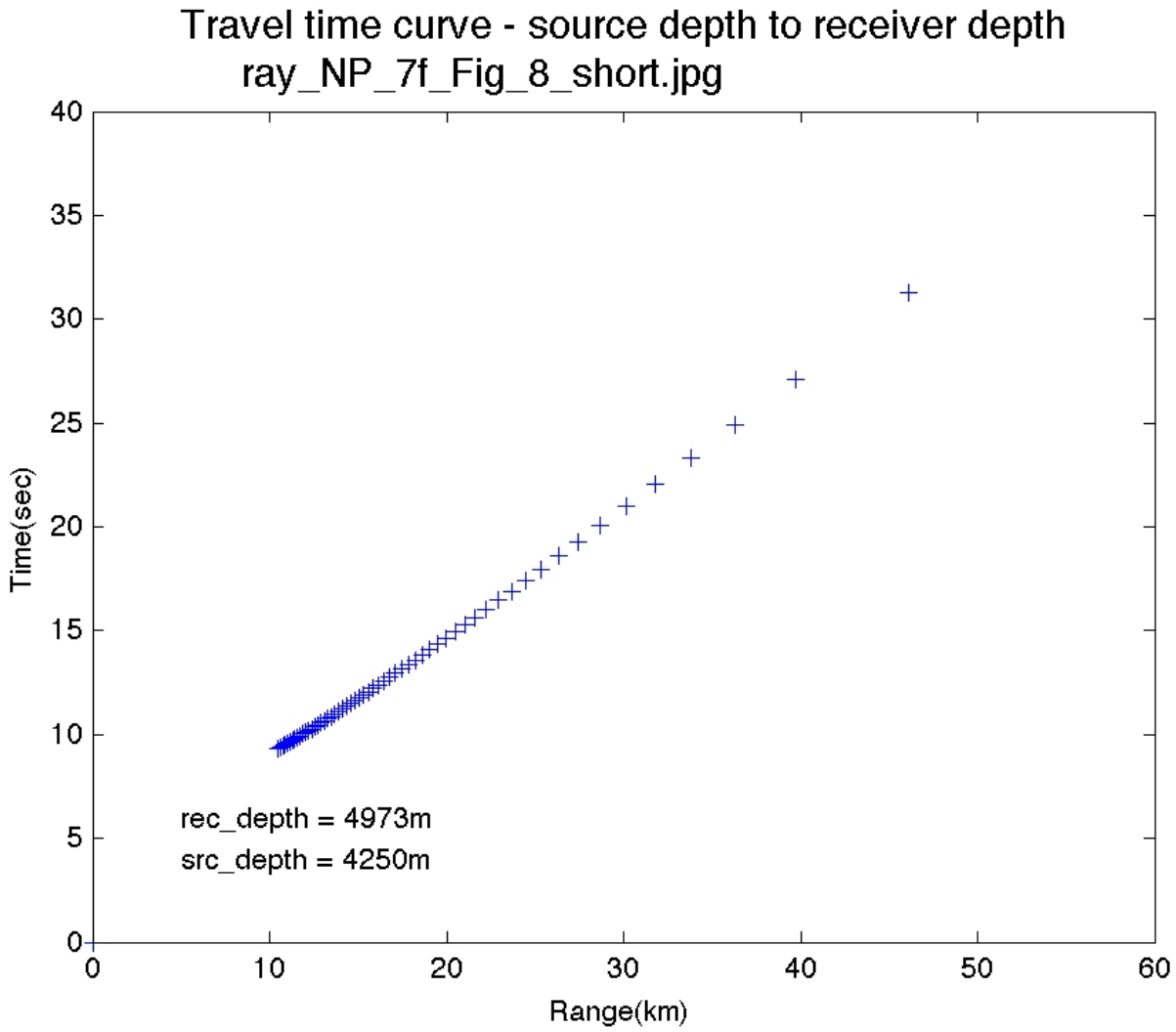

Figure 18b:

Figure 18: Example of ray tracing diagram and travel-time curve for a conversion point depth of 4250m and a receiver depth of 4973m.

Figure 19a: Data-model comparison for Text Point #1.

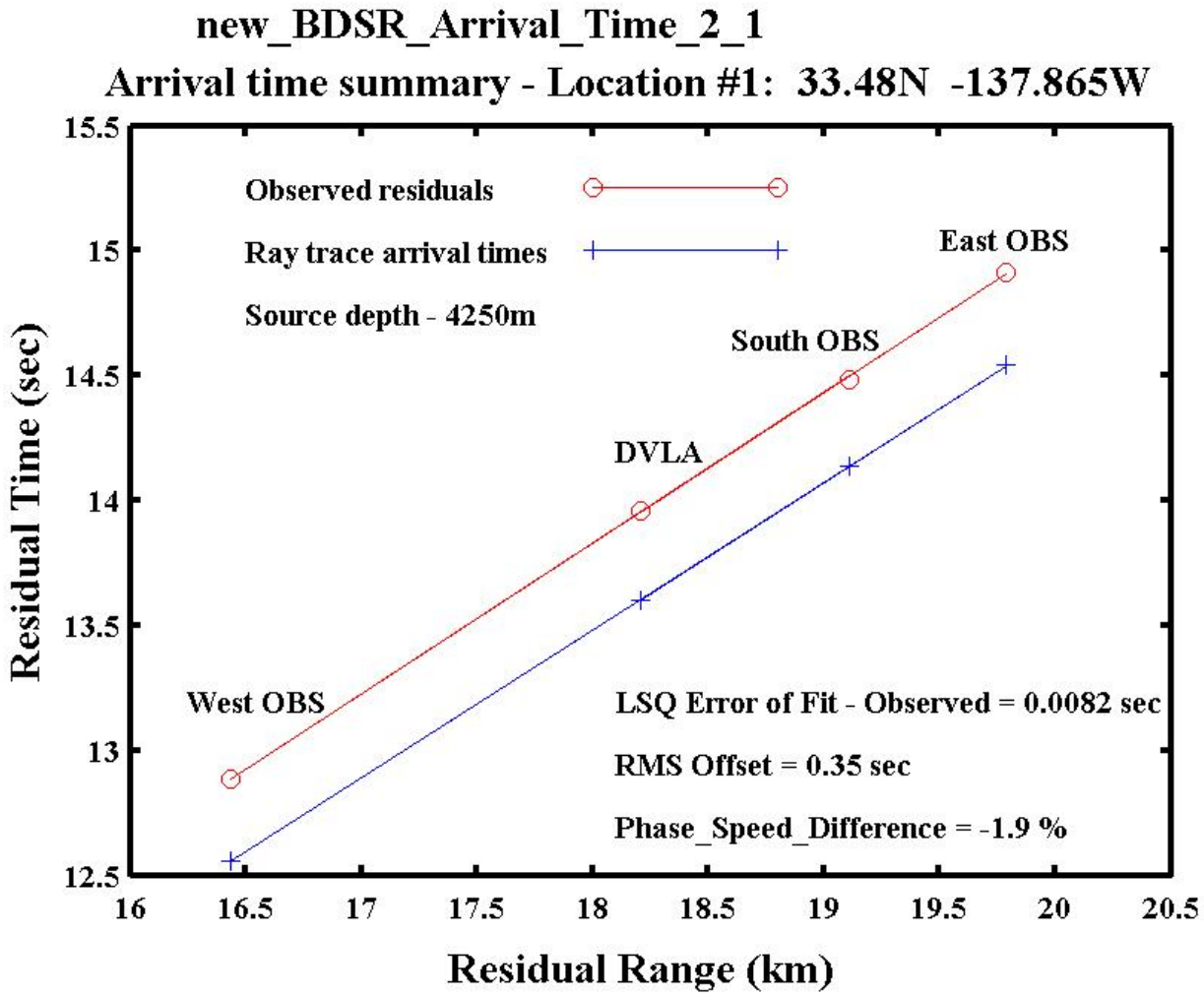

Figure 19a: Example of arrival time data-model comparison for PEP to BDSR conversion at Test Point #1 (see Figure 22) on the south-east slope of Seamount B. Goodness of fit was determined three ways: a) the RMS offset of the ray-traced arrival time from the observed arrival time at the four receiver ranges, b) the phase speed (inverse slope) difference between the observed and modeled linear fits, and c) the least-square error of the linear fit to the observed arrival times (as was done for the triangulation procedure in Section C-3). [new_BDSR_Arrival_Time_2_1.jpg]

Figure 19b: Data-model comparison for Text Point #2.

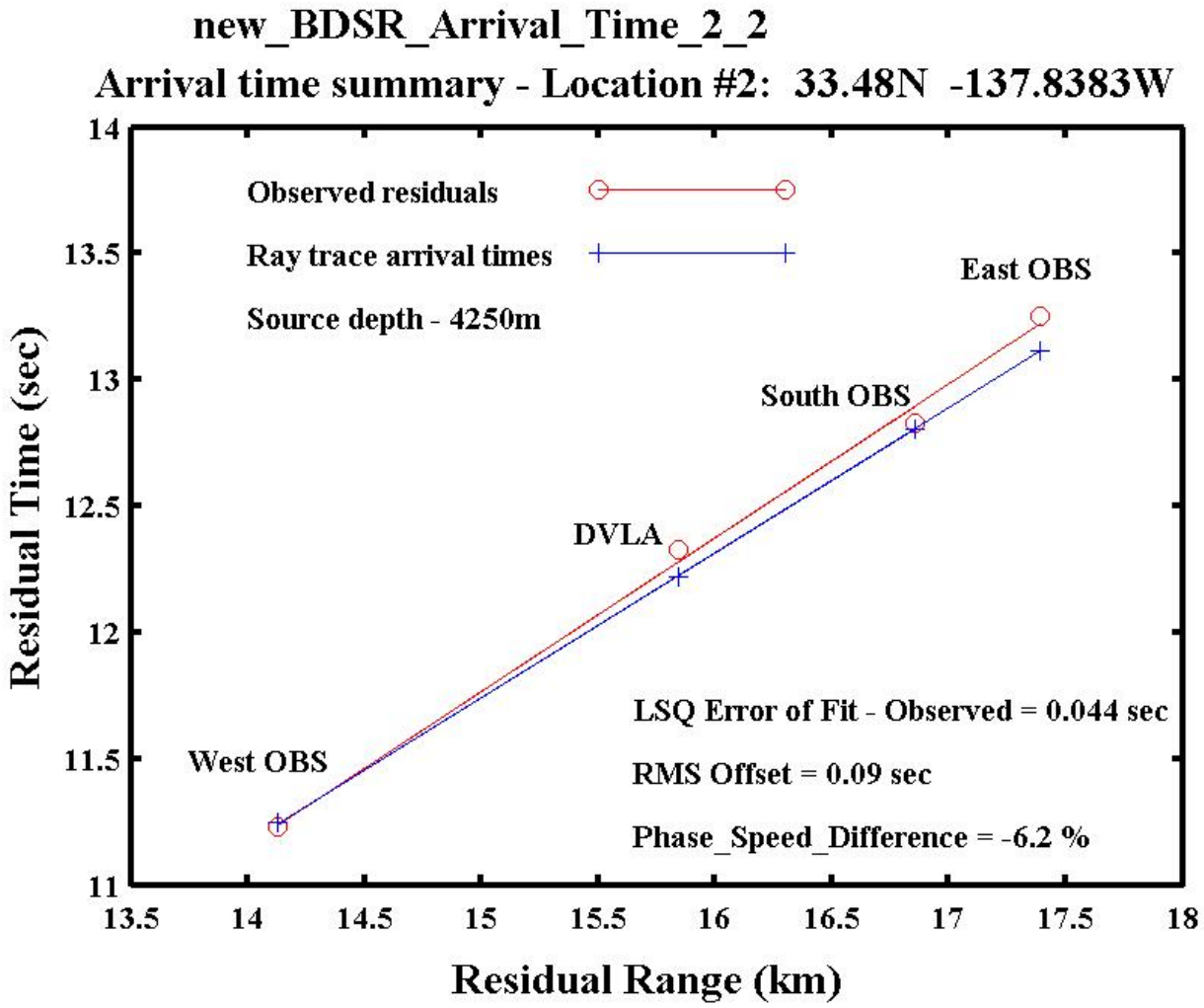

Figure 19b: As Figure 19a, for PEP to BDSR conversion at Test Point #2, on the south-west slope of Seamount B. [new_BDSR_Arrival_Time_2_2.jpg]

Figure 20: Error surfaces covering all six seamounts (OBS and BDSR arrivals).

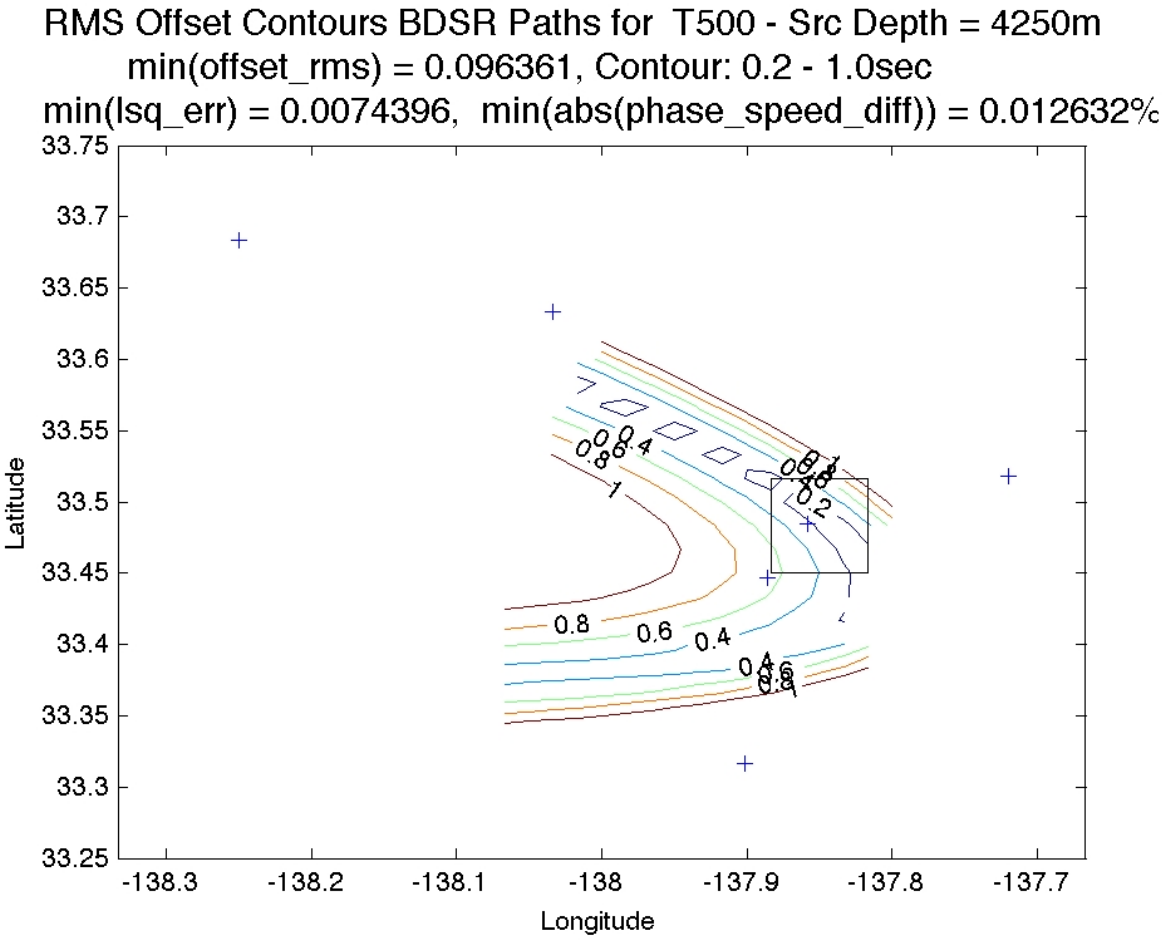

20a) [new_BDSR_err_contour_sixSM_2.jpg]

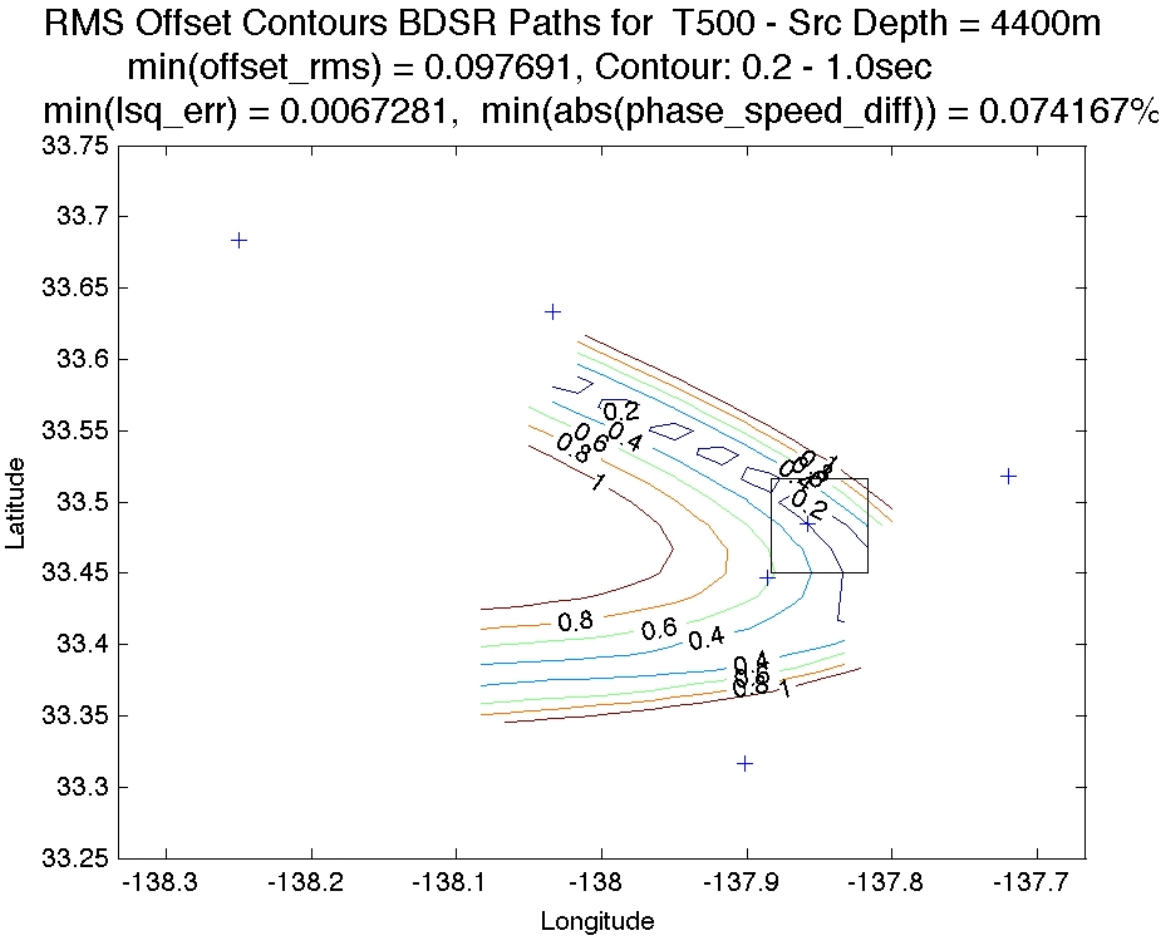

20b) [new_BDSR_err_contour_sixSM_5.jpg]

Figure 20: RMS offset error surface for the coarse grid over all six seamounts. a) Error surface assuming a scatterer depth of 4250m, the depth of DVLA-4250, whose arrival pattern is replicated on the OBSs. b) Error surface assuming a scatterer depth of 4400m, the shallowest depth of Seamount C. The change in source depth of 150m results is a very slight change in the error surface.

Figure 21: RMS offset error surface over Seamount B (OBS and BDSR arrivals).

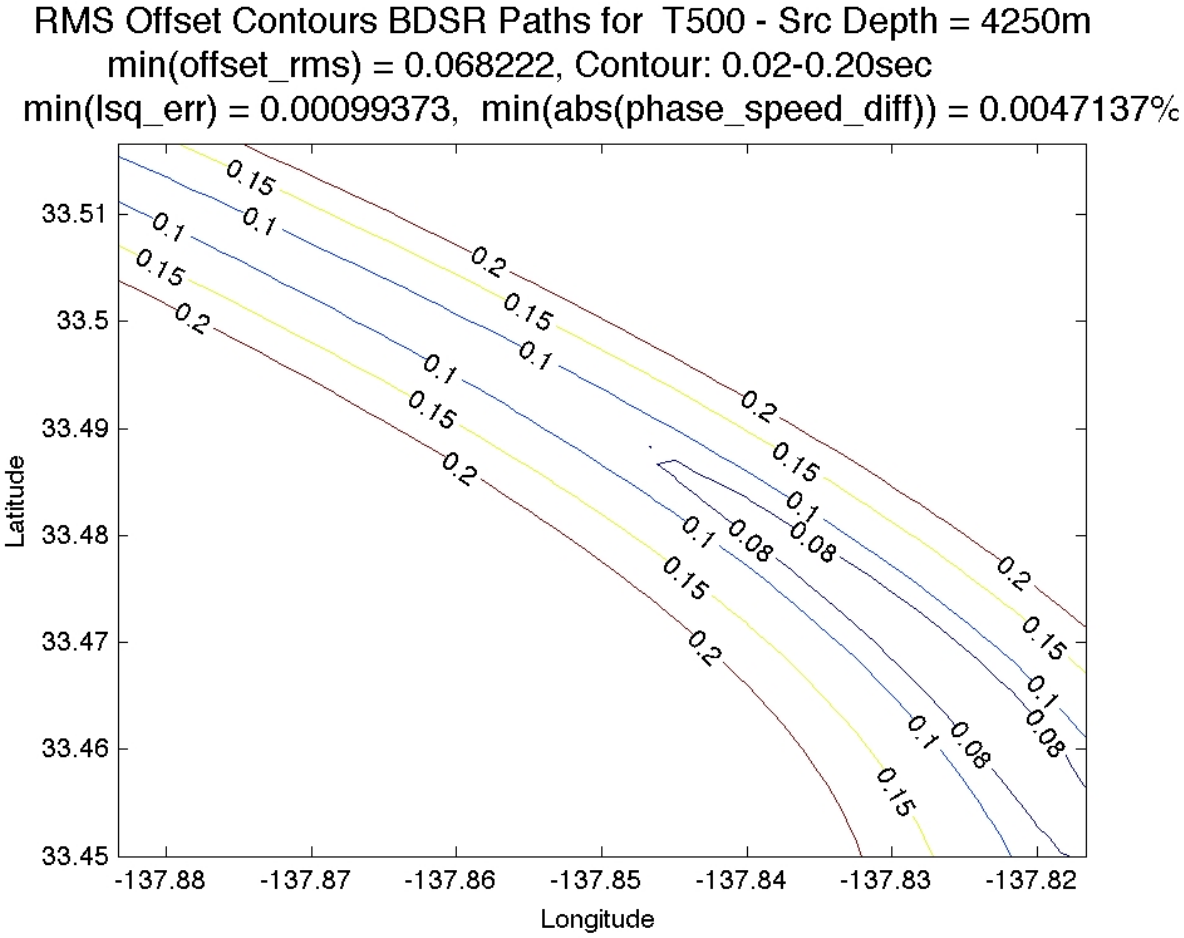

Figure 21: RMS offset error surface for the fine grid over Seamount B and assuming a scatterer depth of 4250m. The pair of 0.1sec contours is overlain on the bathymetry of Seamount B along with similar curves for the LSQ error and the phase speed difference in Figure 22. [new_BDSR_err_contour_2_2.jpg]

Figure 22: Three error surfaces over Seamount B (OBS and BDSR arrivals).

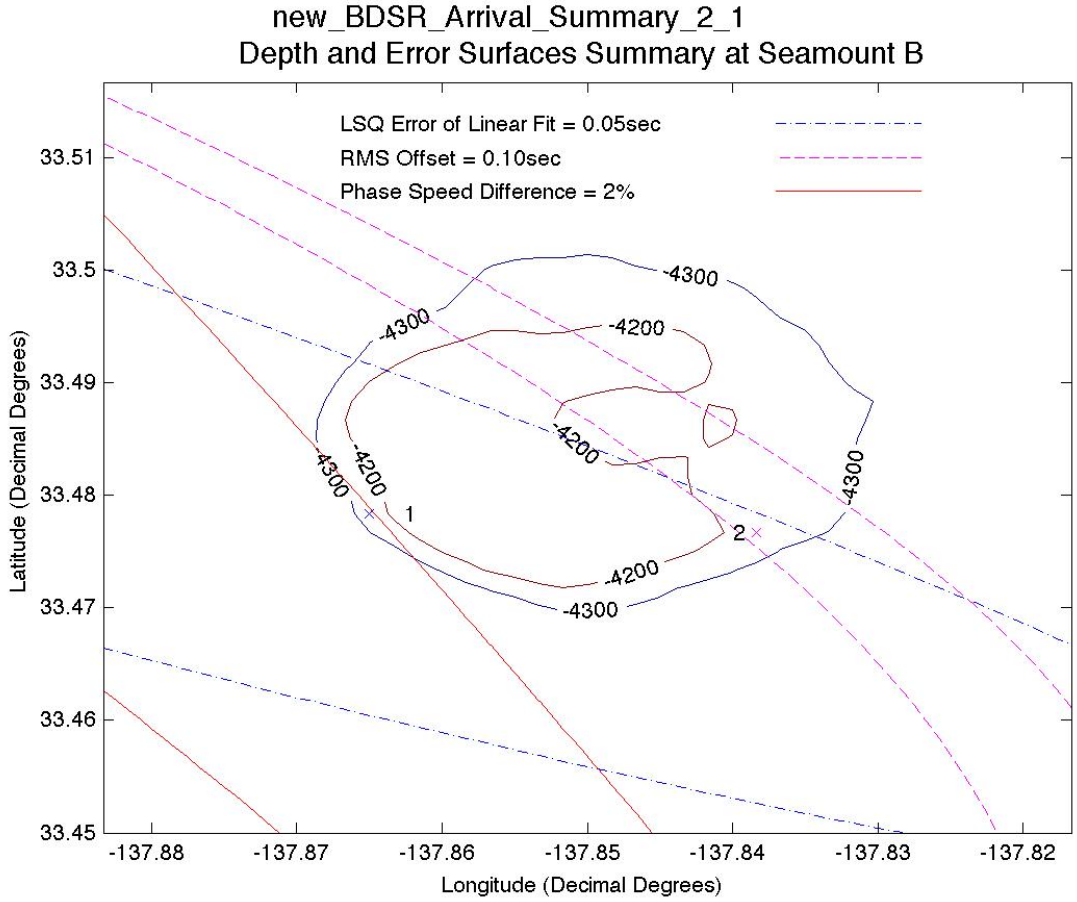

Figure 22: Error contours are overlain on the 4200 and 4300m isobaths at Seamount B. Three error contours are shown: a) least-square fit of the linear regression to the observed residual arrival times, b) the RMS offset between the observed and ray traced arrival times at the four ranges, and c) the difference in the phase speed (slope of the linear fits) for the observed and ray traced arrivals. In each case the minimum values of each surface fall between the two contours shown. The travel time curves for test points #1 and #2 are given in Figure 19. [Figure_16_new_BDSR_Arrival_Summary_2_1a.tif]

Figure 23: DSFA path geometry (OBS and BDSR arrivals).

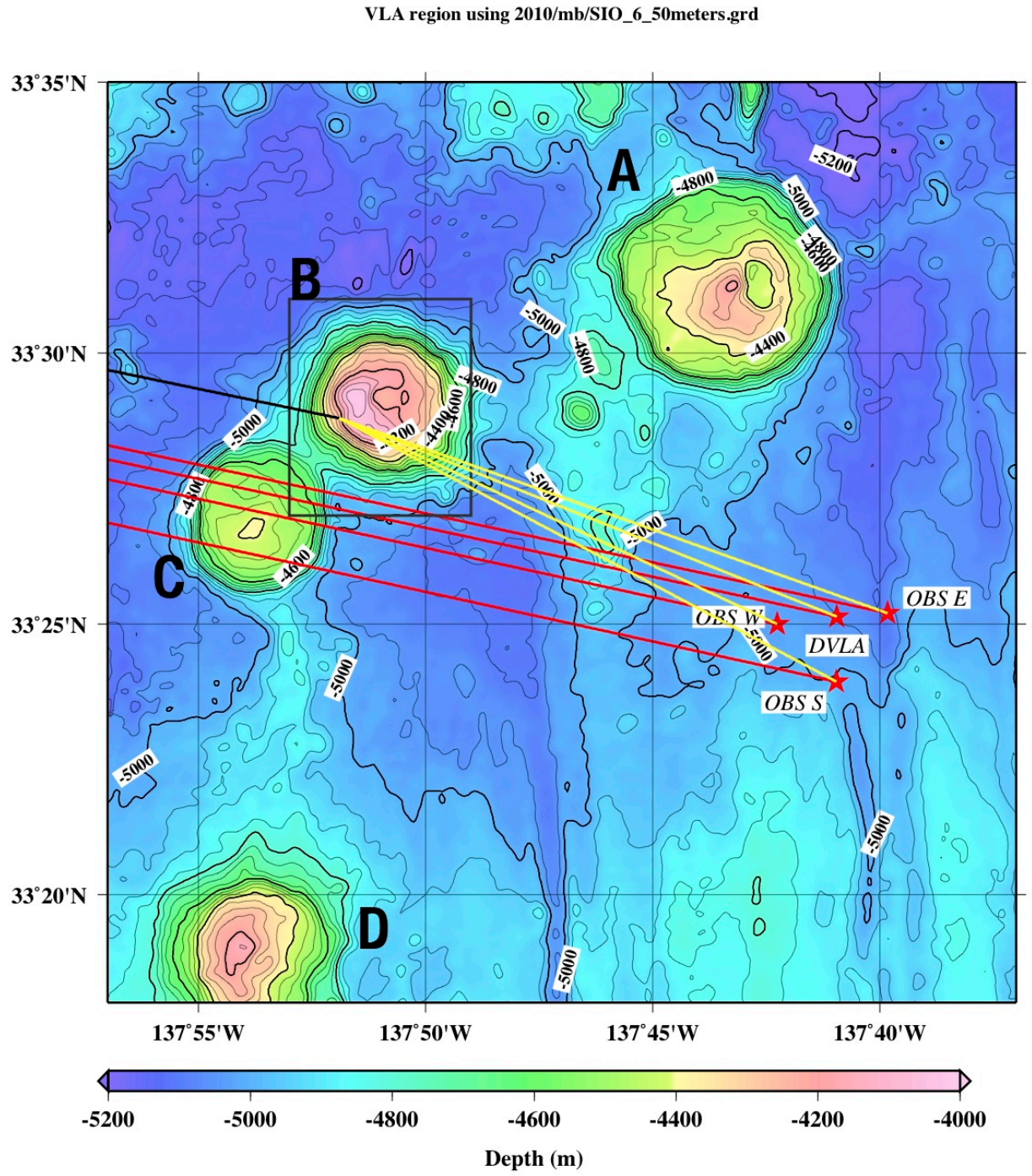

Figure 23: New PEP (black) and BDSR (yellow) trajectories for the conversion point at Location #1 in Figure 22 (travel time curve in Figure 19a). The trajectories are based on triangulation using arrival times at all three OBSs and the DVLA. Figure 11 is similar but was based on arrival times to just the three OBSs. [VLA_region_6.jpg]

Figure 24: Contour map of the bathymetry at Seamount B on the 0.1minute grid.

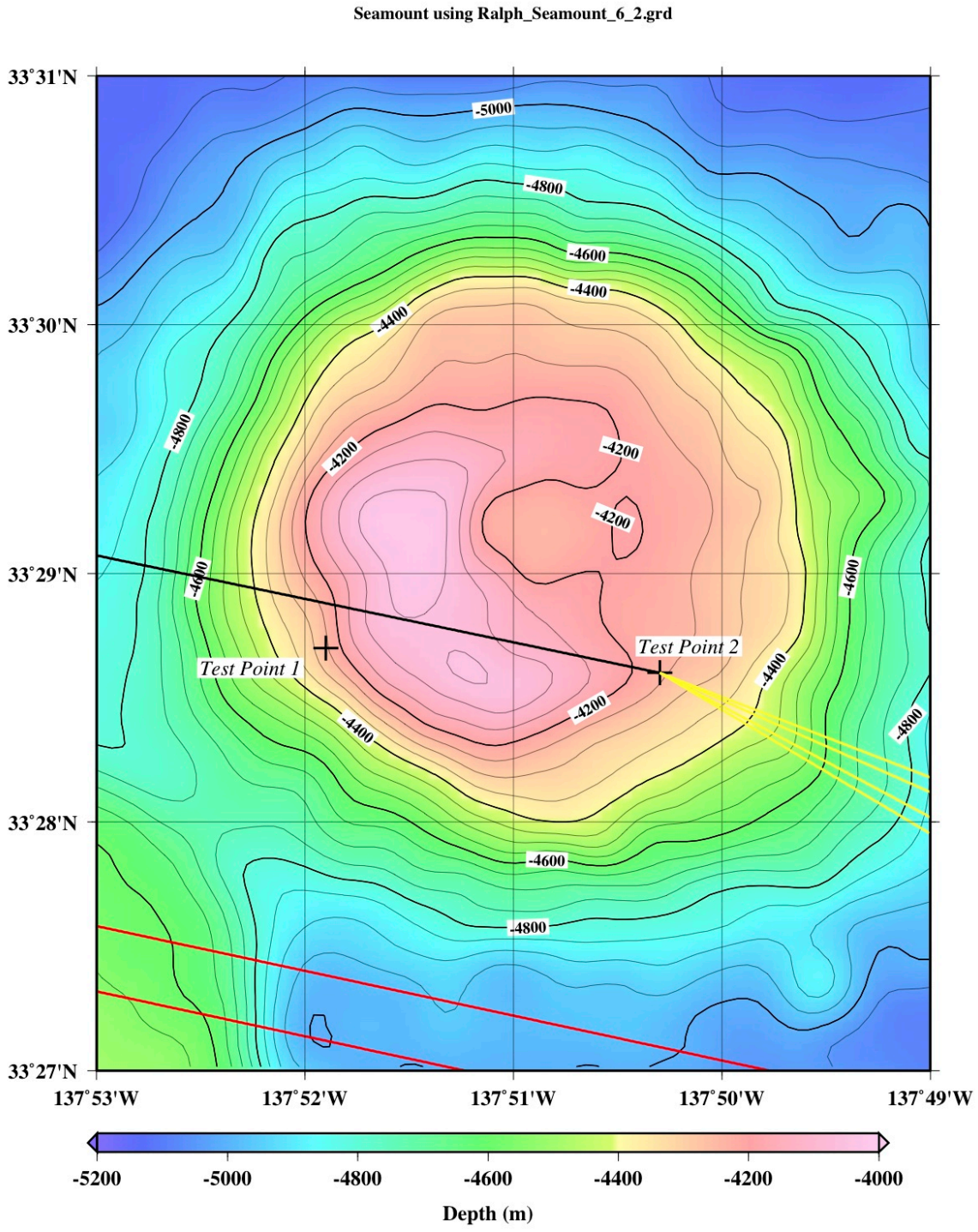

Figure 24: Contour map of the bathymetry on the 0.1minute grid. The map was generated from an interpolated bathymetry data set with values at every 0.1minute in latitude and longitude. The PEP (black) and BDSR (yellow) trajectories are based on test point #2 from Figures 19 and 22. [Ralph_Seamount_6.jpg]

6) PE-predicted propagation to a near-by out-of-plane seamount with conversion to a seafloor interface wave (Out-of-plane IW)

Originally, we had seriously considered this mechanism because we thought that DSFA arrivals were not observed on the DVLA. This changed when we confirmed that the third arrival (at 331.3sec in Figure 15c) on DVLA-L20-Hyd for T500 (M68.2) was actually consistent with a BDSR arrival from Seamount B (see the previous section). The BDSR mechanism from Seamount B explains the data so well that we no longer consider a seafloor interface wave mechanism necessary or viable for the arrivals.

E) Re-interpretation of the 2009 Arrival Pattern

There are sixteen late arrivals on the south OBS (Figures 2a and 3c). These are discussed in Section 5e) of the 2008 technical report. Of these, only six have been interpreted here as seamount scattering, BDSR arrivals (highlighted in yellow in Figure 3). For the ten other late arrivals on the south OBS we do not see similar arrivals on the other OBSs. Whether or not these ten DSF arrivals are generated by the BDSR mechanism is an open question.

There are seven arrivals for T1600 on the south OBS (Figure 1). These are labeled P, Z, S, Z, Z, Z, and S. (P for PE predicted, Z for deep shadow zone and S for deep seafloor arrivals.) The BDSR explanation only applies to the fourth and fifth arrivals, previously misinterpeted as deep shadow zone arrivals. The first and second (P and Z) make sense as PEP and DSZ arrivals. The third (the largest), sixth and seventh arrivals (S, Z and S) are still unexplained. The arrivals for T1600 on the south OBS could be re-labeled P, Z, S, B, B, Z, and S (P for PE predicted, Z for deep shadow zone, B for BDSR, and S for still unexplained deep seafloor arrivals).

The DSF/BDSR arrival for T500 to the South OBS occurs about 0.5sec after the finale of the time front (at 332sec in Figure 5-19 of Stephen et al (2008)) and would not be confused with DSZ arrivals. The DSF/BDSR arrival for T1000 occurs between cusps in the travel time curve (at 668.8sec in Figure 5-20 of Stephen et al). The first of the two DSF/BDSR arrivals for T2300 (at 1548.5sec) occurs just before a cusp and the second arrival (at 1550.2sec) occurs just after a cusp (Figure 5-22 in Stephen et al). So the existence of BDSR paths will confuse a time-front interpretation based on dispersal of the PEP and DSZ arrivals.

F) Discussion of Dushaw et al (1999)

Studying ocean acoustic thermometry, Dushaw et al. (1999) observed arrivals on deep seafloor receivers that they called "shadow zone arrivals" and that were similar to DSF arrivals: "To date, no known mechanism, e.g. diffraction leakage from the caustics or diffusion of acoustic energy by internal wave scattering can explain the extreme depth diffusion of acoustic energy that must be occurring. Because the forward problem for the shadow-zone arrivals is unknown, it is not known how to apply these data correctly to determine ocean temperature changes." Understanding the physical mechanisms for DSF arrivals could have important implications for ocean acoustic thermometry as well as for the ocean ambient noise budget.

Van Uffelen at al. (2009) discussed Dushaw et al.'s shadow zone arrivals in terms of penetration below cusps (caustics) of time fronts due to internal wave variability. In this paper we present another hypothesis for energy to penetrate into the deep shadow zone. Like Dushaw et al. our observations are made on seafloor receivers but unlike Van Uffelen et al. our hypothesis predicts deterministic arrivals at times that do not necessarily correspond to cusps of time fronts and may in some cases be seconds after the finale of the time front.

Dushaw et al. postulated that all of the shadow zone arrivals were "PE arrivals" except in regions of strong bottom interaction. They did discuss problems at receiver "l" which had poor SNR and required a 4sec offset between predicted and measured times. This magnitude of offset is of the same order as the delays we are seeing for DSF arrivals. That the later arrivals are larger in amplitude than the first PE arrival, by as much as 20dB in some cases, was also observed in Dushaw et al.'s data (see their Figure 6a). Although the acquisition geometries, bathymetry along the propagation path, and post-processing differ in some respects, our LOAPEX results are showing similar features to Dushaw et al. and provide additional insights.

Dushaw et al.'s observation of "shadow zone arrivals" on deep arrays in both the Atlantic and Pacific oceans, indicates that the LOAPEX observations are not unique or isolated events. Of course, the converted BDSR mechanism presented here requires seamounts that protrude into the sound channel (above the conjugate depth), but these relatively small seamounts are extremely common on the deep ocean floor. This analysis shows that a complete understanding of deep seafloor signals and ambient noise (at least in the 50-100Hz band) requires consideration of the detailed bathymetry around the receivers.

G) Future Work

1) We should revisit the PE runs with bottom interaction to see why the BRSR arrivals are so diffuse. If we redo this work we should upgrade the bottom model to the one used by Ilya Udovydchenkov in his 2012 paper.

2) Clearly we need to do as much as we can to improve the SNR in the DVLA data, perhaps by beamforming. Unambiguous identification of late, water-born energy would take us a long way to understanding the late arrivals on the OBSs. Note that in "correcting" the DVLA data for array motion the direction the sound is assumed. Usually it is assumed that the sound comes along the geodesic. But for out-of-plane BDSR it is mostly likely coming from Seamount B. Beamforming the DVLA data would need to take this into consideration.

3) Now that we are confident that at least some DSF arrivals are following BDSR paths, it would be more correct to explicitly model the T-station to seamount path and to use the actual depth of the test points on the seamounts.

4) We should check what amount of seafloor slope would be necessary to "reflect" the PE energy into BDSR energy at the seamount as opposed to diffraction. Remember that strictly speaking, reflections occur at very specific locations on the seafloor for a given source-receiver range as determined from ray theory.

5) The ray tracing for the BDSR path used a SSP from Matt Dzieciuch based on the WOA and the LOAPEX path from T1000 to the DVLA. Obviously a SSP for a region within 50km of the DVLA for September conditions would have been better.

ACKNOWLEDGMENTS

The OBS/Hs used in the LOAPEX/NPAL04 field program were provided by Scripps Institution of Oceanography under the U.S. National Ocean Bottom Seismic Instrumentation Pool (SIO-OBSIP - http://www.obsip.org). The OBS/H deployments themselves were co-funded through direct funding to SIO-OBSIP by the National Science Foundation and by Woods Hole Oceanographic Institution under a grant from the WHOI Deep Ocean Exploration Institute. The OBS/H data are archived at the IRIS **(**Incorporated Research Institutions for Seismology**)** Data Management Center. The LOAPEX source deployments and the moored DVLA receiver deployments were funded by the Office of Naval Research under Award Nos. N00014-1403-1-0181 and N00014-03-1-0182. The data reduction and analysis in this paper were funded by the Office of Naval Research under Award Nos. N00014-06-1-0222 and N00014-10-1-0510. Additional post-cruise analysis support was provided to RAS through the Edward W. and Betty J. Scripps Chair for Excellence in Oceanography.

REFERENCES

Dushaw, B. D., Howe, B. M., Mercer, J. A., et al. (**1999**). "Multimegameter-range acoustic data obtained by bottom-mounted hydrophone arrays for measurement of ocean temperature," IEEE J. Ocean. Eng. **24**, 202-214.

Stephen, R. A., Bolmer, S. T., Dzieciuch, M. A., et al. (**2009**). "Deep seafloor arrivals: An unexplained set of arrivals in long-range ocean acoustic propagation," J. Acoust. Soc. Am. **126**, 599-606.

Stephen, R. A., Bolmer, S. T., Udovydchenkov, I., et al. (**2008**), NPAL04 OBS data analysis part 1: Kinematics of deep seafloor arrivals, WHOI Technical Report 2008-03, (Woods Hole Oceanographic Institution, Woods Hole, MA).

Stephen, R. A., Bolmer, S. T., Udovydchenkov, I. A., et al. (**submitted**). "Deep seafloor arrivals in long range ocean acoustic propagation," J. Acoust. Soc. Am.

Stephen, R. A., and Swift, S. A. (**1994**). "Modeling seafloor geoacoustic interaction with a numerical scattering chamber," J. Acoust. Soc. Am. **96**, 973-990.

Udovydchenkov, I. A., Stephen, R. A., Duda, T. F., et al. (**in press**). "Bottom reflections from rough topography in the Long-range Ocean Acoustic Propagation Experiment," J. Acoust. Soc. Am.

Van Uffelen, L., Worcester, P., and Dzieciuch, M. (**2008a**). "Absolute intensities of acoustic shadow zone arrivals," J. Acoust. Soc. Am. **123**, 3464(A).

Van Uffelen, L., Worcester, P. F., and Dzieciuch, M. A. (**2008b**), Absolute intensities of acoustic shadow zone arrivals, in *11th NPAL Workshop, Borrego Springs, CA*, edited, Scripps Institution of Oceanography, La Jolla, CA.

Van Uffelen, L. J., Worcester, P. F., Dzieciuch, M. A., et al. (**2009**). "The vertical structure of shadow-zone arrivals at long range in the ocean," J. Acoust. Soc. Am. **125**, 3569-3588.

Van Uffelen, L. J., Worcester, P. F., Dzieciuch, M. A., et al. (**2006**). " The vertical structure of shadow-zone arrivals at long range in the ocean," J. Acoust. Soc. Am. **119**, 3344(A).

Appendix A: Clock Offset and PEP Arrival Times

Clock offsets and drifts to an accuracy of 0.02sec were determined by comparing PEP waveforms in the data (red lines in Figs A-1 to A-5) with the PE model (black lines) as discussed in the main text. Picked PEP arrival times are indicated by the horizontal dashed black lines. These are also given in Table A-1.

Figure A-1: Clock check at T250 (three OBSs and DVLA).

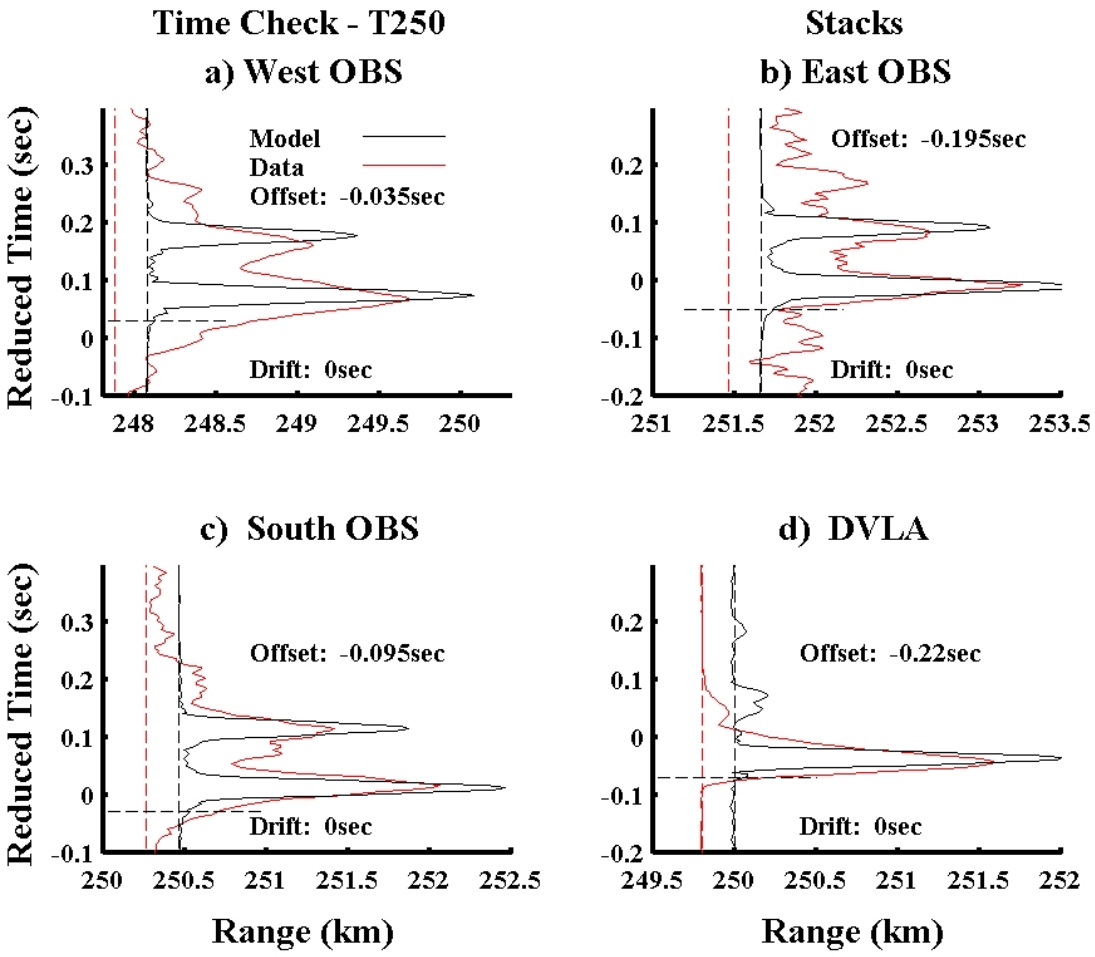

Figure A-1: At T250 there was good SNR for the PEP arrival and waveforms were consistent enough to get good clock offsets between the observed data and the model. [Clock_Check_T250_2012a.jpg]

Figure A-2: Clock check at T500 to T2300 (west OBS).

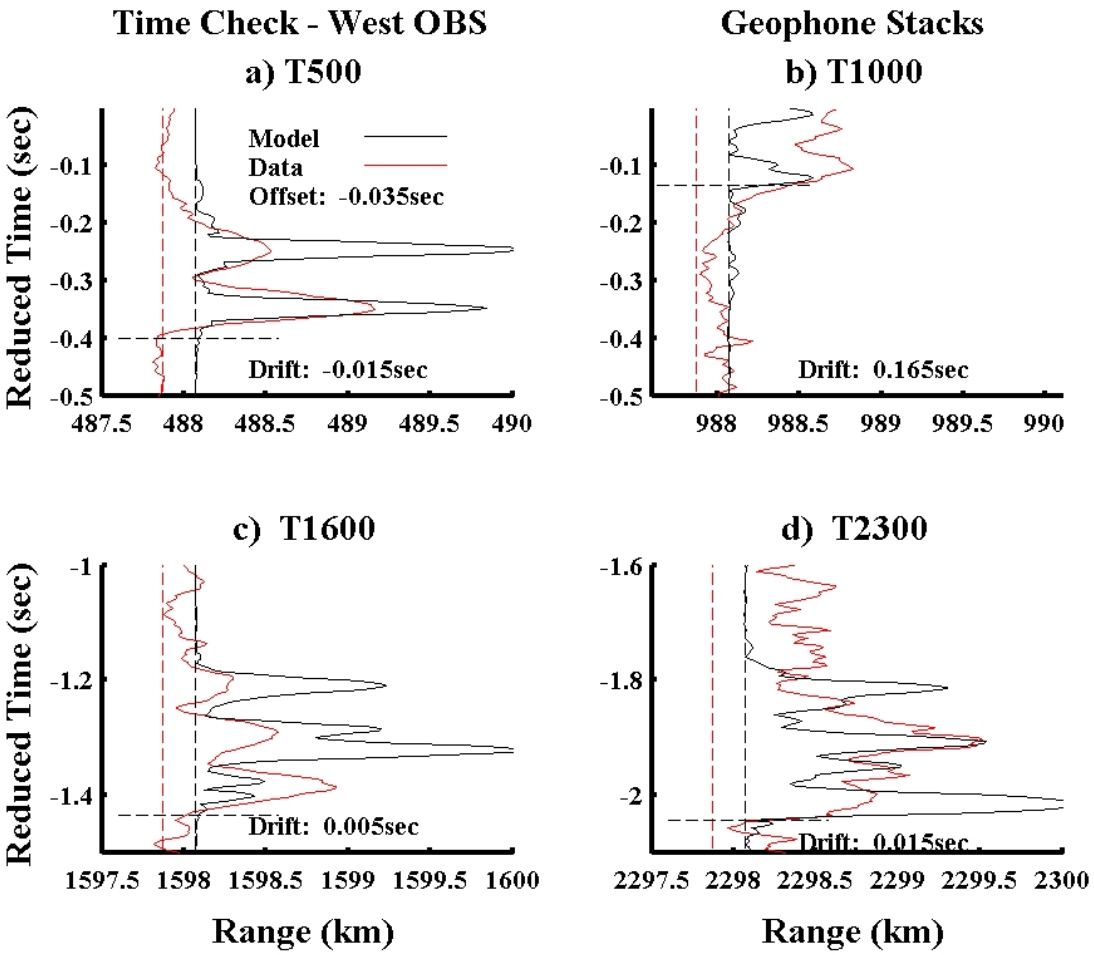

Figure A-2: [Clock_Check_2012a_Fig_1.jpg]

Figure A-3: Clock check at T500 to T2300 (east OBS).

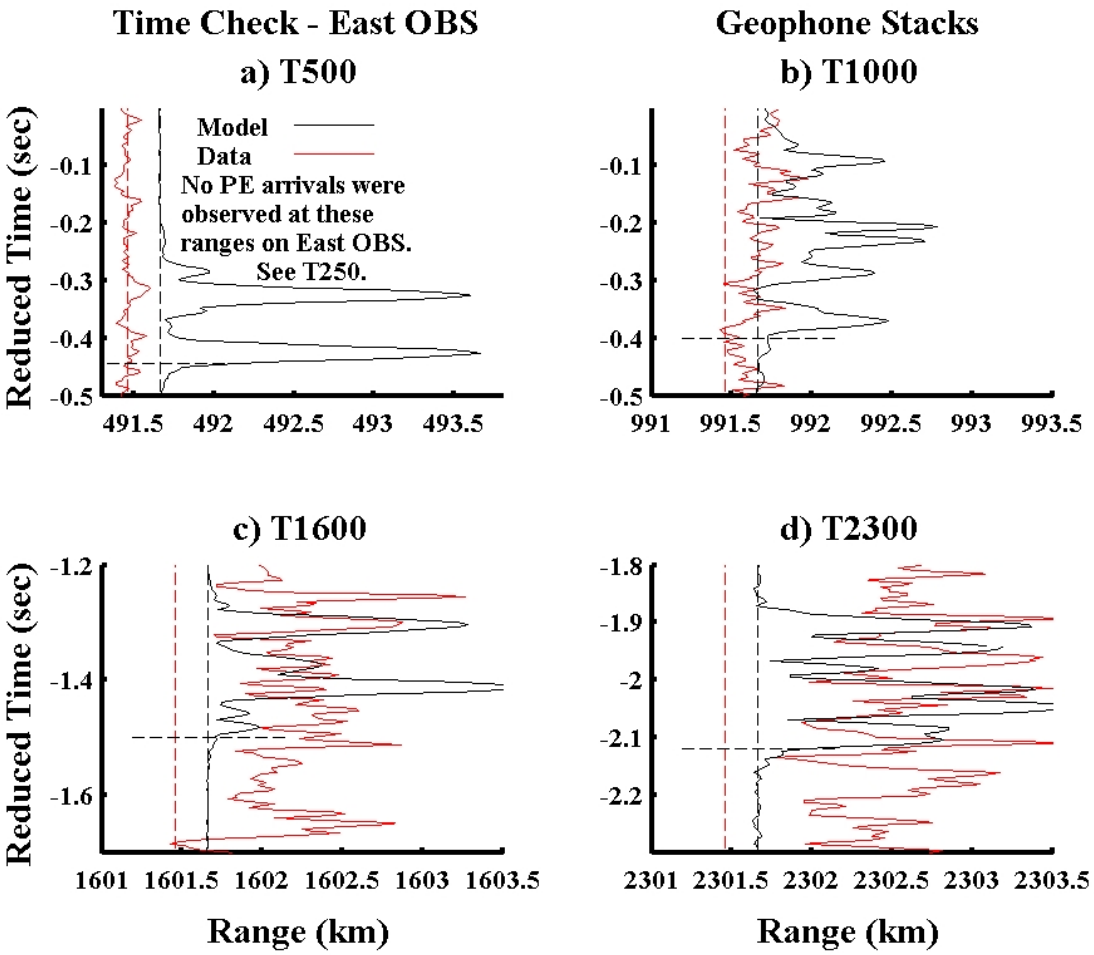

Figure A-3: SNR was too poor on the East OB PEP arrivals was too poor to get clock drifts at T500 and beyond. It was assumed that the offset at T250 would apply well at T500. [Clock_Check_2012a_Fig_2.jpg]

Figure A-4: Clock check at T500 to T2300 (south OBS).

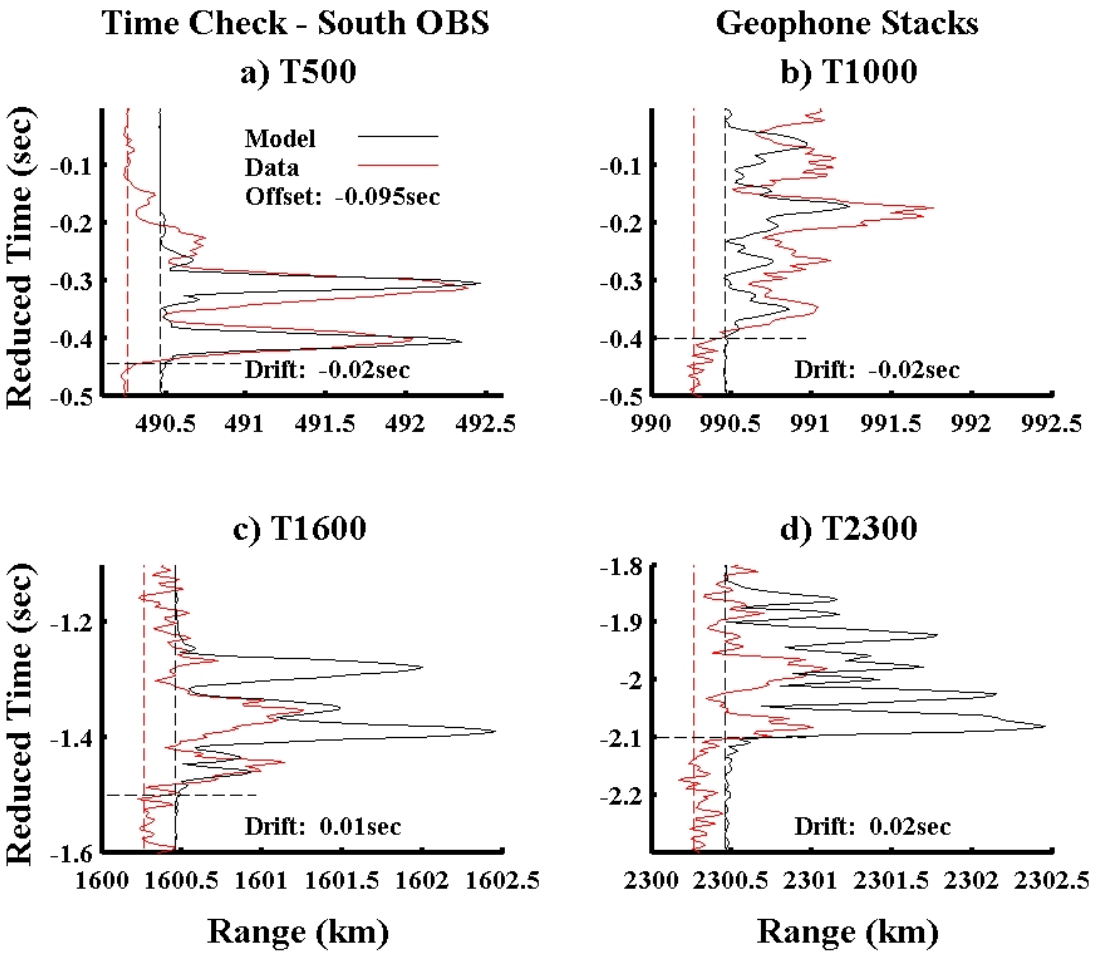

Figure A-4: [Clock_Check_2012a_Fig_3.jpg]

Figure A-5: Clock check at T500 to T2300 (DVLA).

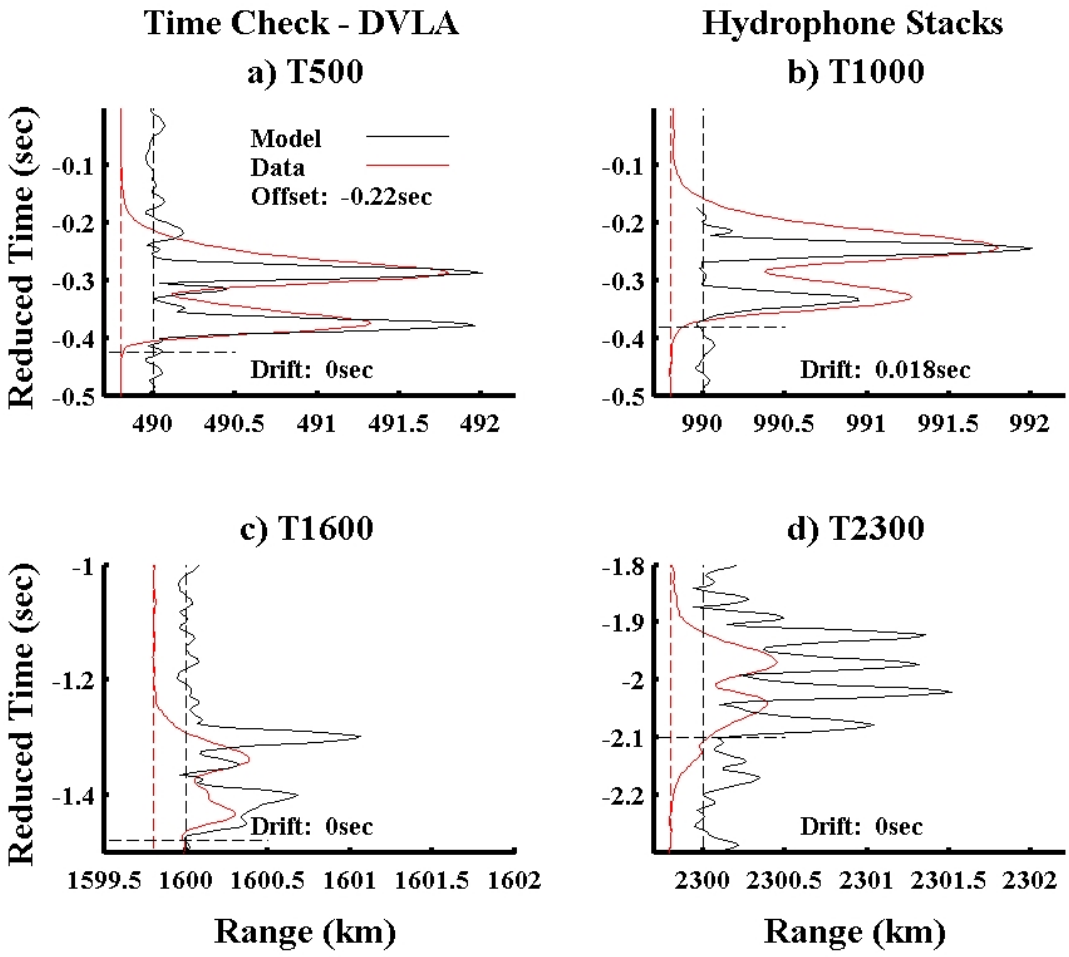

Figure A-5: [Clock_Check_2012a_Fig_4.jpg]

Table A-1: Reduced and unreduced arrival times for first PEP arrival

	DVLA	South OBS	West OBS	East OBS
T250- Reduced Time (sec)	-0.070	-0.030	+0.03	-0.05
T500- Reduced Time (sec)	-0.425	-0.445	-0.400	-0.445**
T1000- Reduced Time (sec)	-0.380	-0.400	-0.135*	-0.400**
T1600- Reduced Time (sec)	-1.480	-1.500	-1.435	-1.500**
T2300- Reduced Time (sec)	-2.100***	-2.100	-2.045	-2.120**
T250 - Range (km)	250.001	250.469	248.073	251.663
T500 - Range (km)	490.001	490.464	488.072	491.662
T1000 - Range (km)	990.002	990.462	988.072	991.662
T1600 - Range (km)	1600.001	1600.461	1598.072	1601.662
T2300 - Range (km)	2300.001	2300.460	2298.071	2301.661
T250- Unreduced Time (sec)	168.281	168.636	167.082	169.420
T500- Unreduced Time (sec)	329.542	329.834	328.268	330.641**
T1000- Unreduced Time (sec)	666.288	666.578	665.234*	667.386**
T1600- Unreduced Time (sec)	1075.962	1076.251	1074.708	1077.060**
T2300- Unreduced Time (sec)	1546.722	1547.031	1545.478	1547.820**
* - This arrival seems delayed by about 2.5sec in the model.	** - Poor SNR in the data		*** - Poor data- model comparison	

Appendix B: BRSR arrivals at the DVLA

Samples of data are plotted for each of the NPAL04 - LOAPEX transmissions for every working element in the DVLA. The average of all the transmissions in the first five minutes has been taken for each format (10 or 11 transmissions depending on source configuration, up to T1600; T2300 and T3200 used first 18minutes) and the displays have been corrected for array motion in the direction of the geodetic (compared to my work which stacked all available traces with no regard for array motion). BRSR or BDSR arrivals are seen on T50-800m, T50-350m, T250-800m, T500-800m, and T500-350m, but not on T250-350m. DSFAs were not identified on the OBSs for the 350m source depth at ranges of T250 and less. We should look more carefully at the OBS data (using the same transmissions as Ilya) for T50 and the 800m transmissions. [The color bars are normalized to the peak value and a fixed dynamic range of 50dB.]

Figure B-1: DVLA time fronts - T50 range, 75Hz, 800m depth.

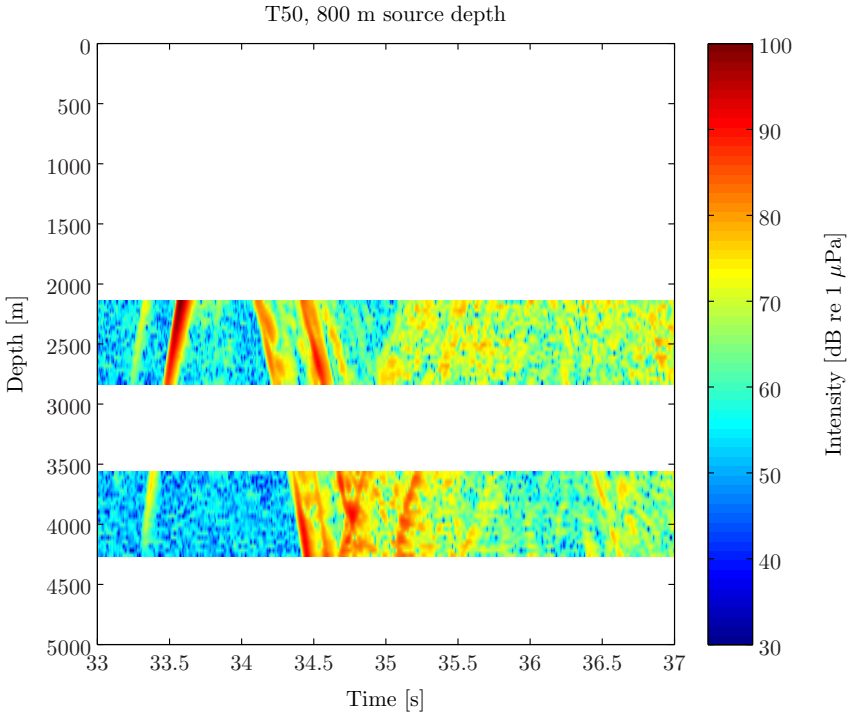

Figure B-1a: [fig1_T50_DVLA.pdf]

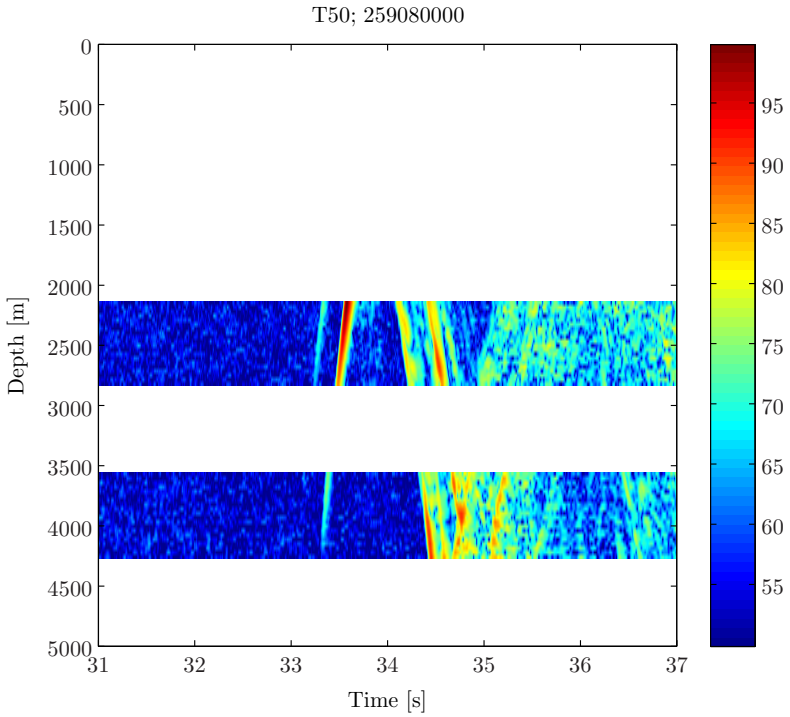

Figure B-1b: [T50_75_Hz_800_m_addSVLA_off_LOAPEX_DVLA_processed_it_1.pdf]

Figure B-2: DVLA time fronts - T50 range, 68.2Hz, 350m depth.

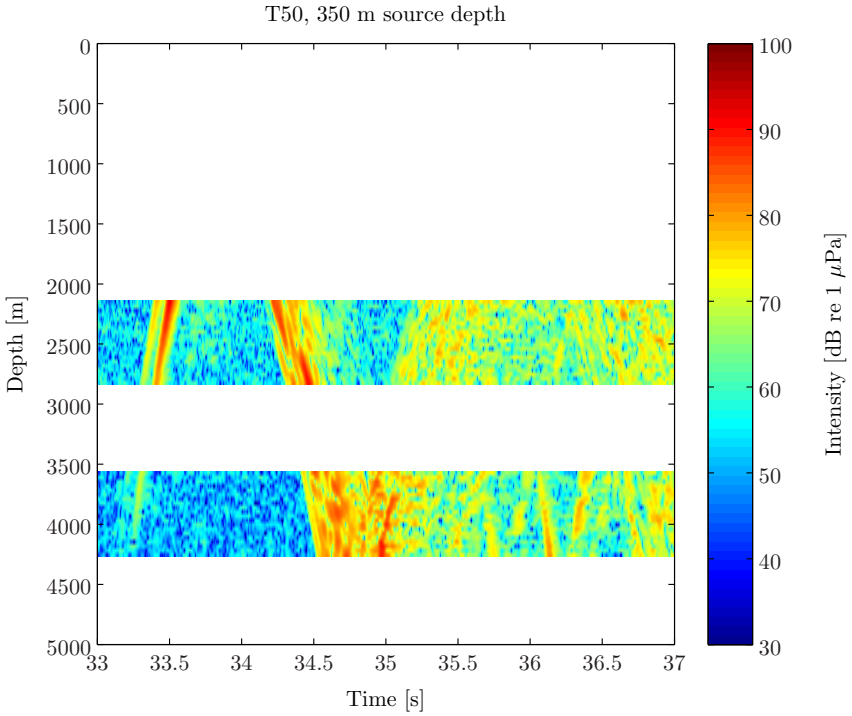

Figure B-2a: [fig1a_T50_DVLA.pdf]

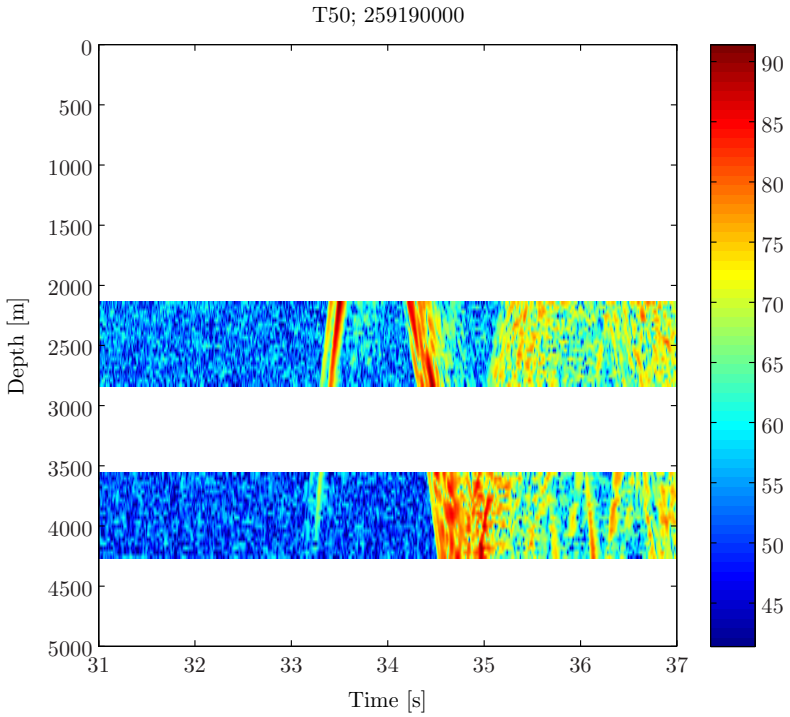

Figure B-2b: [T50_68_2_Hz_350_m_addSVLA_off_LOAPEX_DVLA_processed_it_1.pdf]

Figure B-3: DVLA time fronts - T250 range, 75Hz, 800m depth.

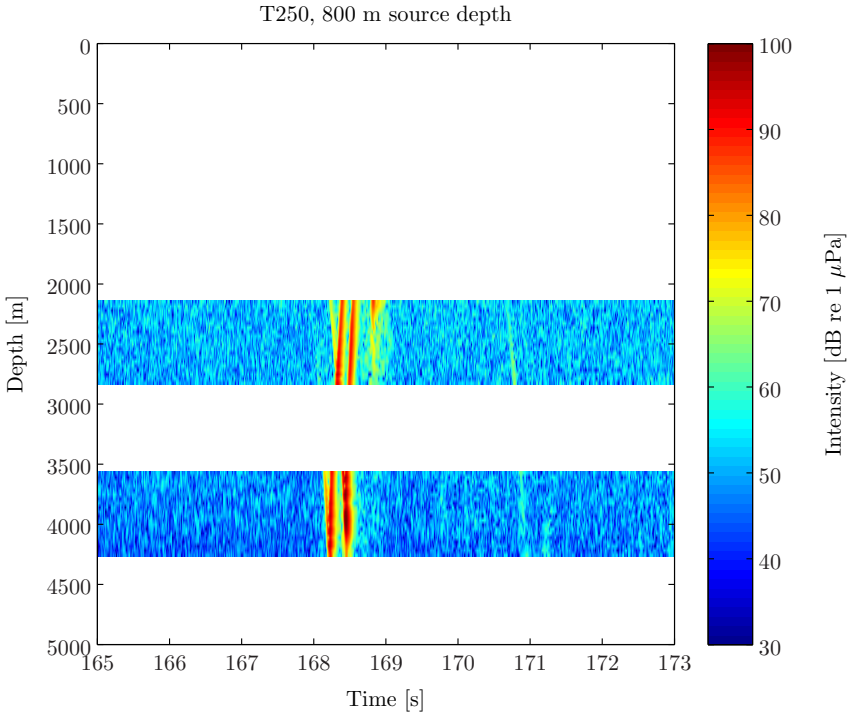

Figure B-3a: [fig2_T250_DVLA.pdf]

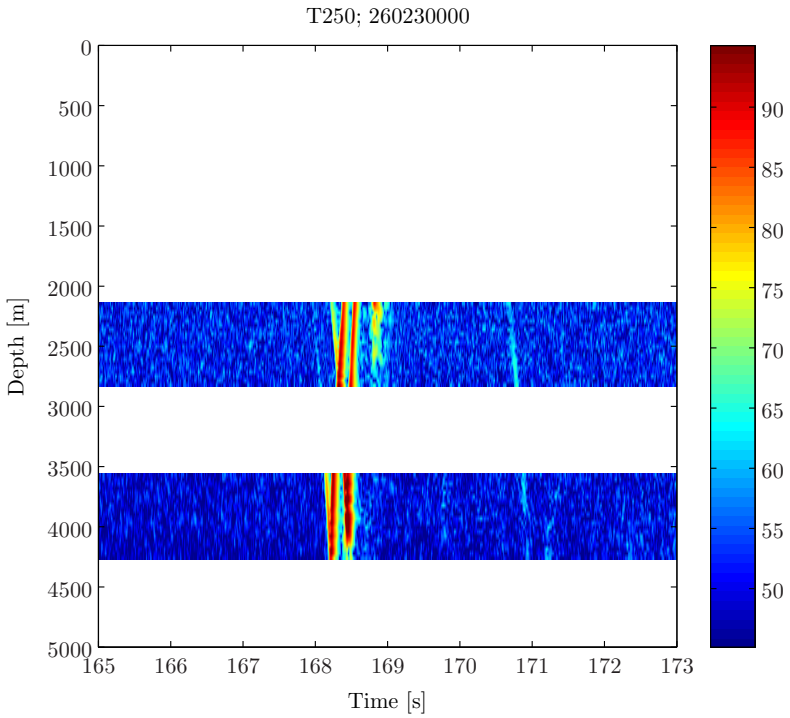

Figure B-3b: [T250_75_Hz_800_m_addSVLA_off_LOAPEX_DVLA_processed_it_4.pdf]

Figure B-4: DVLA time fronts - T250 range, 68.2Hz, 350m depth.

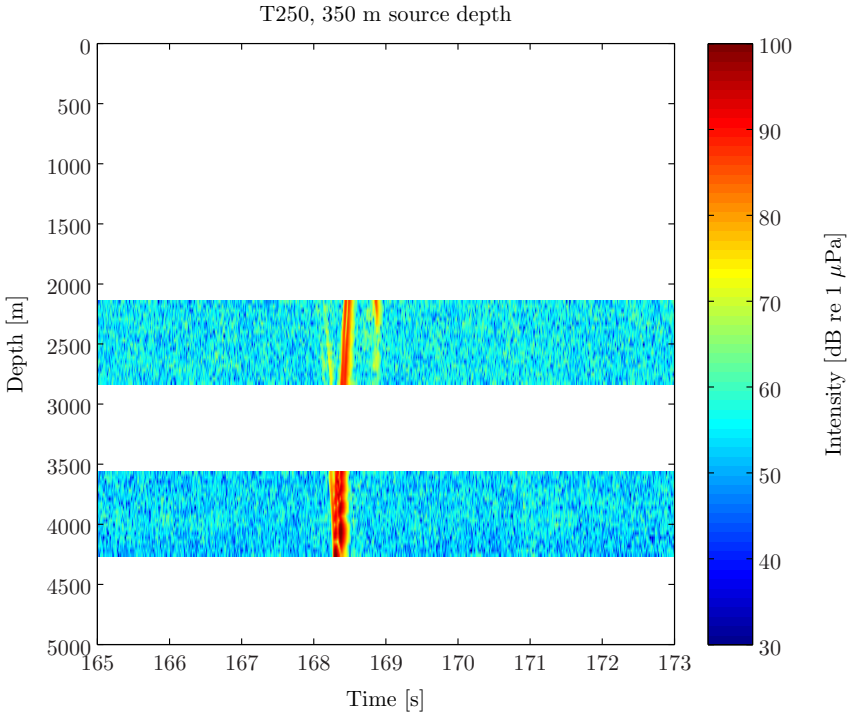

Figure B-4a: [fig2a_T250_DVLA.pdf]

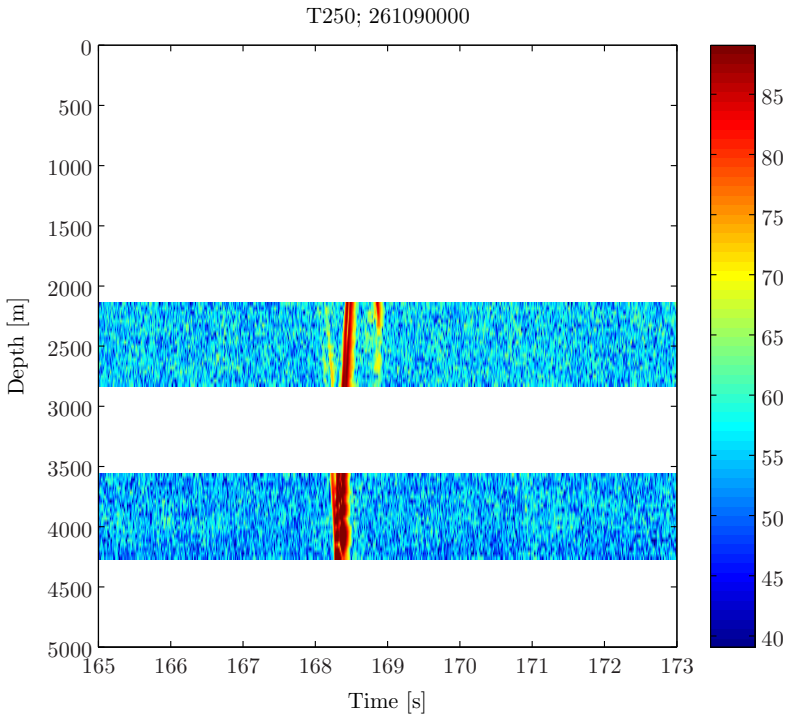

Figure B-4b: [T250_68_2_Hz_350_m_addSVLA_off_LOAPEX_DVLA_processed_it_1.pdf]

Figure B-5: DVLA time fronts - T500 range, 75Hz, 800m depth.

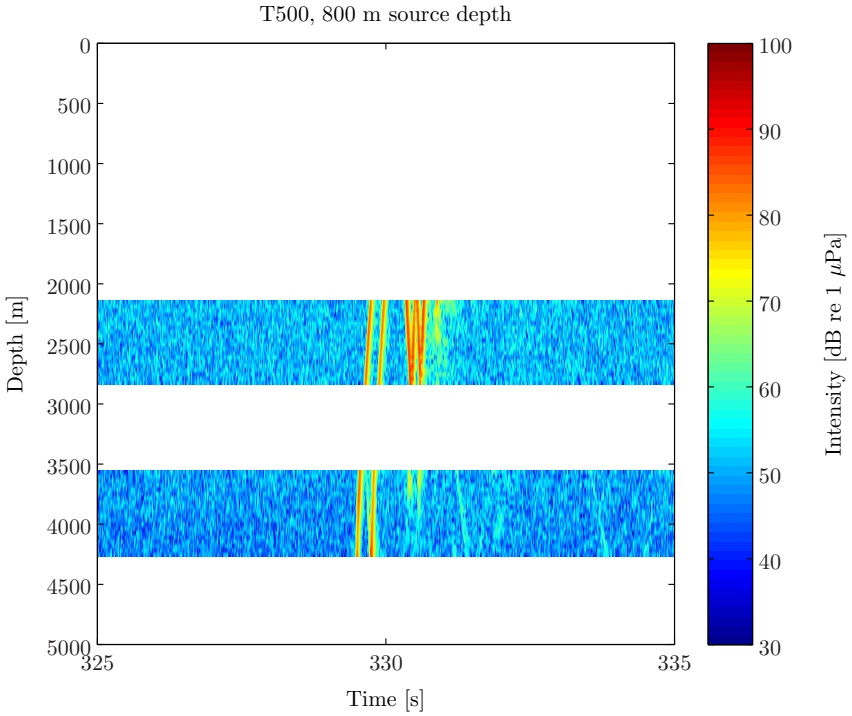

Figure B-5a: [fig3_T500_DVLA.pdf]

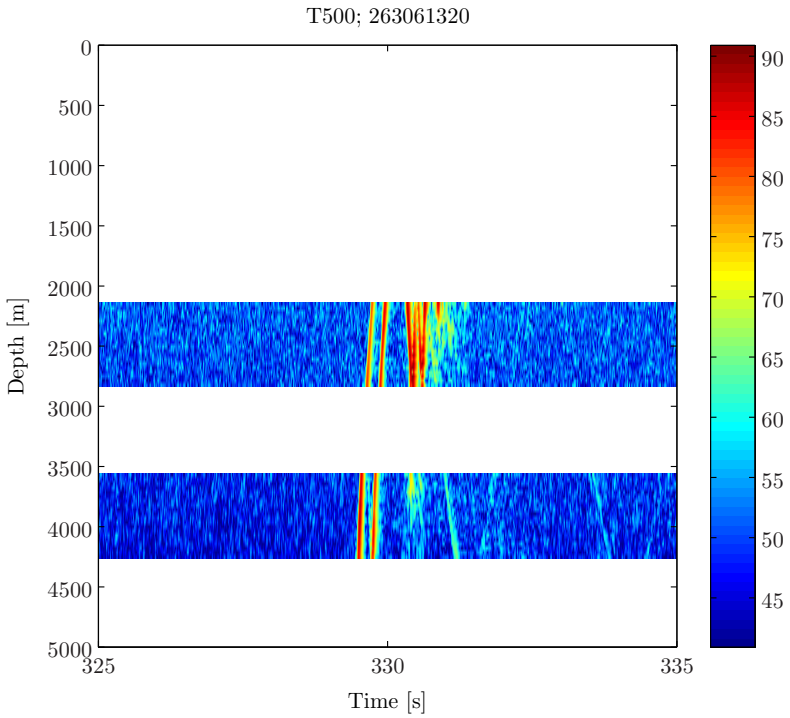

Figure B-5b: [T500_75_Hz_800_m_addSVLA_off_LOAPEX_DVLA_processed_it_9.pdf]

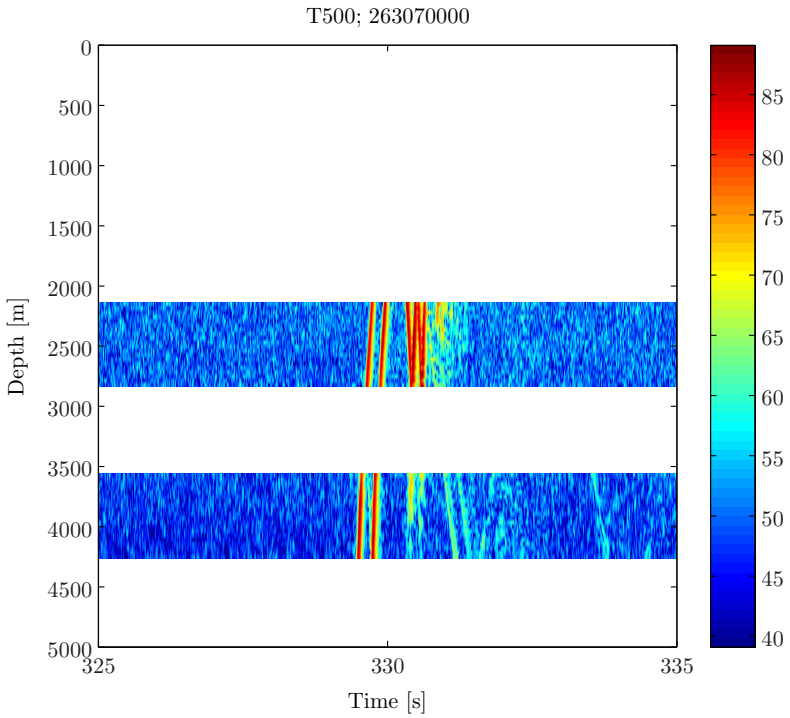

Figure B-5c: [T500_75_Hz_800_m_addSVLA_off_LOAPEX_DVLA_processed_it_10.pdf]

Figure B-5: T500 - 800m. This figure is very similar to Figure 5-4b in Stephen et al (2008). That caption said: "This figure shows the same data as the upper right panel in Figure 5-4a but with a color scale spanning 75dB instead of 35dB. Although the time axes are referenced differently, the arrivals in the bottom panel between 327 and 328sec (for the 75Hz LOAPEX source) are similar to the SRBR arrivals observed in the upper plot of Figure 5-1 [(Van Uffelen *et al.*, 2008b)] between 339 and 340sec (for the 250Hz SPICEX source). The color scale in Figure 5-1 spans only 40dB, so there is an indication that these arrivals at 75HZ are much weaker relative to the other time fronts than at 250Hz. There is also a weak arrival appearing in the lower panel just before 330sec. Unlike Figure 5-1 (at 250Hz), the SRBR time fronts here (at 75Hz) only appear clearly towards the bottom of the DVLA, possibly because the background noise is weaker. [Ilya_T500_LOAPEX_Data_75_dB_scale.pdf]" The figures are discussed in Sections 5a) and 5c) of Stephen et al (2008).

Figure B-6: DVLA time fronts - T500 range, 68.2Hz, 350m depth.

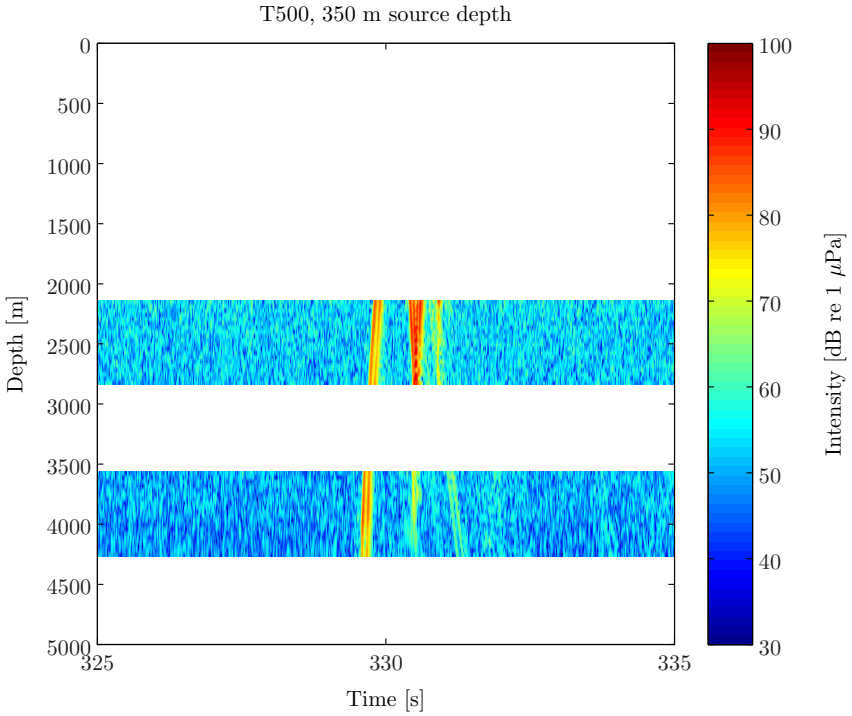

Figure B-6a: [fig3a_T500_DVLA.pdf]

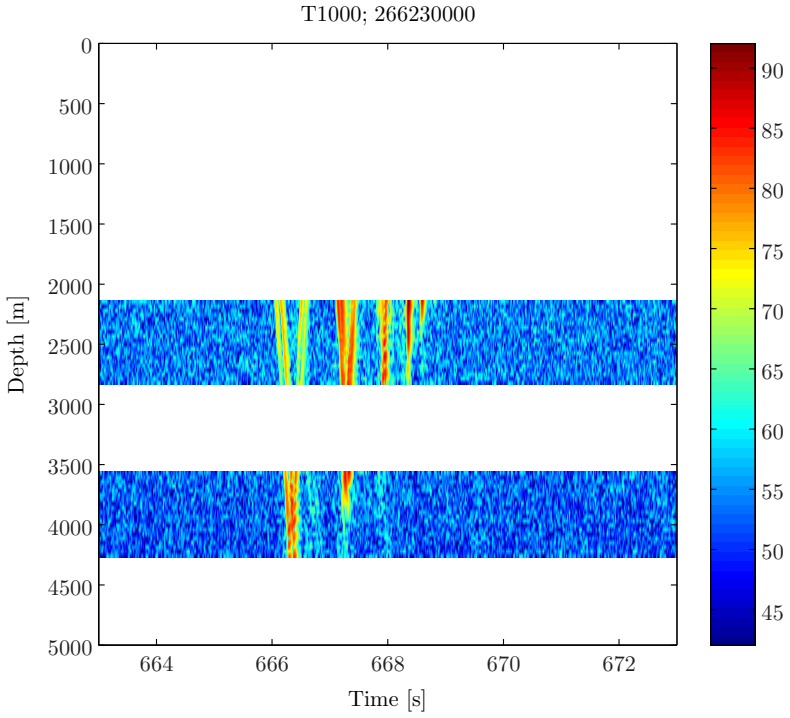

Figure B-6b: [T500_68_2_Hz_350_m_addSVLA_off_LOAPEX_DVLA_processed_it_1.pdf]

Figure B-7: DVLA time fronts - T1000 range, 75Hz, 800m depth.

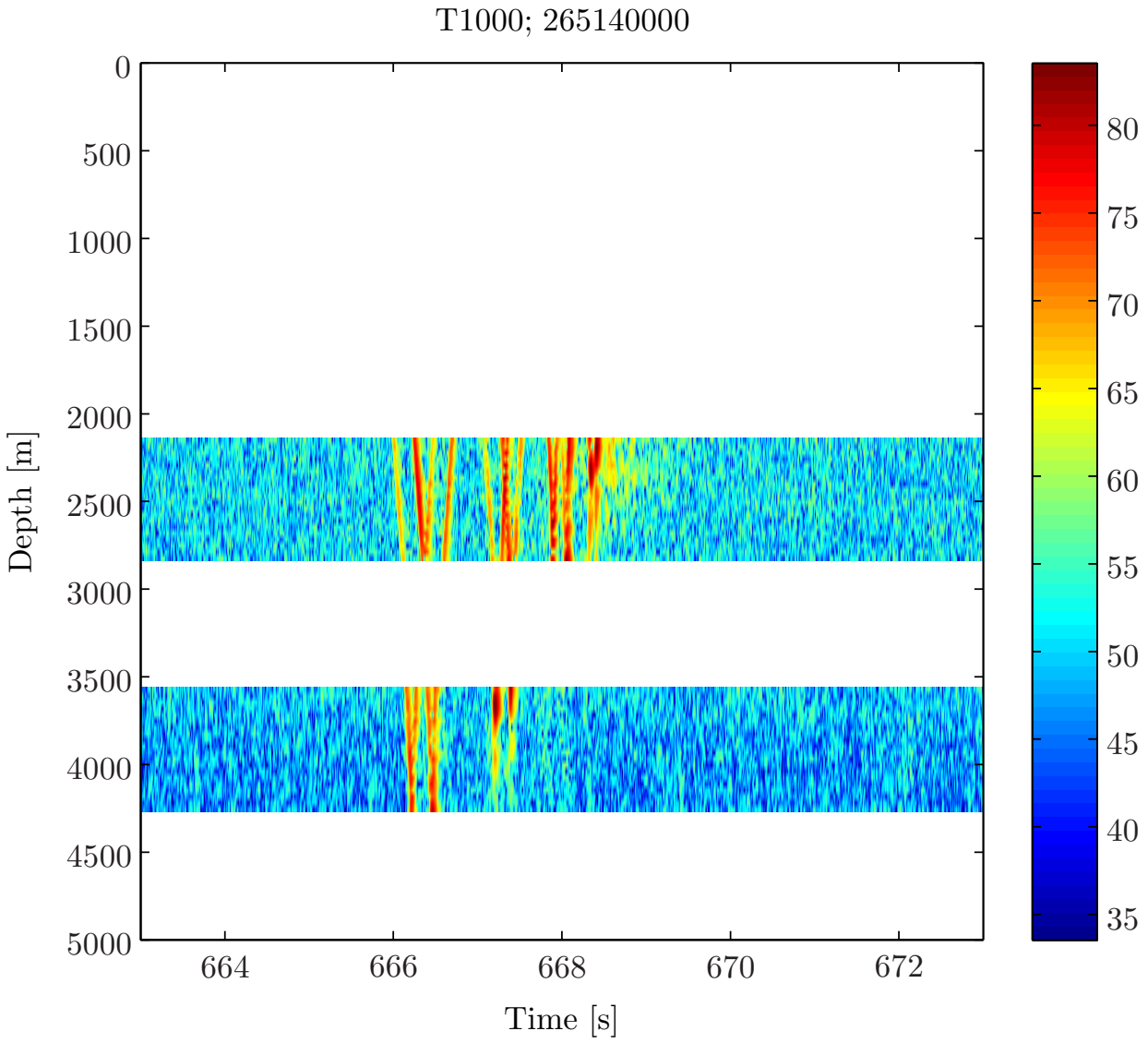

Figure B-7: [T1000_75_Hz_800_m_addSVLA_off_LOAPEX_DVLA_processed_it_1.pdf.pdf]

Figure B-8: DVLA time fronts - T1000 range, 68.2Hz, 350m depth.

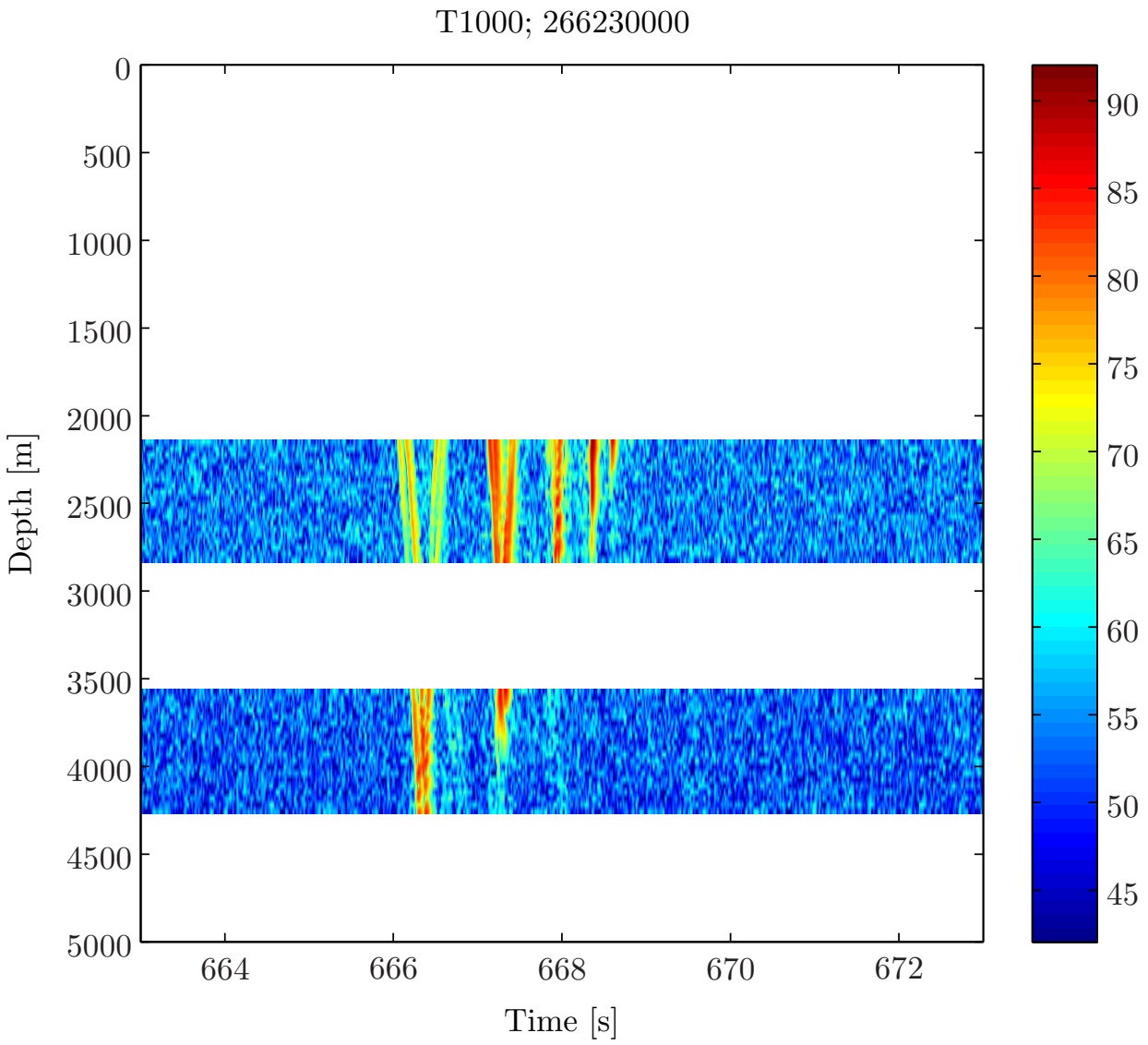

Figure B-8: [T1000_68_2_Hz_350_m_addSVLA_off_LOAPEX_DVLA_processed_it_1.pdf]

Figure B-9: DVLA time fronts - T1600 range, 68.2Hz, 350m depth.

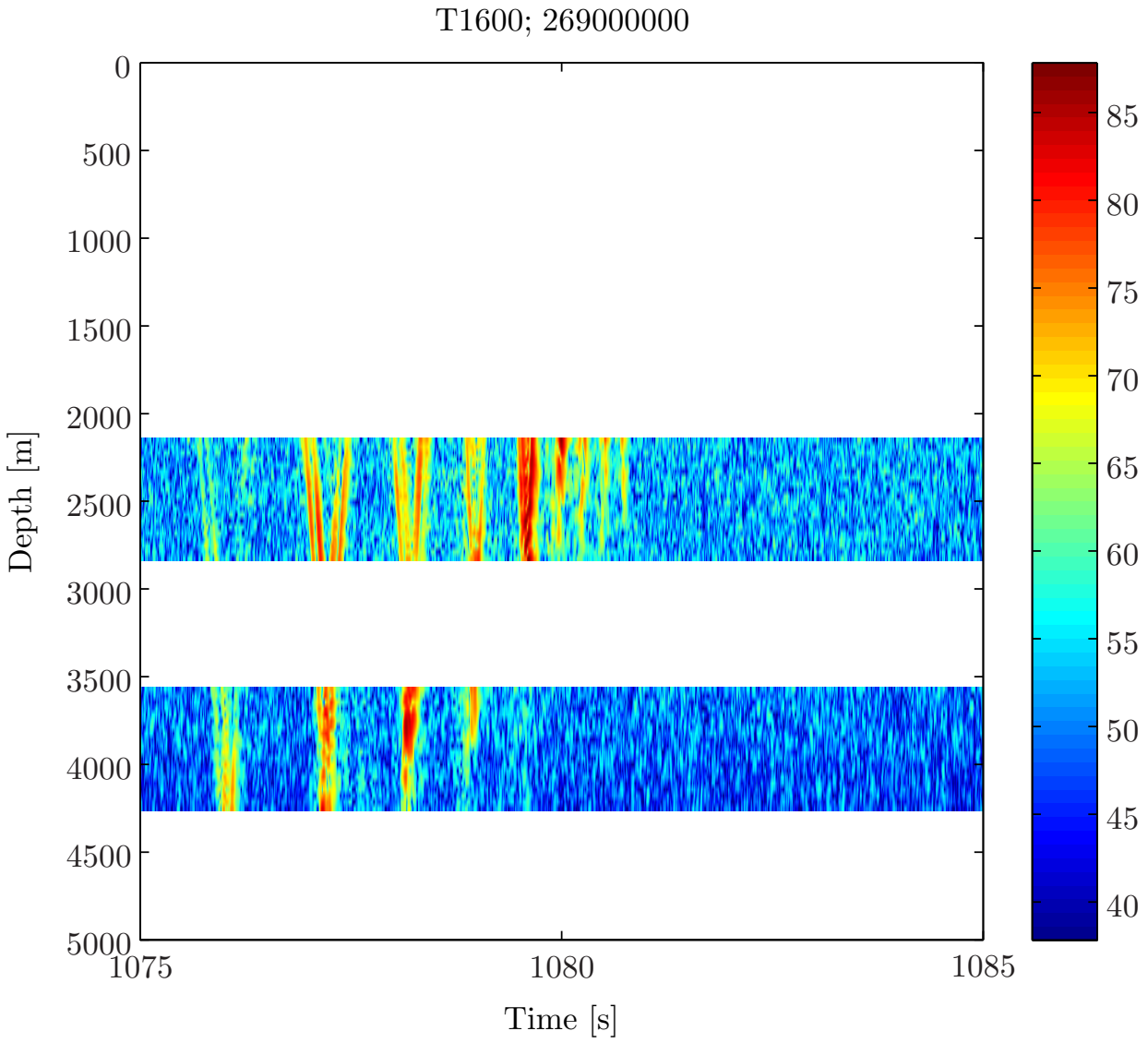

Figure B-9: [T1600_68_2_Hz_350_m_addSVLA_off_LOAPEX_DVLA_processed_it_1.pdf]

Figure B-10: DVLA time fronts - T2300 range, 68.2Hz, 500m depth.

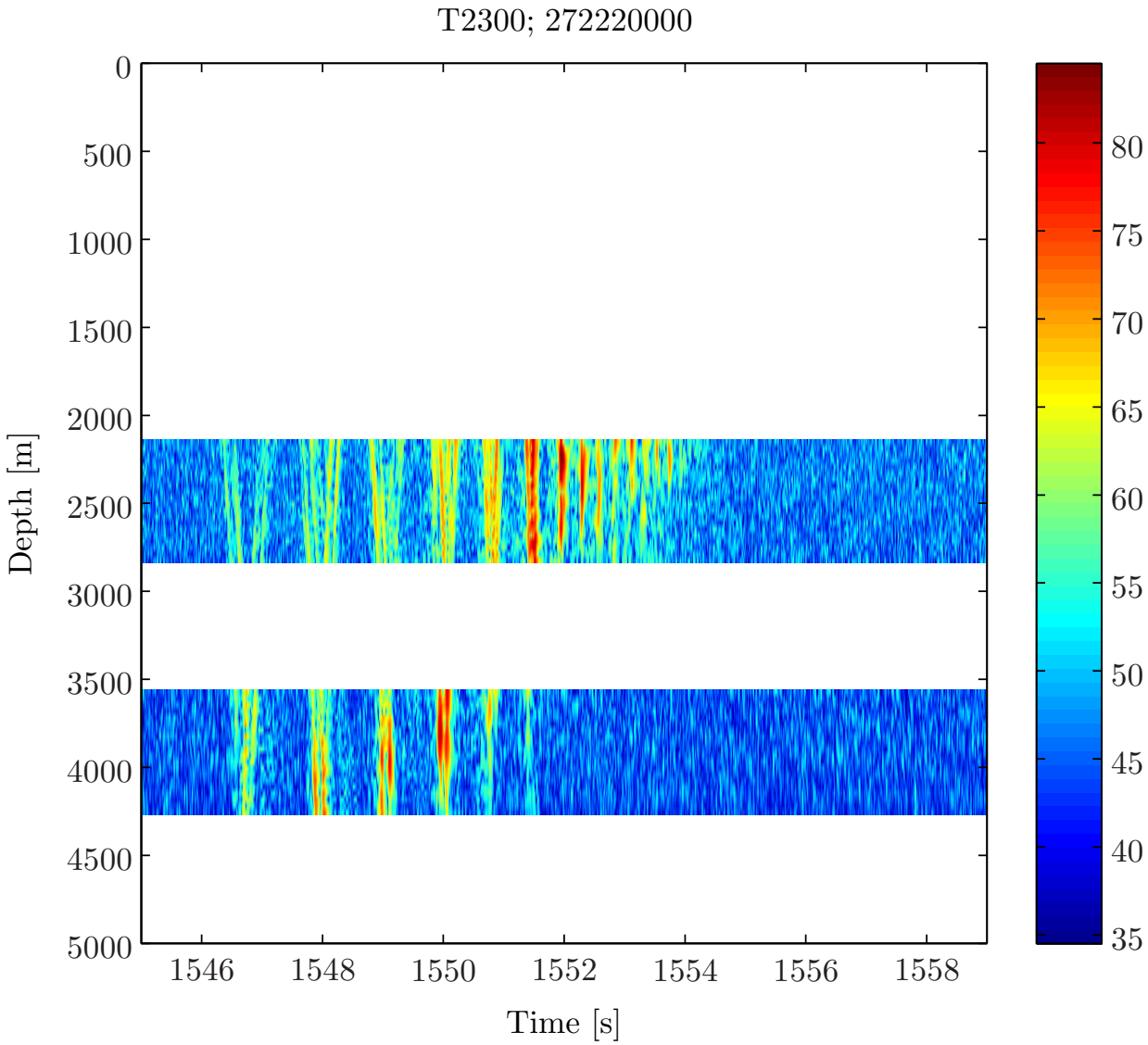

Figure B-10: [T2300_68_2_Hz_500_m_addSVLA_off_LOAPEX_DVLA_processed_it_1.pdf]

Figure B-11: DVLA time fronts - T2300 range, 68.2Hz, 350m depth.

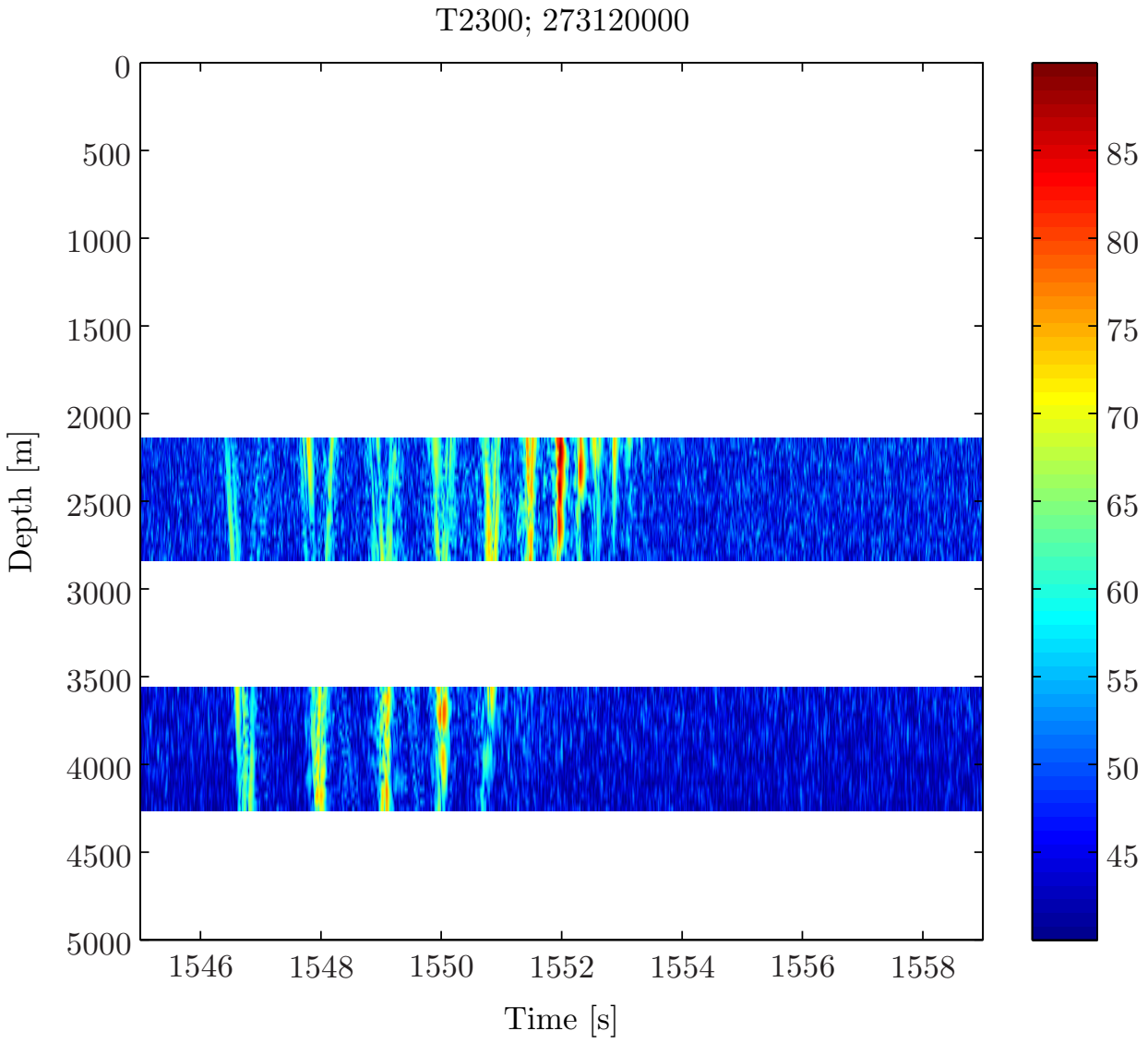

Figure B-11: [T2300_68_2_Hz_350_m_addSVLA_off_LOAPEX_DVLA_processed_it_1.pdf]

Figure B-12: DVLA time fronts - T3200 range, 68.2Hz, 500m depth.

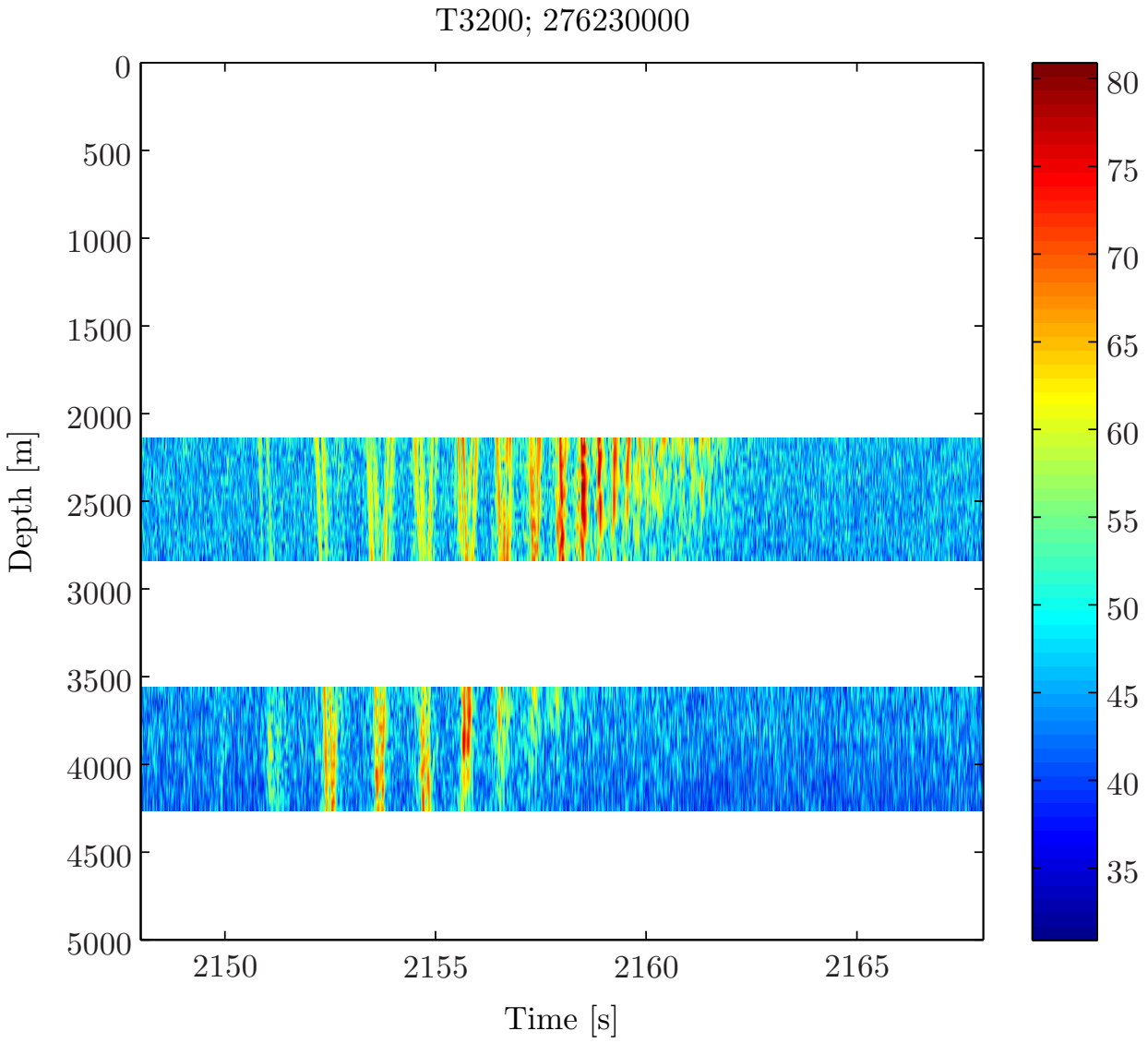

Figure B-12: T3200_68_2_Hz_500_m_addSVLA_off_LOAPEX_DVLA_processed_it_1.pdf]

Figure B-13: DVLA time fronts - T50 range, 68.2Hz, 350m depth.

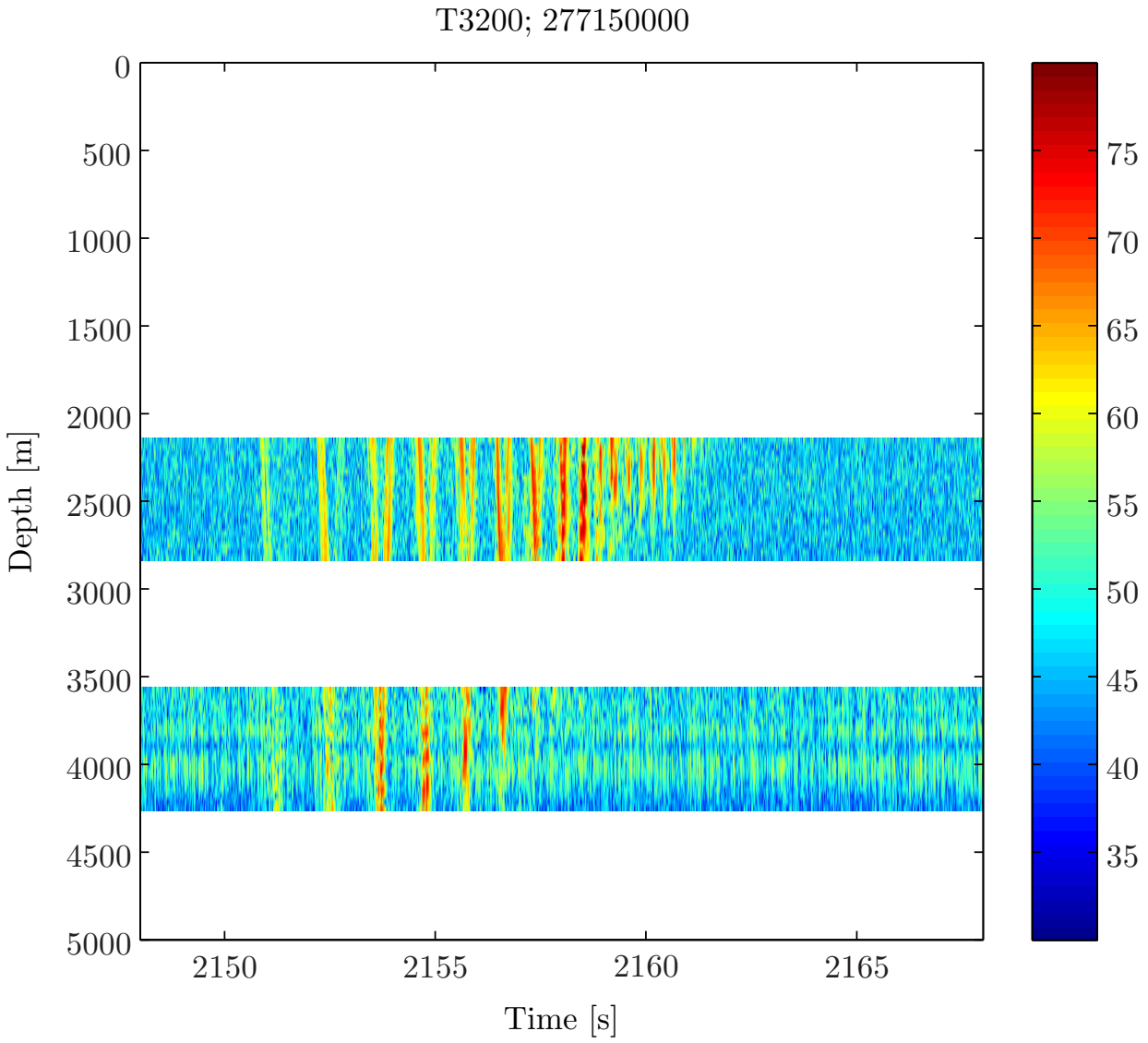

Figure B-13: [T3200_68_2_Hz_350_m_addSVLA_off_LOAPEX_DVLA_processed_it_1.pdf]

Appendix C: Ray tracing analysis for BDSR paths from all six seamounts

All of these ray tracing results use "cwmean" which is a typical SSP for NPAL from Matt Dzieciuch. "It is extracted from WOA04 and is the mean along the 1000km LOAPEX path. These are the same range dependent profiles that I used in the calculations I did for you previously." There are values every meter which is much finer than the profile I estimated from Figure 5.4 of the LOAPEX cruise report. Obviously a SSP for a region within 50km of the DVLA for September conditions would have been better.

The seamount bathymetric profiles are taken from Figure C-1 and the scatterers are assumed to be at the peak of the seamounts (Figure C-2). Ray tracing was carried out from the peak of the seamount to the sea surface and back down to 5000m (for example, Figures C-3 and C-4). Figure C-5 compares the observed and BDSR modeled travel times for conversion at the top of the six seamounts. Seamount B gave the closest agreement. Figure C-6 shows that changing the conversion point depth from 3,640 to 4,400m is insufficient to bring the modeled phase velocity into agreement with the observed phase velocity.

Figure C-1: Bathymetry over the six seamount region.

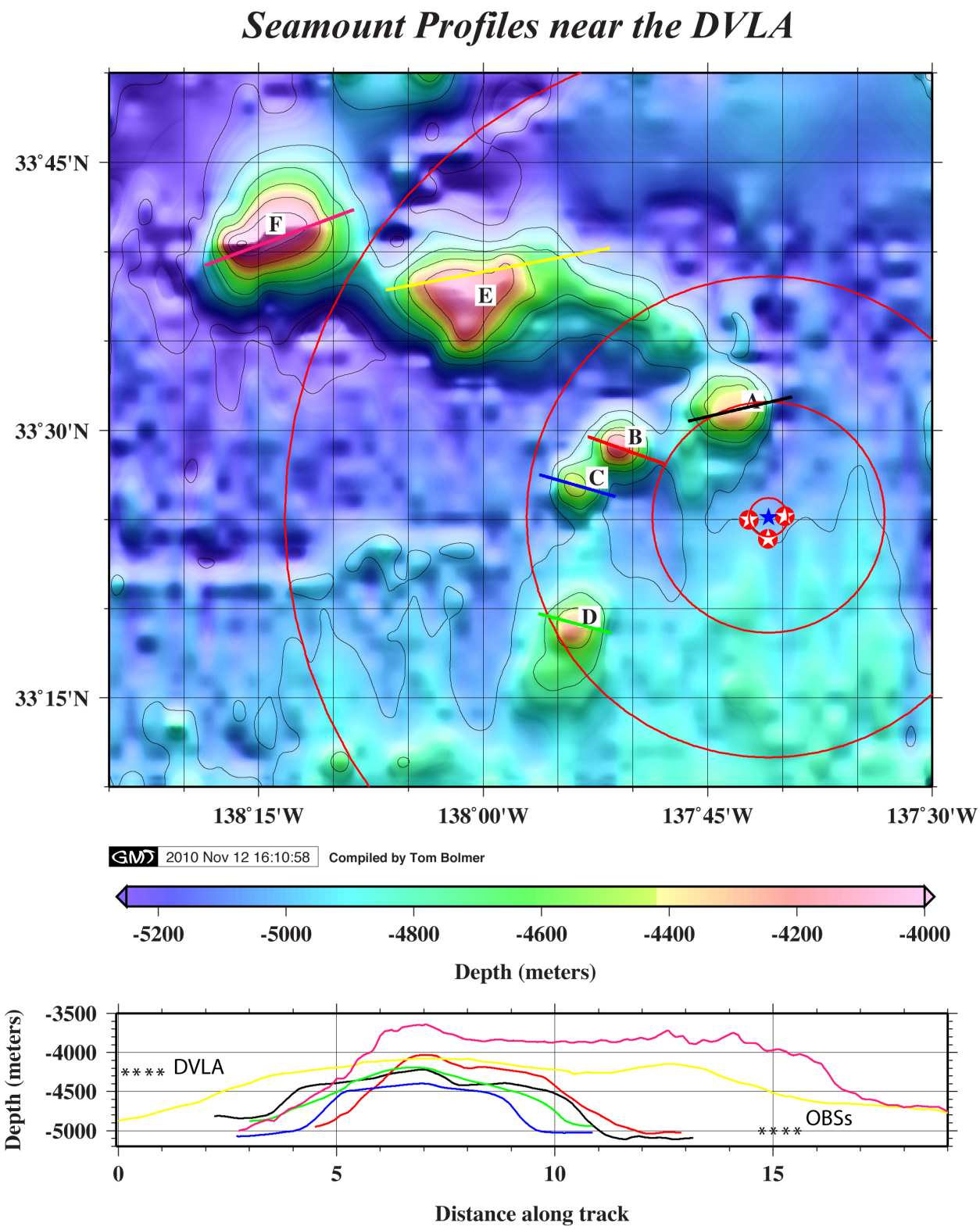

Figure C-1: [VLA_region_5_Profiles.jpg]

Figure C-2: Profiles across the six seamounts.

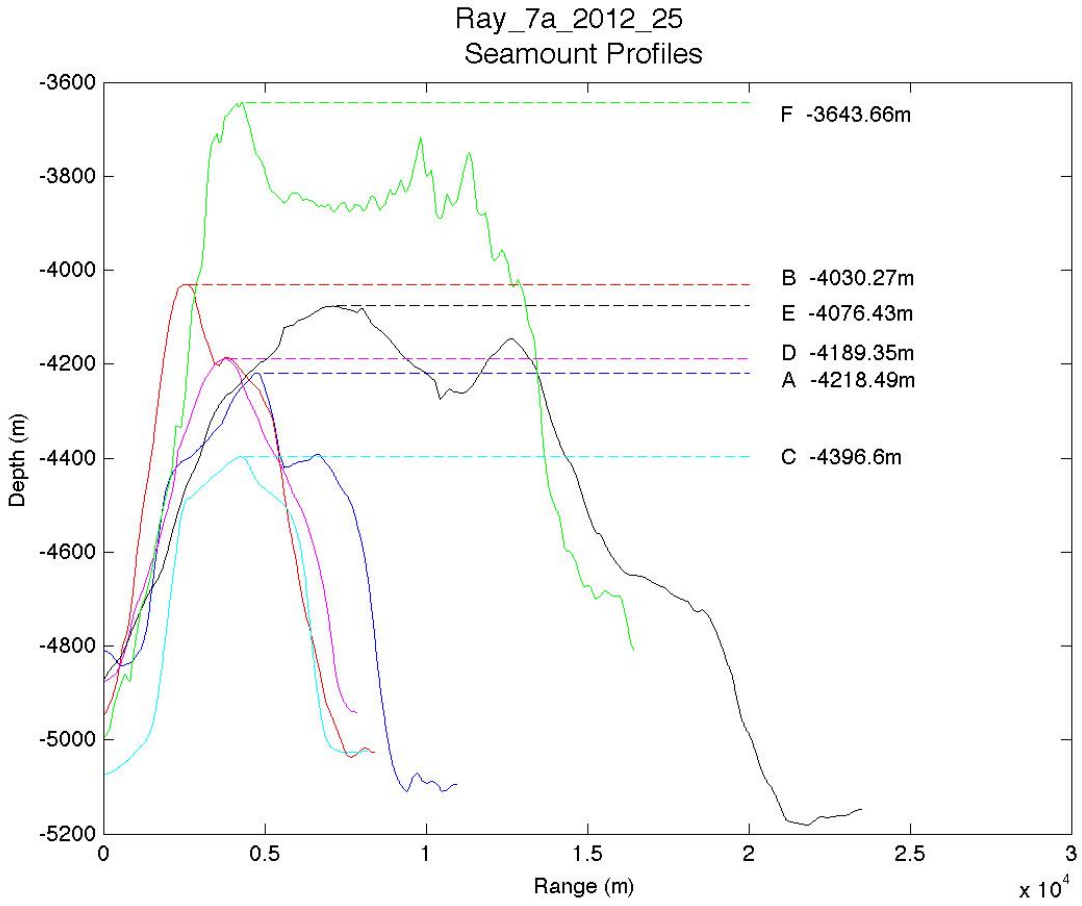

Figure C-2: [Ray_7a_2012_25.jpg]

Figure C-3: Ray tracing example.

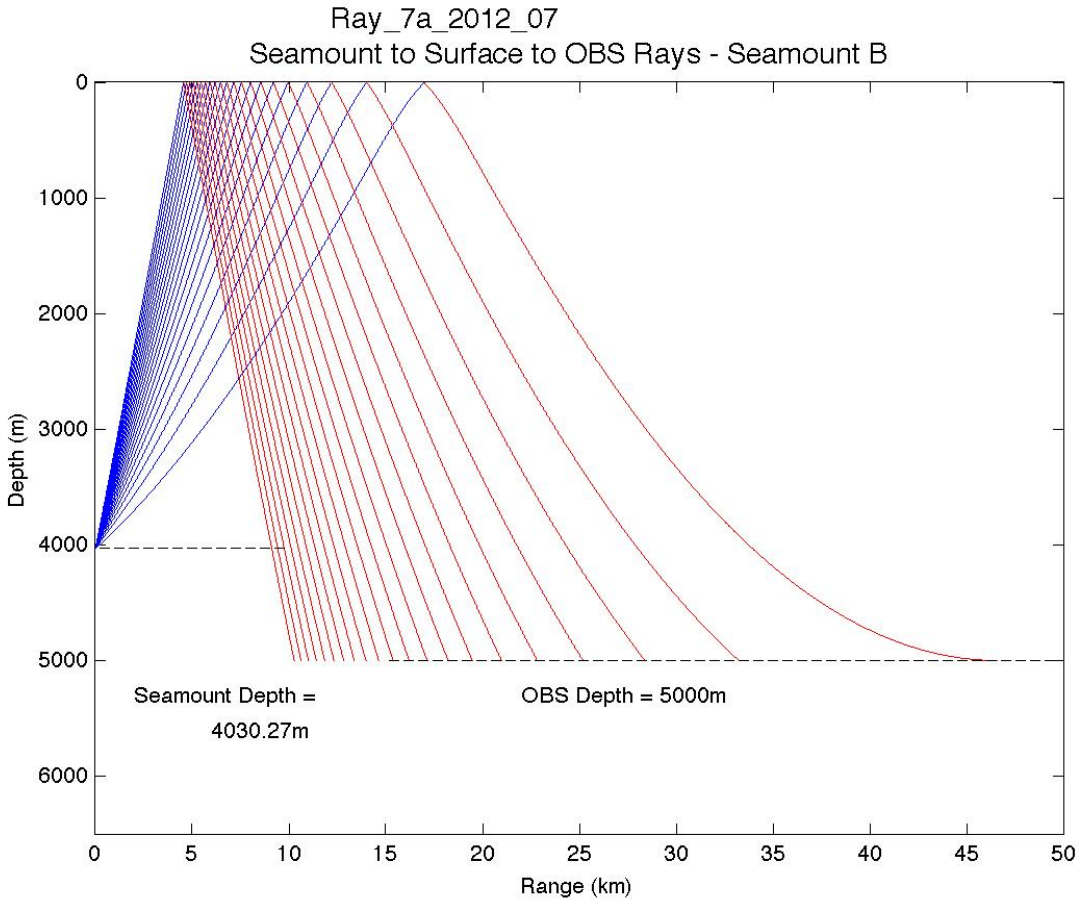

Figure C-3: Example of the ray tracing calculation for a scatterer **at the top of Seamount B**. This is not the same conversion point as in Figures 19, 22, 23 and 24 and Table 7. [Ray_7a_2012_07.jpg]

Figure C-4: Travel-time example.

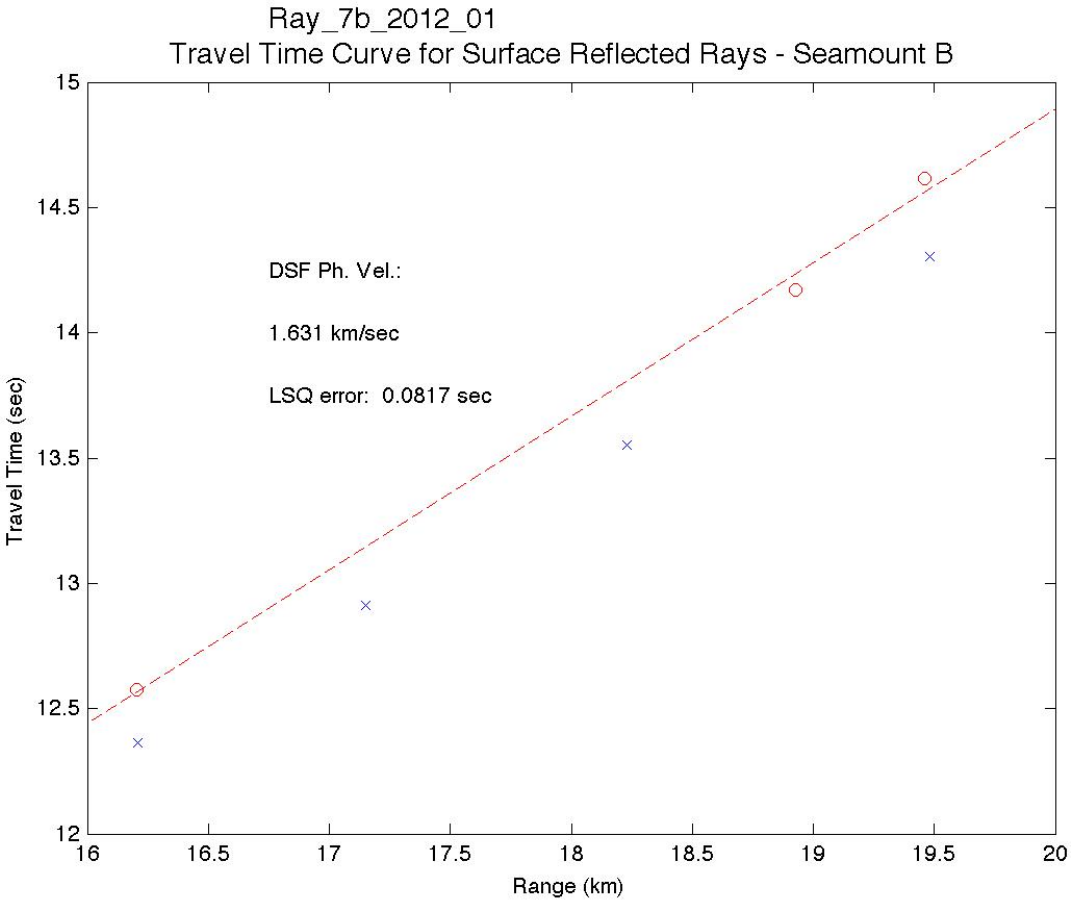

Figure C-4: The travel time curve from the ray tracing in Figure C-3 (blue x's) is compared with the observed residual times and ranges for DSFAs (red circles). [Ray_7b_2012_01.jpg]

Figure C-5: BDSR travel-times for the six seamounts.

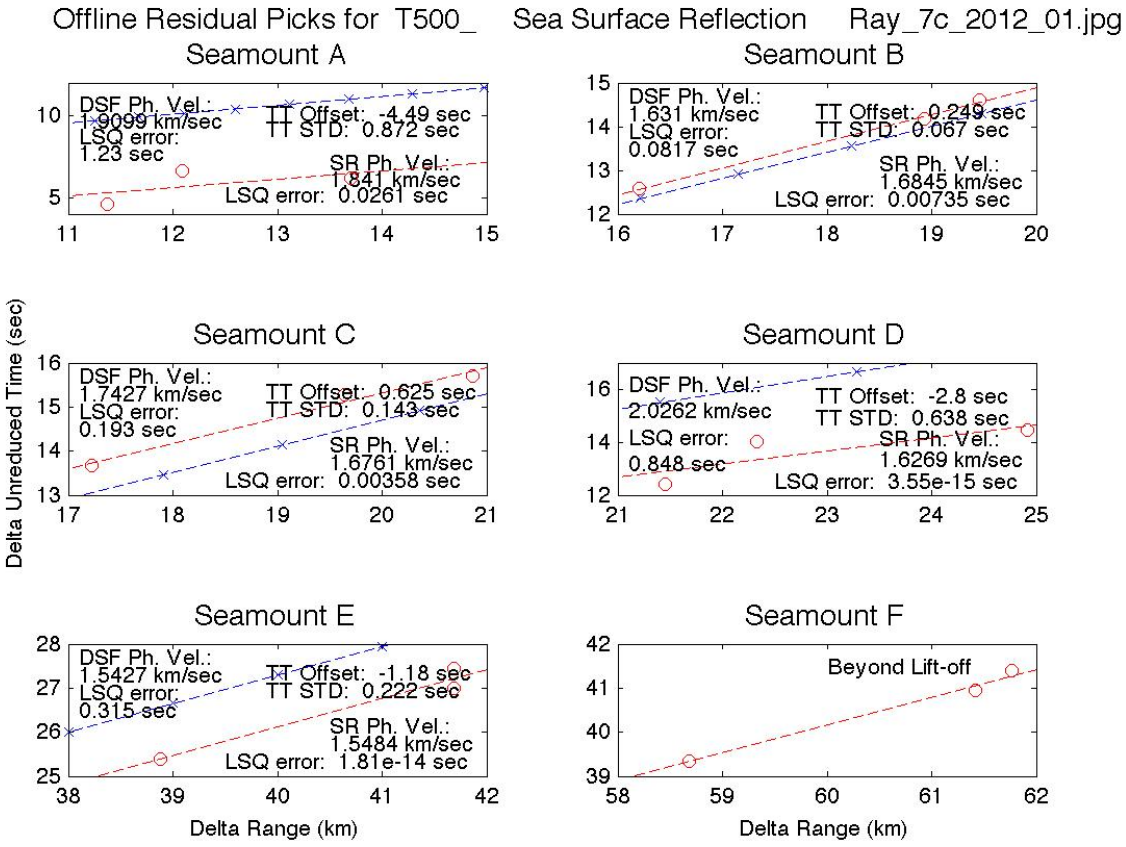

Figure C-5: Summary of the ray tracing versus observed arrival times for the six seamounts. BDSR from Seamount B comes closest to matching to the observed residual times and ranges, ie smallest TT Offset, the time difference between ray trace and observed times at the three residual ranges. [Ray_7c_2012_01.jpg]

Figure C-6: Depth dependence of modeled phase speed.

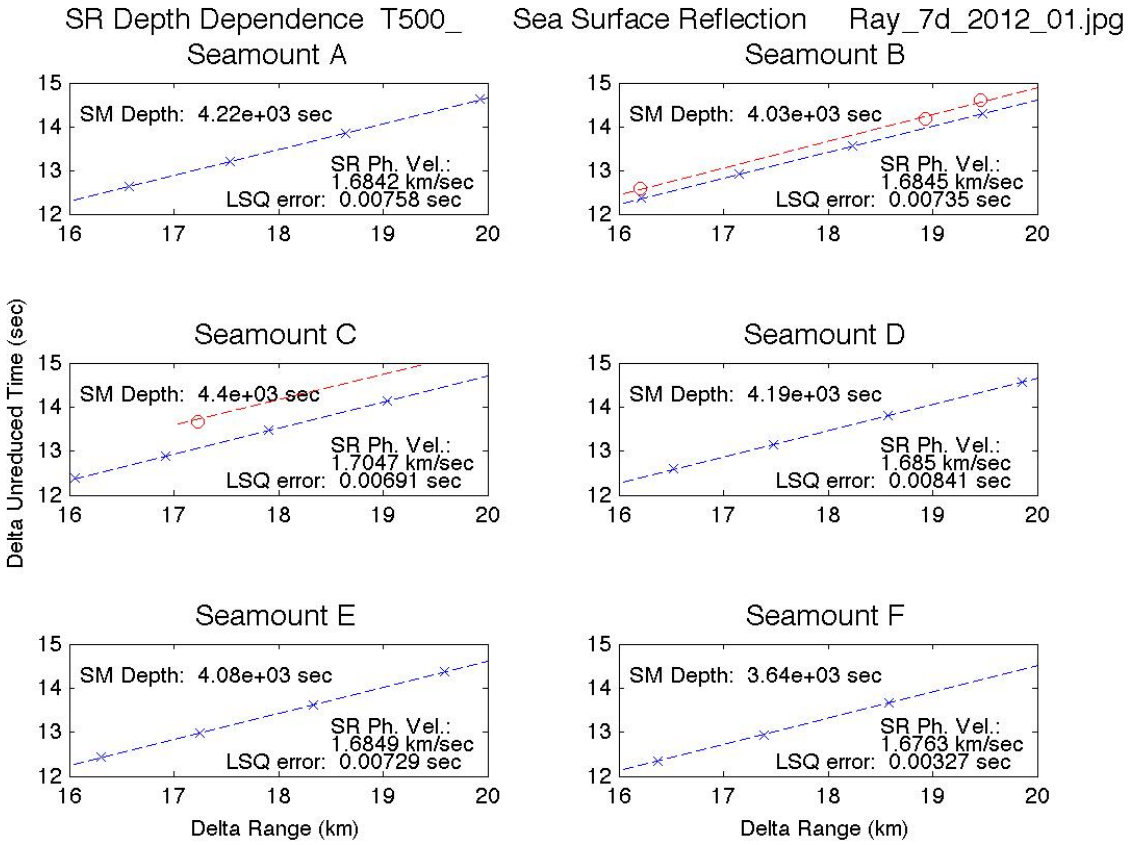

Figure C-6: The goal here was to see if different scatterer heights (SM Depth) could change the BDSR phase velocity at the Seamount B ranges (16-20km) enough for agreement with the observed DSFA phase velocity of 1.631km/sec (crude, from Figure C-5) or 1.6484 km/sec (accurate). None of the scatterer depths from 3,640m to 4,400m could do this (to receivers at 5,000m depth). [Ray_7d_2012_01.jpg]

50272-101

REPORT DOCUMENTATION PAGE	1. REPORT NO. WHOI-2012-09	2.	3. Recipient's Accession No.

4. Title and Subtitle
Analysis of Deep Seafloor Arrivals Observed on NPAL04

5. Report Date
December 2012

6.

7. Author(s) Ralph A. Stephen, S. Thompson Bolmer, Ilya A. Udovydchenkov, Matthew A. Dzieciuch, Peter F. Worcester, Rex K. Andrew, James A. Mercer, John A. Colosi, & Bruce M. Howe

8. Performing Organization Rept. No.

9. Performing Organization Name and Address
Woods Hole Oceanographic Institution
Woods Hole, Massachusetts 02543

10. Project/Task/Work Unit No.

11. Contract(C) or Grant(G) No.
(C)N00014-10-1-0510
(G)

12. Sponsoring Organization Name and Address
Office of Naval Research

13. Type of Report & Period Covered
Technical Report

14.

15. Supplementary Notes
This report should be cited as: Woods Hole Oceanographic Institution Tech Report, WHOI-2012-09.

16. Abstract (Limit: 200 words)
This report gives an overview of the analysis that was done on Deep Seafloor Arrivals since they were initially presented in Stephen et al (2009). All of the NPAL04/LOAPEX (North Pacific Acoustic Laboratory, 2004/ Long Range Ocean Acoustic Propagation Experiment) data on three ocean bottom seismometers (OBSs) at ~5,000m depth and the deepest element of the deep vertical line array (DVLA) at 4250m depth has been analyzed. A distinctive pattern of late arrivals was observed on the three OBSs for transmissions from T500 to T2300. The delays of these arrivals with respect to the parabolic equation predicted (PEP) path were the same for all ranges from 500 to 2300km, indicating that the delay was introduced near the receivers. At 500km range the same arrival was observed throughout the water column on the DVLA. We show that arrivals in this pattern converted from a PEP path to a bottom-diffracted surface reflected (BDSR) path at an off-geodesic seamount.

17. Document Analysis a. Descriptors

bottom-interacting ocean acoustics
long-range ocean acoustics
ambient ocean acoustic noise

b. Identifiers/Open-Ended Terms

c. COSATI Field/Group

18. Availability Statement
Approved for public release; distribution unlimited.

19. Security Class (This Report)
UNCLASSIFIED

20. Security Class (This Page)

21. No. of Pages
91

22. Price

(See ANSI-Z39.18) *See Instructions on Reverse*

OPTIONAL FORM 272 (4-77)
(Formerly NTIS-35)
Department of Commerce